PERFORMANCE-BASED ASSESSMENTS OF BUCKLING-RESTRAINED BRACED STEEL FRAMES RETROFITTED BY SELF-CENTERING SHAPE MEMORY ALLOY BRACES

A Thesis
Presented to
The Academic Faculty

by

Huy Van Pham

In Partial Fulfillment
of the Requirements for the Degree
Master in the
School of Civil and Environmental Engineering

Georgia Institute of Technology
August of 2013

PERFORMANCE-BASED ASSESSMENTS OF BUCKLING-RESTRAINED BRACED STEEL FRAMES RETROFITTED BY SELF-CENTERING SHAPE MEMORY ALLOY BRACES

Approved by:

Dr. CS. Walter Yang, Advisor
School of Civil and Environmental Engineering
Georgia Institute of Technology

Dr. Bruce R. Ellingwood
School of Civil and Environmental Engineering
Georgia Institute of Technology

Dr. Donald White, Co-Advisor
School of Civil and Environmental Engineering
Georgia Institute of Technology

Dr. Reginald DesRoches, Co-Advisor
School of Civil and Environmental Engineering
Georgia Institute of Technology

Date Approved: May 14, 2013

To my present and future family …

ACKNOWLEDGEMENTS

I would like to dedicate my deep gratitude to Dr. CS Walter Yang for all his guidance and support along the way. It's my honor and pleasure to work with him on this project. Thank you for everything.

I would like to express special thanks Dr. Donald White, Dr. Reginald DesRoches and Dr. Bruce R. Ellingwood for their significant suggestions throughout the project. This project wouldn't be complete without their help.

Finally, I dedicate the greatest gratitude to my family for their supports and motivation. I'm grateful to you for being with me at every step I have made. Nothing would be meaningful without you.

TABLE OF CONTENTS

LIST OF TABLES

LIST OF FIGURES

LIST OF ABBREVIATIONS

AISC	American Institute of Steel Construction
ASCE	American Society of Civil Engineers
A_f	Finishing Temperature of Austenite Phase of Shape Memory Alloy
A_s	Starting Temperature of Austenite Phase of Shape Memory Alloy
BRB	Buckling-Restrained Brace
BRBF	Buckling-Restrained Braced Frame
CBF	Concentric Braced Frame
CBF	Concentrically Braced Frame
CP	Collapse Prevention
EBF	Eccentric Braced Frame
EBF	Eccentrically Braced Frame
EDP	Engineering Demand Parameter
FEMA	Federal Emergency Management Agency
GM	Ground Motion
IDA	Incremental Dynamic Analysis
IM	Intensity Measure
IO	Immediate Occupancy
ISDR	Interstory Drift Ratio
LA	Los Angeles
LS	Life Safety
MCE	Maximum Considered Earthquake
MRF	Moment Resisting Frame

M_f	Finishing Temperature of Martensite Phase of Shape Memory Alloy
M_s	Starting Temperature of Martensite Phase of Shape Memory Alloy
NEHRP	National Earthquake Hazard Reduction Program
NSPA	Nonlinear Static Pushover Analysis
NTHA	Nonlinear Time History Analysis
Ni-Ti	Nickel and Titanium
O	Operational
PDR	Permanent Drift Ratio
PGA	Peak Ground Acceleration
RDR	Roof Drift Ratio
SAC	Partnership of the Structural Engineers Association of California(SEAOC), the Applied Technology Council (ATC), and the Consortium Universities of Research in Earthquake Engineering (CUREE)
SC-BRBF	Self-Centering Buckling-Restrained Braced Frame
SCBF	Special Concentrically Braced Frame
SCBF	Special Concentrically Braced Frame
SEAOC	Structural Engineers Association of California
SMA-BF	Shape Memory Braced Frame
SMA	Shape Memory Alloy
SMRF	Special Moment Resisting Frame
SMRF	Steel Moment Resisting Frame
Sa(T1)	Spectral Acceleration at Fundamental Period
UBC	Uniform Building Code
UBF	Unbonded Braced Frame
USGS	United States Geological Survey

SUMMARY

This thesis presents research designed to enable current buckling-restrained braced steel frames (BRBFs) to add a self-centering capacity in addition to their original well-known energy dissipation, so that the BRBFs can return to the original configuration after a seismic event. The original strength of the buildings then can be recovered by replacing only damaged buckling restrained braces (BRBs) which will reduce their downtimes and economic losses. This thesis assesses and compares the seismic performance of frames prior to and after rehabilitation and retrofit by the addition of innovative self-centering SMA braces. The first model considered was a conventional BRBF model designed in compliance with the latest versions of the ASCE Standard 7-10 and the 2010 AISC Seismic Provisions for a typical office building located in downtown Los Angeles, CA. Its dynamic properties, a nonlinear static pushover analysis (NSPA) and a nonlinear time history analysis (NTHA) were performed using the Open System for Earthquake Engineering Simulation (OpenSEES) analysis platform. The cyclic strain hardening behavior of BRBs was considered in the brace modeling. Thirty pairs of ground motion records for downtown Los Angeles that have 2%, 10% and 50% probability of exceedance in 50 years were used to quantify the seismic demands for the BRBFs.

This conventional BRBF model with three buckling restrained braced bays in a lateral force-resisting frame (Model-1) was rehabilitated by adding the innovative SMA braces in the fourth bay, which originally had no braces, to provide additional lateral force-resisting strength and re-centering capacity. This rehabilitated model (Model-2) has

the same beams, columns and BRBs as the first model, but has additional SMA braces and exhibits a larger lateral force-resisting capacity than the original BRB model. Finally, in the retrofitted model (Model-3), the BRBs are replaced by new designed braces and SMA braces are added in the fourth bay so that the model has the same lateral force-resisting capacity as the original BRB model. A design procedure for hybrid BRB-SMA frames is proposed and used to design the retrofitted model. Finally, seismic performance of the rehabilitated and retrofitted models was assessed using the same analyses as used for the original conventional BRBF model.

The numerical results show that the BRBFs retrofitted and rehabilitated by SMA braces have better seismic performance in term of residual drifts and interstory drift than the original frame (Model-1). Compared to the original frame, the rehabilitated model reduces the average maximum interstory drift by 35% while the retrofitted model increases an average of maximum interstory drift demand by 8%. As from standpoint of residual drift, both rehabilitated and retrofitted models show superior performance to the original model, with 79% and 83% reductions, respectively. The averages of maximum SMA strain demand are 0.785% and 2.3% for the rehabilitated and retrofitted models respectively, which are less than the strain limit of 6% (the point beyond which re-centering cannot be guaranteed). Finally, SMA brace and system fragility curves that can be further used for the assessment of downtime and repair cost.

CHAPTER 1

INTRODUCTION

1.1 Motivation

Many regions in California are vulnerable to extreme seismicity. A report of Estimation of Future Earthquakes losses in California (Rowshandel et al., 2005) has stated that average annual losses of in California due to earthquakes during 1970-2000 were about $2.2 billion per year. Among total loss of $2.2 billion, the county of Los Angeles suffered the greatest portion which was approximately $780 million or about one-third of the state-wide annual loss. Moreover, the estimated losses for Los Angeles have been projected as more than $200 billion in building damages if the 1971-2000 earthquakes were to be repeated (Rowshandel et al., 2005).

The buckling-restrained braced frame (BRBF) has been developed during the past decade as a seismic force-resisting system. Although BRBFs are believed to have an enhanced capability of withstanding severe earthquakes, the potential for large residual drifts in this system diminish the practical feasibility of repairing the building after an earthquake more difficult and financially costly. These issues imply a need for developing a system in which structural damage following an earthquake is minimized and the building can be restored to its original condition with reasonable effort.

1.2 Objectives and Research Approaches

The objective of this study is to assess the performance buckling-restrained braced frames (BRBFs) and to evaluate the effectiveness of SMA braces as a retrofit and rehabilitating option. Steps to accomplish this objective are summarized as the following:

1. A 3-story BRBF building model was designed for Los Angeles downtown according to ASCE Standard 7-10 and the 2010 AISC Seismic Provisions.
2. Three suites of 60 ground motion records for downtown Los Angeles (LA01 to LA60, SAC Steel Project). A scaling factor was applied for all ground motion records in this thesis so that the mean response of the 10% ground motion suite reflects the new seismic coefficients of downtown Los Angeles specified in the current USGS. The probabilities of exceedance in 50 years of the suites are 2% for LA21-LA40 records, 10% for LA01-LA20 records and 50% for LA41-LA60 records.
3. Eigenvalue analysis, nonlinear static pushover analysis (NSPA) and nonlinear time history analysis (NTHA) are carried out to assess the seismic response of the frames.
4. The frame response parameters, such as maximum inter-story drift and maximum residual deformation, are converted to performance levels. A seismic fragility assessment is then developed to measure the probability of failure of the frame to meet pre-set performance limits under the possible future seismic events
5. The original BRBF model is modified by installing additional SMA braces as into a bay containing, no steel BRBs, which create self-centering buckling-restrained braced frames, or hybrid BRB-SMA frames. Besides the additional SMA braces, the retrofitted model has the BRBs redesigned so that it has the same lateral force-

resisting capacity as the original model. In the rehabilitated model, everything remains the same as the original model, except the addition of SMA braces. Then, steps 1-4 are repeated for comparison of seismic performance among three frames.

Finally, based on the analyses of the three frames, conclusions regarding the effectiveness of hybrid BRB-SMA systems are made. Suggestions for future research can be found at the end of the thesis

CHAPTER 2

BACKGROUND AND LITERATURE REVIEW

2.1 Buckling-Restrained Braced Frames

Since buckling of braces in conventional CBFs causes degradation in the brace strength under compression and large unbalanced vertical load in beams, an alternative approach to designing CBF systems to prevent brace buckling was developed. The system was called buckling-restrained braced frames (BRBFs). The concept of buckling-restrained braces (BRBs) was first developed in Japan in the 1980s. After the 1994 Northridge Earthquake, the BRBF systems have been used with increasing frequency in the U.S. and has been accepted in the AISC Seismic Specification for Steel Buildings (ANSI/AISC 341-10).

2.1.1 Components of BRB

A typical BRB is composed of five components: a restrained yielding segment, a restrained non-yielding segment, an unrestrained non-yielding segment, unbonding material, and a buckling-restraining mechanism, as shown in Figure 2.1.

1. Restrained yielding segment: This segment, also called steel core, is usually mild steel such as A36 steel, and has a rectangular or cruciform cross-section. It is designed to carry only axial force and is the only portion permitted to yield under loading.
2. Restrained non-yielding segment: This segment is an extension of the restrained yielding segment. The cross-section of this segment is enlarged to ensure that its response remains in the elastic range.

3. Unrestrained non-yielding segment: This segment is an extension from the restrained non-yielding portion. It is projected from the steel tube for connection to the frame. The connection between BRB and frame is usually designed as a pin or bolt connection.
4. Unbonding material: This is a material between mortar/concrete and restrained yielding segment to prevent the segments from contacting each other under loading so that the yielding segment can deform longitudinally independent of the buckling-restraining mechanism.
5. Buckling-restraining mechanism: This mechanism is composed of mortar/concrete and steel tube with the purpose to prevent the steel core from buckling.

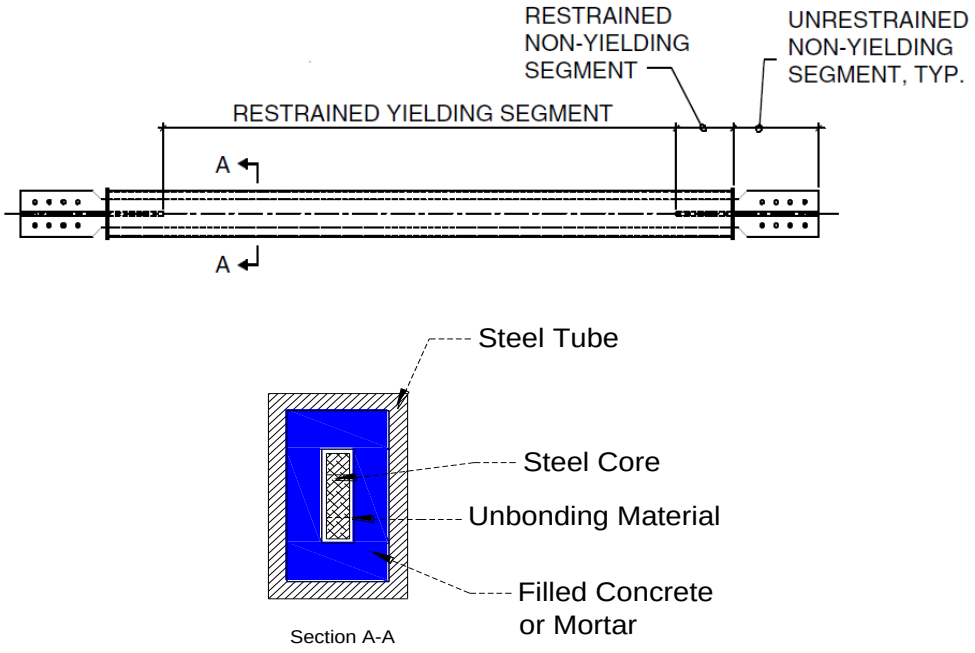

Figure 2.1 Components of buckling-restrained braces (Lopez, 2001).

2.1.2 Behaviors of BRB

With the buckling-restraining mechanism described as above, the BRB is allowed to yield in both tension and compression, while conventional braces experience buckling in compression, which reduces their compression capacity significantly. Figures 2.2 and 2.3 compare the hysteretic behavior of a BRB and an ordinary brace. In Figure 2.3, the BRB shows very stable and predictable behavior under inelastic cycling, with a capacity that is slightly higher in compression than tension by up to 10% higher) and nearly no degradation in stiffness (Clark et al., 2000). Furthermore, BRBs possesses large ductility capacity, the cumulative inelastic deformation in BRBs under cyclic loading can exceed 300 times the initial yield deformation before failure (Sabelli et al., 2003).

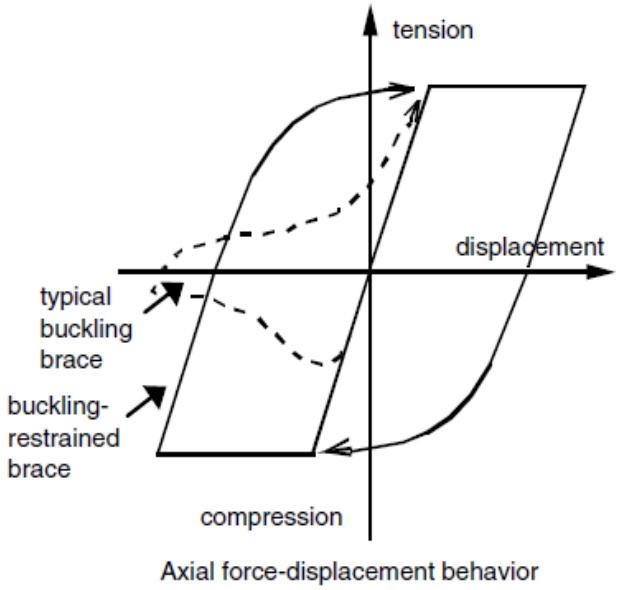

Figure 2.2 Behavior of conventional brace versus buckling-restrained brace (ANSI/AISC 341-10)

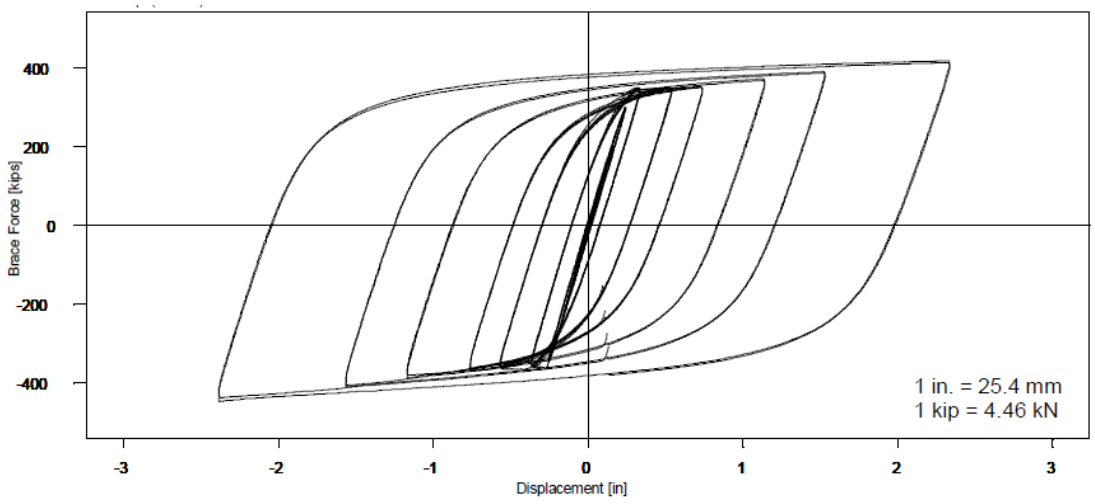

Figure 2.3 Hystereic behavior of brace specimen T-2 under Basic SAC loading history (Clark et al., 2000).

2.1.3 Previous Research on BRBs and BRBFs

Watanabe et al. (1988) conducted experiments on five BRBs to investigate the effect of the strength of the steel tube on the strength of the steel core. The results suggested that, in order to prevent buckling of BRBs, the steel tube must have an elastic buckling strength greater than the yield strength of the steel core (or $P_e \geq P_y$). Furthermore, in order to prevent global buckling, the ratio of P_e/P_y must be greater than 1.5.

Clark et al. (1999) conducted a study that compared the seismic performance of a Special Moment Resisting Frame (SMRF) and a BRBF. The BRBF was redesigned from an Eccentrically Braced Frame (EBF) by using the equivalent lateral force procedure in accordance with the 1994 Uniform Building Code (UBC). As a result, the total weight of steel in the BRBF was reduced significantly by 50% compared to the SMRF. The result from static pushover analyses showed that the BRBF (called a UBF in Figure 2.4) has larger lateral stiffness but lower yield strength compared to the SMRF. The overstrength of the BRBF was much smaller compared to that of the SMRF because design of the

SMRF was governed by drift, while the design of BRBF was governed by strength. The results from a series of nonlinear time history analyses (NTHA) under EL Centro , Tafl and Kobe ground motions are shown in Figure 2.5. The maximum roof drifts of BRBF are about 50 - 70% that of SMRF.

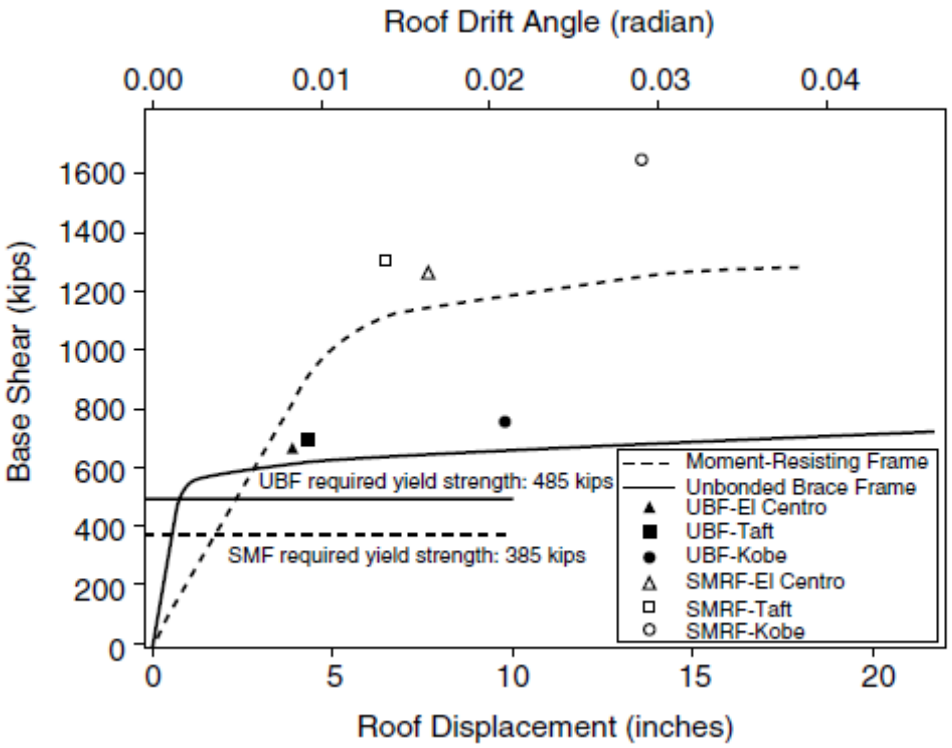

Figure 2.4 Results from static pushover analyses of UBF and SMRF (Clark et al., 1999).

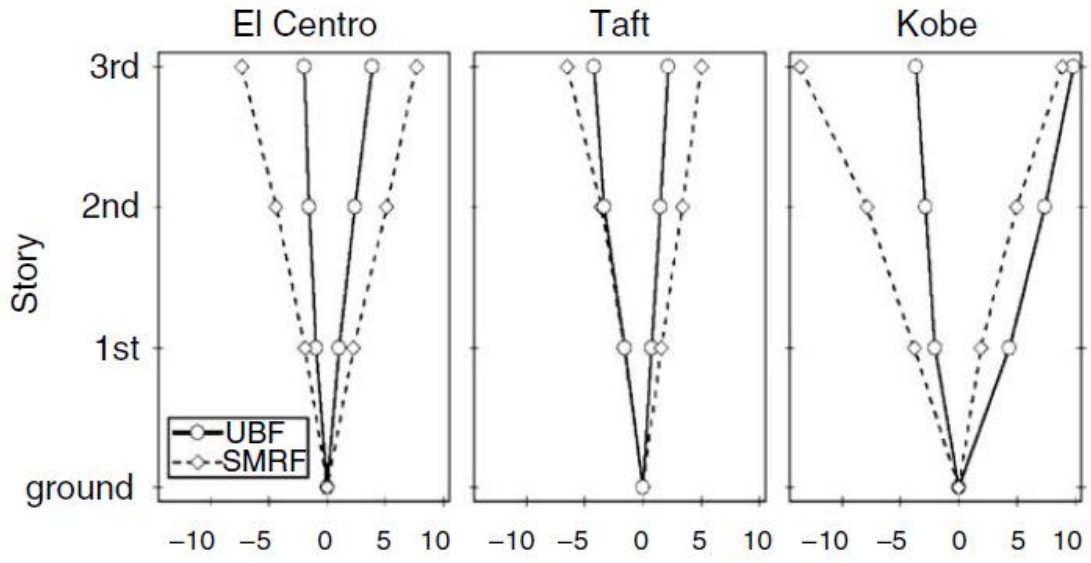

Figure 2.5 Story drift profiles of UBF and SMRF (Clark et al., 1999).

Sabelli et al. (2003) conducted a study that evaluated seismic responses of BRBFs and CBFs in three-story and six-story buildings. Both building models were assumed to be located in Los Angeles with braced arranged in an inverted-V configuration. Both building were designed using the equivalent lateral force procedure with both R = 6 and R = 8, and Ω_o (overstrength factor) = 2. A suite of 20 ground motion records scaled to correspond to NEHRP design spectrum was used for NTHA. The following conclusions were drawn from the study. 1) Changing from R= 6 to R=8 doesn't affect seismic responses or maximum drifts of buildings. 2) Variation in brace ductility has the same pattern as maximum story drifts. Maximum brace ductility is similar for the three-story and six-story buildings. However, cumulative brace ductility is higher in the six-story building. 3) Residual drift is about 40-60% of maximum drift. 4) Stiffening the beam to limit upward displacement at mid-span of the beam has little effect on maximum drift of the buildings but reduces the brace ductility demand significantly. 5) Response appears to be sensitive to proportioning. Sabellis' study suggested that better estimations of the

lateral force demands using methods other than the equivalent static lateral force method may capture the structure responses more accurately.

Uang and Kiggins (2006) conducted a study that continues from the work done by Sabelli et al. (2003). SMRFs were added in to original three-story and six-story buildings as a dual system, and their seismic responses were compared to the original BRBF systems. The SMRFs were designed to resist 25% of the total base shear. The study concludes that inserting SMRFs into BRBFs reduce the maximum drift demands by 10-12% and reduce the residual drift by 46-55% compared to that of the original BRBFs. However, the standard deviation of the residual story drift results is very high indicating the presence of many uncertainties in the predictions.

Sarno and Elnashai (2008) conducted a study that assessed the seismic performance of steel moment resisting frames (MRFs) retrofitted with different bracing systems. The original MRF was designed with a lateral stiffness that didn't comply with drift limitations in high seismic region. The bracing systems were special concentrically braced frames (SCBFs), mega-braces (MBFs) and BRBFs. Their combination led to a eight retrofitted models as summarized in Table 2.1.

Table 2.1 Summary of frames assessed by Sarno and Elnashai.

Frame label	Brace configuration	Brace type	Brace steel grade
SCBF-N	Concentric	Ordinary	A36
BRBF-CN	Concentric	Unbonded	A36
SCBF-L	Concentric	Ordinary	LYS235
BRBF-CL	Concentric	Unbonded	LYS235
MBF-N	Mega	Ordinary	A36
BRBF-MN	Mega	Unbonded	A36
MBF-L	Mega	Ordinary	LYS235
BRBF-ML	Mega	Unbonded	LYS235

It was found that MBFs have maximum story drifts 70% lower than MRFs and about 50% lower than SCBFs. Although BRBFs have slightly higher reduction in

maximum story drifts than MBFs, their total weights are larger than those of MBFs (18.45 vs 13.5). The study concluded that MBFs are the most cost-effective bracing systems.

Moradi et al. (2013) conducted a study that compared seismic performance of BRBFs and Shape memory alloy braced frames (SMA BFs). Four different bracing configurations (including diagonal, split-X, chevron-V and inverted-V) were examined by using incremental dynamic analysis (IDA) under twenty different ground motion records. In the SMA BFs, the beams and columns were kept the same as in the BRBFs, while the BRBs were replaced by superelastic SMA bar segments that connected to rigid links as seen in Figure 2.6. The SMA BFs were designed such that the overall system would have the same natural period as the BRBFs.

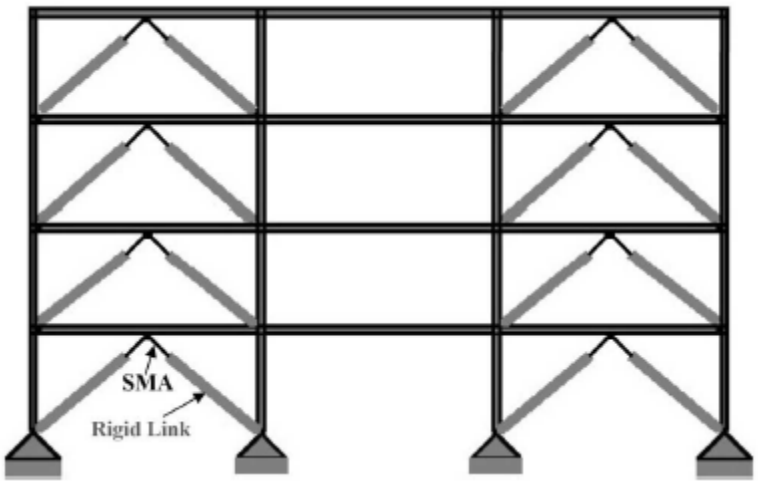

Figure 2.6 SMA inverted-V braced frame (Moradi et al., 2013).

Moradi et al., draw the following conclusions from the study:

1) The responses of BRBFs are little sensitive to higher modes.
2) The SMA braces are effective in reducing maximum interstory drifts.
3) Both SMA BFs and BRBFs satisfy design drift limits

4) Inelastic responses of SMA BFs are distributed more evenly than BRBFs which will mitigate structural damages.
5) SMA BFs experiences negligible residual drifts due to the re-centering capacity of shape-memory alloy braces.
6) SMA BFs are more sensitive to frequency content of input earthquakes. Under severe earthquakes, SMA braces undergo complete phase transformation which allow them dissipate more energy.

2.1.3 Advantages and Disadvantages of BRBFs

BRBFs have the following advantages (Shuhaibar et al., 2002): 1) BRBFs have higher lateral stiffness than MRFs and are better able to satisfy design drift requirements. 2) BRBFs eliminate the issue of buckling of braces in CBFs by allowing yielding in both compression and tension. 3) Cyclic behavior of BRBFs can be predicted and modeled easily. 4) BRBs can be installed through pin or bolted connection to gusset plate which make the installation economical.

However, BRBFs have their own disadvantages. Most importantly, this type of system has large residual drift due to their low post-yield stiffness and lack of recentering capability (Uang and Kiggins, 2006).

2.2 Shape Memory Alloys

Shape memory alloys (SMAs) are classes of metallic alloys that display several characteristics not present in traditional civil engineering materials. At the macroscopic level, SMAs feature two unique properties which are the shape memory effect and the superelastic effect. The effects were first observed by Arne Olander in 1938 (Oksuta and

Wayman, 1998), but serious research on SMAs dates from the 1960's. The most cost effective and widely used SMAs include NiTi, CuZnAl, and CuAlNi.

2.2.1 How Shape Memory Alloys Work

SMAs possess the two unique properties above because their constituent materials them to have a solid phase transformation. Two phases that occur in the transformation are *martensite* and *austenite*.

Martensite, is the relatively soft and easily deformed phase of shape memory alloys, which exists at lower temperatures. *Austenite* is the stronger phase of shape memory alloys, which occurs at higher temperatures. In stress-free state, a SMA is characterized by four transformation temperatures M_s , M_f , A_s and A_f which represent temperature at start and end of each phase.

The shape memory effect is observed when the temperature of SMAs is cooled to below the temperature M_f. At this state, the SMA is completely in *Martensite* phase and can deform easily. After the SMA deforms, the original shape can be recovered simply by applying the heat until the temperature greater than A_f. The deformed *Martensite* is now transformed to the *Austenite* phase, which is configured in the original shape of the SMAs. Figure 2.7 shows the process of how the shape memory effect is achieved.

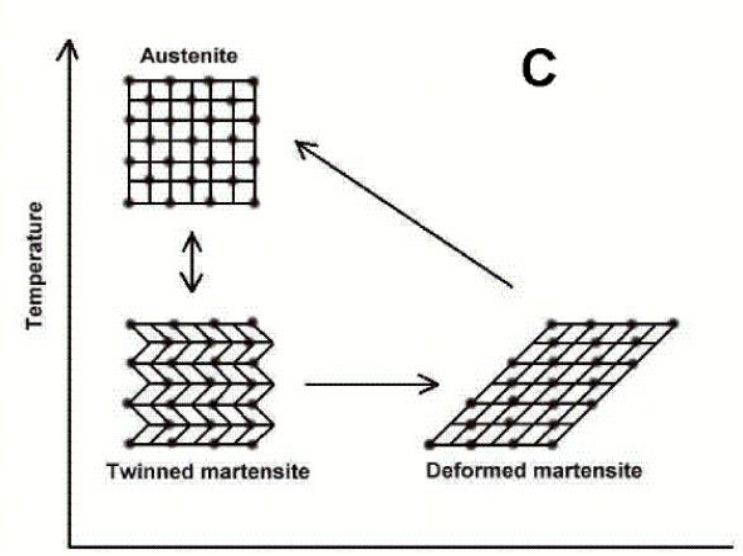

Figure 2.7 Process of achieving shape memory effect (Ryhanen et al., 2002).

The superelastic effect refers to the ability of the SMAs to return to its original shape upon unloading afer deformation without changing temperature as shown in Figure 2.8. The SMAs is loaded until the *Austenite* is transformed into *Martensite*. The loading is absorbed by the softer *Martensite* which makes SMAs deformed, but as soon as the loading is decreased the *Martensite* begins to transform back to *Austenite* provided that the temperature of the SMA is still above A_f, and the SMAs resume their original shape.

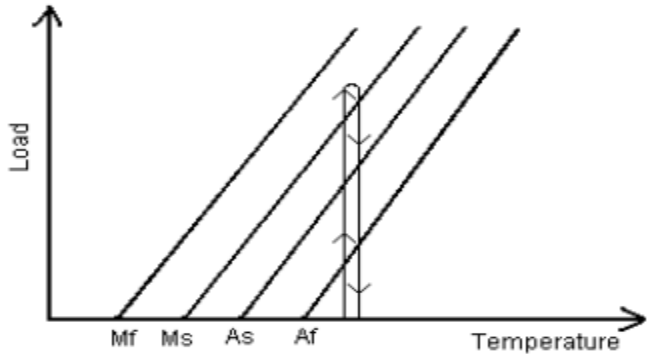

Figure 2.8: Process of achieving superelastic effect (Ryhanen et al., 2002).

2.2.2 Mechanical Properties and Seismic Application of SMAs

Desroches et al. (2004) conducted a series of experiments to investigate the response of SMA wires and bars to gain a better understanding of their characteristic behavior and to explore their possible use in future seismic application. The NiTi SMA specimens were tested to evaluate the effect of loading history, loading rate and section size on loading plateau stress, unloading plateau stress, residual strain and equivalent viscous damping ratio.

The loading history included a 2% strain cycle and 4% strain cycle, following by 4 cycles of 6% strain. The effect of loading rate was examined by using quasi-static 0.025Hz, dynamic 0.5 Hz and dynamic 1 Hz cycling and the effect of section size was tested on 1.8 mm SMA wire and 7.1 mm, 12.7 mm and 25.4 mm SMA bars.

With respect to the section size, the 25.4 mm bar had the highest residual strain; however, the difference in residual strain based on bar sizes was insignificant. The 1.8 mm SMA wire had the highest loading stress and lowest unloading stress which resulted in a higher equivalent viscous damping ratio than SMA bars. The 12.7 mm bar had the largest stress at maximum 6% strain cycle, which induced the highest strain hardening ratio, and the lowest equivalent damping ratio of all the samples. Overall, SMA wires had higher strength and damping potentials than SMA bars. However, damping properties are low for both SMA wires and bars. The SMA specimen size had no effect on residual strain or re-centering capacity.

In term of loading rate, the results show that increasing the loading rates decreased the damping properties in all sample but have negligible effects on residual strains. For results regarding the effect of loading history, both residual strain in SMA

bars and wires increased when cyclic strain increased. However, both wires and bar shows good super-elastic behavior for cyclic strains up to 6%. But for damping properties, strain cycles have significant impact on equivalent viscous damping ratio of SMA wire and bars. As the amplitudes of strain cycles are increased, the equivalent viscous damping ratio increased for up to 5% strain cycles. Beyond 5%, the equivalent viscous damping ratio decreased slightly due to the decrease in forward transformation stress and strain hardening.

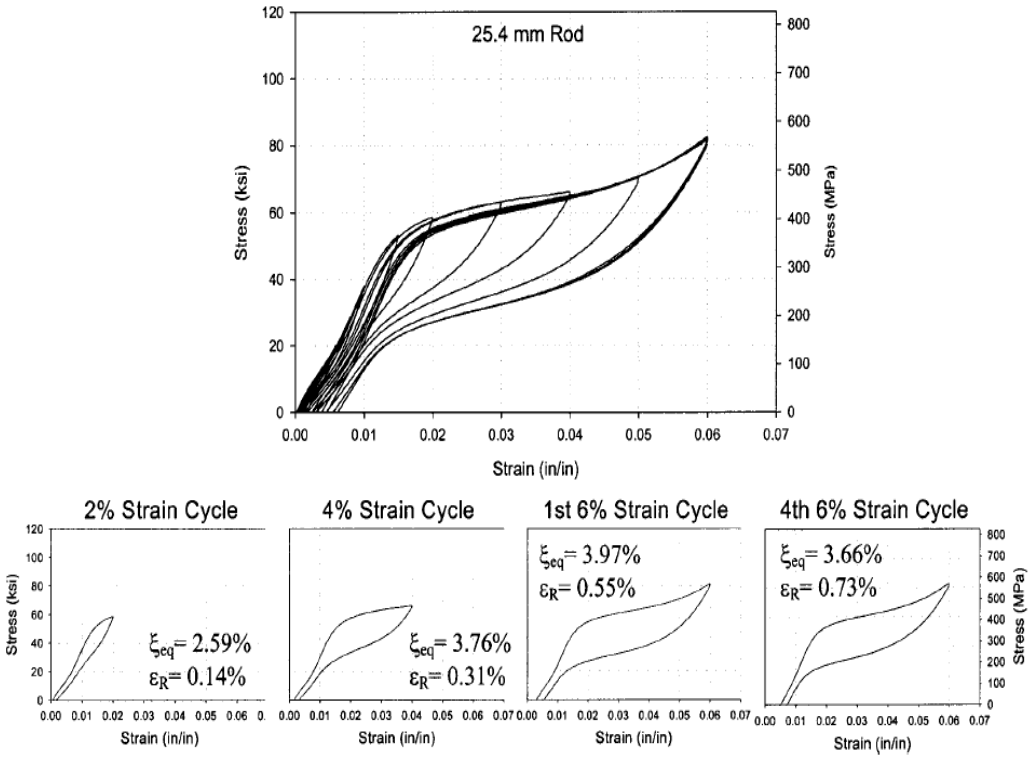

Figure 2.9 Stress-Strain behavior of SMA bar subjected to quasi-static loading (Desroches et al., 2004).

McCormick et al. (2007) conducted a study to investigate cyclic mechanical properties of NiTi SMAs through multi-scale cyclic tensile tests on both coupon and full-scale specimens. Specimens with diameters of 12.7, 19.1 and 31.8 mm were tested along with their respective full-scale specimens. All specimens were subjected to a quasi-static cyclic loading protocol of 20 cycles at 6% strain in tension only. The coupons tests were performed by using 250 KN hydraulic testing frame for the 12.7 mm and 19.1 mm specimens and by using 2.7 MN uniaxial hydraulic testing frame for the 31.8 mm specimen. The test results showed that 1) coupon specimens taken from different locations within the bar provide limited information relative to the properties of full-scale bar due to variation in composition in specimen cross-section. 2) Material properties are strongly dependent on specimen geometry. 3) There is no relationship between section size and forward transformation stresses. 4) Recentering capacity increases with a decrease in bar size, indicating that hot rolling of the bar reduces the accumulated inelastic strain in the specimen. 5) Equivalent viscous damping is inversely proportional to the bar size. 6) Typical earthquake loading has not significant changes on properties of specimen when compared to cyclic tensile tests when run at same rates. 7) Full-scale large diameter hot rolled specimens shows good pseudoelastic (super-elastic) properties and are more cost-effective than cold rolled bars.

Due to the unique behavior mentioned above, SMAs were found to be a promising innovative material to improve performance of civil engineering structures. Several numerical and experimental studies have been carried out to examine the possibility of incorporating SMAs into building systems to limit interstory and residual

drifts during severe earthquakes (Ocel et al., 2004; Auricchio et al., 2006; Asgarian and Moradi, 2011)

McCormick et al. (2007) performed seismic assessments of inverted-V CBF and SMA braced frames. The detail of the SMA brace installation is shown in Figure 2.10. SMA behaviors are assumed to be symmetric and to be buckling restrained. The SMA braces are designed to provide the same initial axial stiffness and yield strength as the steel braces, which lead to the same period for both systems. The dynamic performances of these systems are examined by using nonlinear time history analysis. Major conclusions are drawn as the followings: 1) Story drift ratios are much larger in CBFs than in SMA braced frames. 2) The SMA's recentering capacity permits smaller elongation in SMA braces than in conventional braces. 3) Interstory drift ratios and residual roof drifts are much smaller in SMA braced frames and SMA braces are especially more effective in low-rise buildings. 4) Large interstory drifts and residual drifts occur in the 1^{st} and 2^{nd} stories while results for the upper stories are equivalent to those experienced in SMA braced frames suggesting that SMA braces are most effective if placed in lower stories.

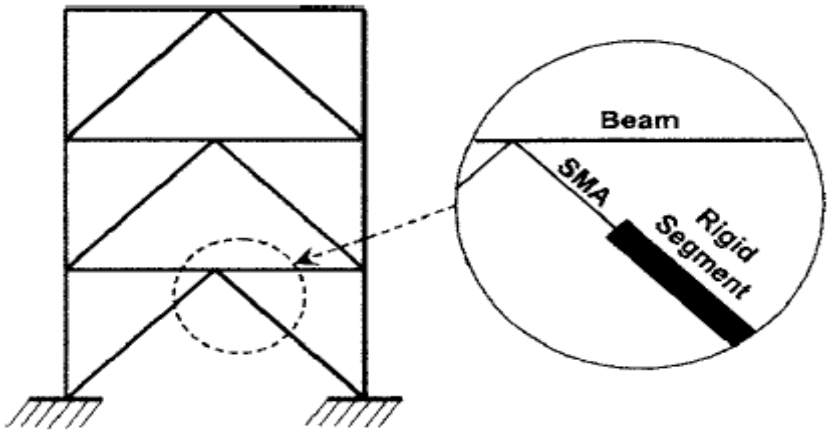

Figure 2.10 Details of SMA braces installation (McCormick et al., 2007).

Yang et al. (2010) proposed an innovative SMA-based device called hybrid steel-SMA device, which provides both energy-absorbing and recentering capabilities. Figure 2.11 shows components of the hybrid device which include a set of recentering SMA wires, two energy-absorbing struts and two high-strength steel tubes. The hybrid device is designed to be stocky and seismically compact or buckling restrained. A nonlinear time history analysis was carried to compare seismic performance of three-story braced frames with the steel-SMA hybrid devices and buckling-restrained braces. The results show that the hybrid steel-SMA devices not only exhibit a re-centering capacity but also maximize energy dissipation. Furthermore, the hybrid braced frames show little larger in interstory drifts but these drifts are distributed more uniformly than in BRBFs.

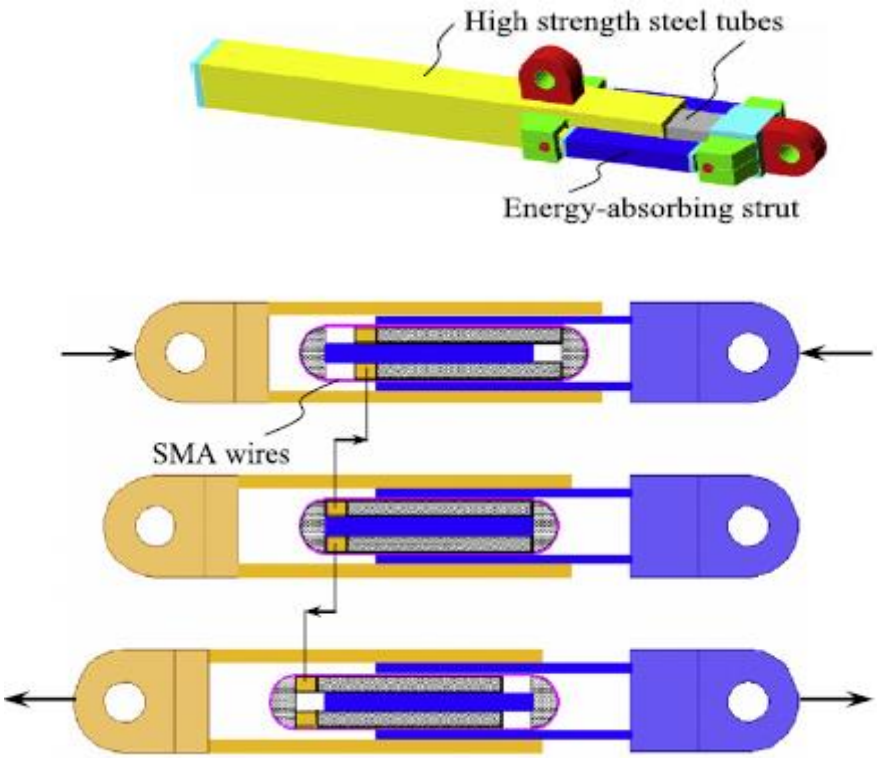

Figure 2.11 Components of hybrid device (Yang et al., 2010).

CHAPTER 3

DESCRIPTIONS AND MODELING OF FRAMES

3.1 General Characteristics of a Typical BRBF in Downtown Los Angeles

A conventional inverted-V buckling-restrained braced steel frame in this study is designed for downtown Los Angeles and according to the equivalent lateral force procedures specified in ASCE Standard 7-10. BRBF building has three stories, 4 bays in the N-S direction and 6 bays in the E-W direction. In each bay, the width is 30 ft and the height of each story is 13 ft as shown in Figure 3.1. The following floor load distributions are used to design the frames (steel weight is assumed to be 13 psf for all design): floor dead load (weight calculation) is 96 psf, roof dead load (exclude penthouse) is 83 psf, penthouse dead load is 116 psf, reduced live load per floor and for roof is 20 psf (FEMA-355C). The seismic mass is 70.90 kip-sec^2/ft for roof and 65.53 kip-sec^2/ft for 2nd and 3rd floor.

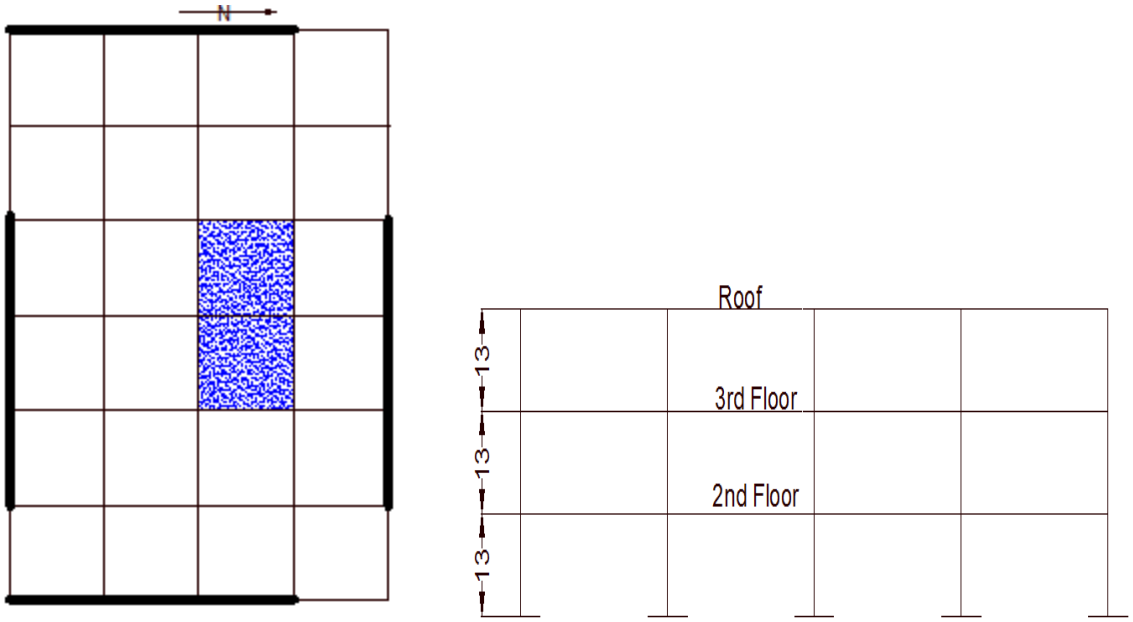

(a) (b)

Figure 3.1 Plan view (a) Elevated view (b) of the typical three-story frames for Los Angeles with the penthouse indicated by the shaded area.

The frame is designed according to the mapped spectral accelerations, 2.415g and 0.846 g, for the short period and the 1-second period respectively. The building is designed on stiff soil, class D. The response modification factor *R* is selected as 8 for BRBF system according to the latest ASCE Standard 7-10 (noted the *R* was 7 in the ASCE Standard 7-5, the older version). The importance factor is taken as 1 for regular buildings. Accordingly, the seismic weight, *W*, for each braced bay is 1084 kips. The seismic response coefficient, C_s, is equal to 0.23. The design base shear, $V = C_s \times W =$ 249.32 kips. This makes total design base shear for each lateral force-resisting frame equal to $V \times 3\ bays = 750$ kips.

3.1.1 As-built Frame (Model-1)

This as-built conventional BRB steel frame, Model-1, is braced by BRBs in inverted-V configuration in 3 bays as shown in Figure 3.2. The beams and columns are designed using A572 Grade 50 steel with the minimum yield stress, F_y , equal to 50 ksi and a ratio of the expected yield stress to minimum yield stress, R_y , equal to 1.1. The BRBs is designed using A36 mild steel having minimum yield stress, F_{ysc} , equal to 36 ksi and R_y equal to 1.5 (ANSI/AISC 341-10). The area of steel core is computed based on the following equation:

$$A_{sc} = \frac{(V \times \rho)}{(2 \times cos\theta \times \phi \times F_{ysc})} \tag{3.1}$$

where V is design shear for each braced bay calculated from equivalent lateral force procedure in ASCE Standard 7-10, ρ is the redundancy factor for seismic-resisting frames, θ is the angle between the brace and beam, ϕ is strength reduction factor and F_{ysc} is the yield stress of steel core. Beams and columns are designed from the loading combinations that include seismic loads based on adjusted strength of braces in tension and compression (refer Appendix A). The adjusted brace strength in tension is $\omega R_y F_{ysc}$ and adjusted brace strength in compression equals $\omega \beta R_y F_{ysc}$ where ω is the cyclic strain hardening adjustment factor and β is the compression strength adjustment factor. The member sizes are given in Table 3.1.

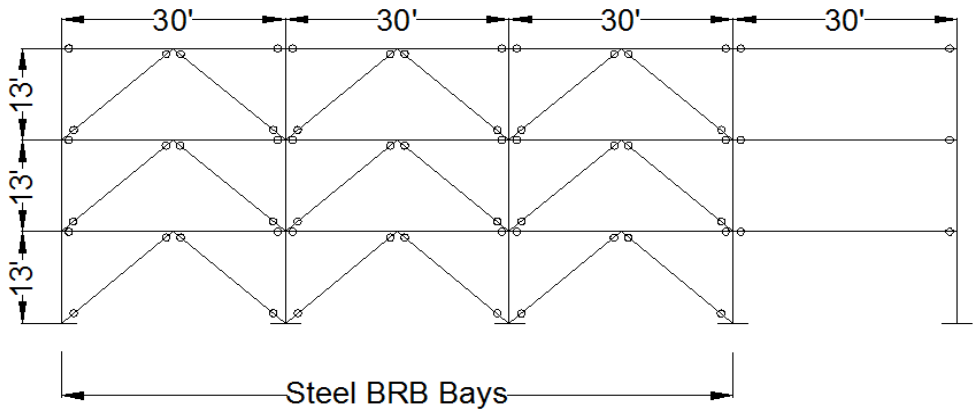

Figure 3.2 Elevated view of Model-1.

Table 3.1 Member sizes for Model-1.

Story	Columns	Beams	Area of BRBs (in^2)	Length of BRB steel core (in)
1	W 12x96	W 14x109	6.00	126
2	W 12x96	W 14x109	5.00	126
3	W 12x96	W 14x82	3.25	126

3.1.2 Rehabilitated Frame (Model-2)

This model is a self-centering BRB frame (SC BRBF), or hybrid BRB-SMA frame, in which SMA braces are added to an unbraced bay to provide re-centering capacities as shown in Figure 3.3. All other member sizes and mechanical properties remain the same as those in the as-built model (Model-1). The SMA braces installed in this model are assumed to have a forward transformation yield stress (loading plateau stress, F_{ysma}) of 60ksi, modulus of elasticity of 6000ksi and strain hardening ratio of 1%. These properties are adopted from previous tests on Ni-Ti SMA material (DesRoches et al., 2004, Dolce and Cardone, 2001). The yielding segment length of SMA brace is taken as 62 inches (refer Appendix A for the design concept). The ratio of the reverse transformation yield stress to the forward transformation yield stress, α, is assumed to be 0.75 for this model.

In order to obtain recentering capacity, Equation 3.2 requires that the total strength of SMA braces at unloading point corresponding to the reverse transformation yield displacement must be equal to or greater than the summation of the strength of the BRBs in each story. This means the SMA braced bay is designed to have lateral-force resistance equals to $\sum F_{sc} / \alpha$; hence, the lateral force resistance of this model is now increased up to $1 + 1/\alpha = 2.33$ times compared to that of Model-1.

$$[\sum F_{sma.r} = \alpha \times \sum F_{sma.f}] \geq \sum F_{sc} \tag{3.2}$$

in which $F_{sc} = A_{sc} \times F_{ysc}$, $F_{sma.f} = A_{sma} \times F_{ysma}$

Then, required area for SMA braces are determined as following:

$$A_{sma} = \frac{\sum F_{sma.f}}{N_{sma} \times F_{ysma}} \tag{3.3}$$

where N_{sma} is number of SMA braces in a story.

It is noted that the above design calculations are for only one story. The repetition may be required if the required lateral strength for each story is different.

The SMA braces installed in this model are assumed to be buckling restrained, or a self-centering devices developed by Yang et al. (2010). The member sizes are summarized in Table 3.2.

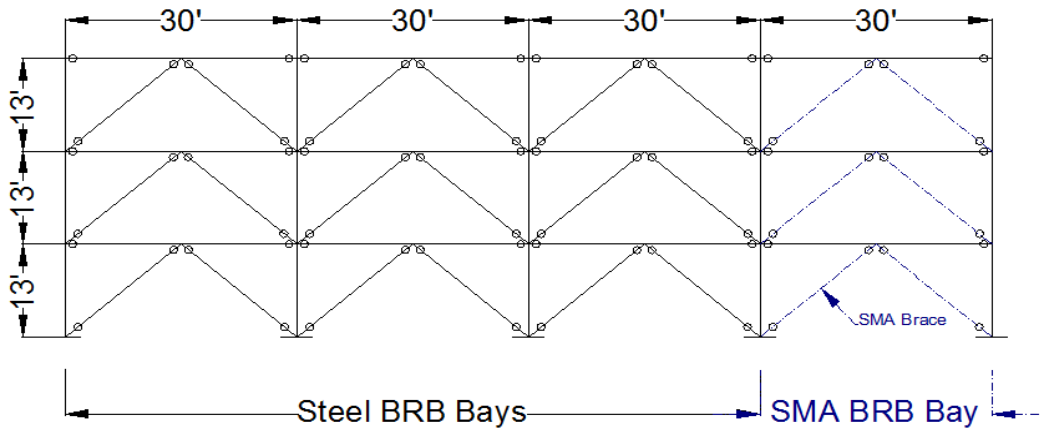

Figure 3.3 Elevated view of Model-2.

Table 3.2 Member sizes for Model-2.

Story	Columns	Beams	Area of BRBs (in^2)	Area of SMA Braces (in^2)
1	W 12x96	W 14x109	6.00	21.75
2	W 12x96	W 14x109	5.00	18.00
3	W 12x96	W 14x82	3.25	11.75

3.1.3 Retrofitted Frame (Model-3)

This self-centering BRB frame is a retrofitted model from the as-built frame in which the originally existing BRBs are removed and new designed BRBs and SMA braces are installed as shown in Figure 3.4. The BRBs and SMA braces are designed to resist the same seismic forces as the Model-1 does. Beams and columns sizes are kept the same as they were in Model-1. SMA braces have the same material properties as described in Model-2, except for areas and length. The yielding length of SMA is selected at 42 inches (refer Appendix A for the design concept). The SMA reverse transformation stress is now taken as one half of the forward transformation stress, or $\alpha = 0.5$. Design procedure of SMA braces and BRBs in a hybrid frame is expressed below:

$$\sum \phi F_{sma.f} + \sum \phi F_{sc} \geq \frac{V_{total}}{cos\theta} \quad (3.4)$$

in which V_{total} is the design interstory shear for each story and equals to V multiplied by the number of BRB bays in the as-built model (Model-1). Solving Equations 3.2 and 3.4 obtains the force distribution into the BRB braces and SMA braces:

$$\sum F_{sc} = \frac{1}{\phi} \times \frac{\alpha}{1+\alpha} \times \frac{V_{total}}{cos\theta} \quad (3.5)$$

$$\sum F_{sma.f} \geq \frac{1}{\phi} \times \frac{1}{1+\alpha} \times \frac{V_{total}}{cos\theta} \quad (3.6)$$

Then, areas of BRBs and SMA braces can be determined by using Equations 3.7 and 3.8 respectively:

$$A_{sc} = \frac{\sum F_{sc} \times \rho}{F_{ysc} \times N_{brb}} \quad (3.7)$$

$$A_{sma} = \frac{\sum F_{sma.f} \times \rho \times R_y \times \omega}{F_{ysma} \times N_{sma}} \quad (3.8)$$

in which N_{brb} and N_{sma} is number of buckling-restrained braces and SMA braces respectively. Also, the consideration of R_y and ω in Equation 3.8 is due to the effects of the expected yield stress of the BRBs and cyclic strain hardening (isotropic strain hardening) of BRBs on the SMA braces. Based on the proposed design procedure above for hybrid BRB-SMA frame system with the same design base shear as the as-built BRBF system (R=8), the sizes for the BRB and SMA braces in the hybrid Model-3 are determined as listed in Table 3.3.

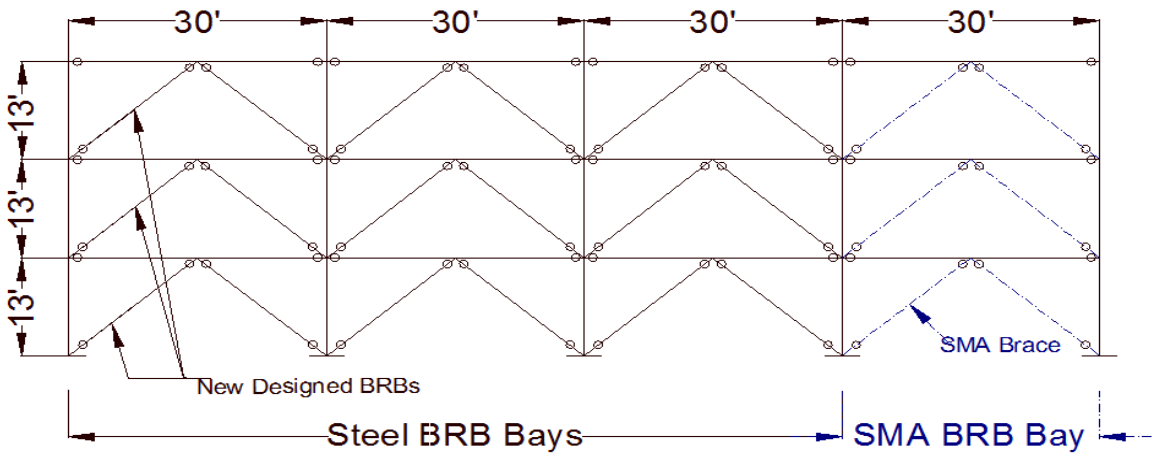

Figure 3.4 Elevated view of Model-3.

Table 3.3 Member sizes for Model-3.

Story	Columns	Beams	Area of BRBs (in^2)	Area of SMA Braces (in^2)
1	W 12x96	W 14x109	2.00	12.00
2	W 12x96	W 14x109	1.75	10.25
3	W 12x96	W 14x82	1.25	6.25

3.2 Numerical Modeling of Frames

In order to examine the seismic performance of BRBFs and SC BRBFs, nonlinear pushover static analyses and nonlinear time history analyses are carried out using the Open System for Earthquake Engineering Simulation (OpenSEES) analysis platform. Due to the symmetrical floor plan, lateral force-resisting frames are modeled for only one side of the building. Floor masses are taken into account and are applied to the columns at each story and to the middle of the beams. All beams and columns are modeled using nonlinear beam-column elements with fiber sections. Beams are divided into 10 elements for each bay while columns are divided into 2 elements for each story. All beam-column

connections are simple connections. The bilinear force-deformation relation for all beam and column members includes 3% strain hardening. All bracing connections are also idealized as pinned connections to resist axial load only. The gusset plates at brace connections are neglected for simplicity. Both materials and geometric nonlinearities are taken into consideration. A 5% Rayleigh damping coefficient is assumed for the first and third modes.

3.2.1 Modeling of Buckling-Restrained Steel Braces

Each BRB is simulated by three nonlinear beam-column elements which represent two non-yielding segments (rigid connections) at both ends and a yielding segment (steel core) at the middle of the brace. Moments are released at both ends. The steel core is assumed to have 53% of the total length of brace. The percentage of the middle portion, 53%, is obtained from a seismic design example for BRBF I Steel Tips (Lopez and Sabelli, 2004). Since the steel casing and concrete are not modeled, a factor is applied to increase the moment of inertia of steel core to match its realistic value while the area of the steel core remains the design value; hence, the steel core is prevented from buckling. A constitutive model of BRB is shown in Figure 2.2, which is assumed to have equal capacity in both tension and compression. However, the cyclic strain hardening, observed in the experimental results (Cofie, 1983) is taken into account in the investigated frame models.

The BRBs are modeled using the "Steel02" material with the expected strength, F_{ysc} x R_y = 36 ksi x 1.5 = 54 ksi (ANSI/AISC 341-10). The post-yield stiffness is 0.008

times modulus of elasticity, and the isotropic strain hardening ratio (an increase of tension/compression yield envelope as a portion of yield strength after plastic strain) is 4%. These properties were determined by matching the numerical cyclic stress-strain curves shown in Figure 3.7 to experimental ones shown in Figure 3.6 for A36 steel under the same loading protocol (Figure 3.5).

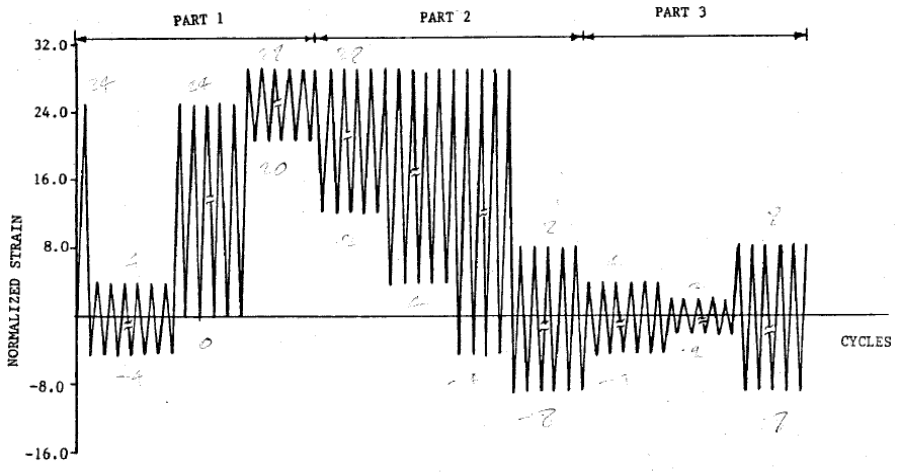

Figure 3.5 Loading Protocol (Cofie, 1983).

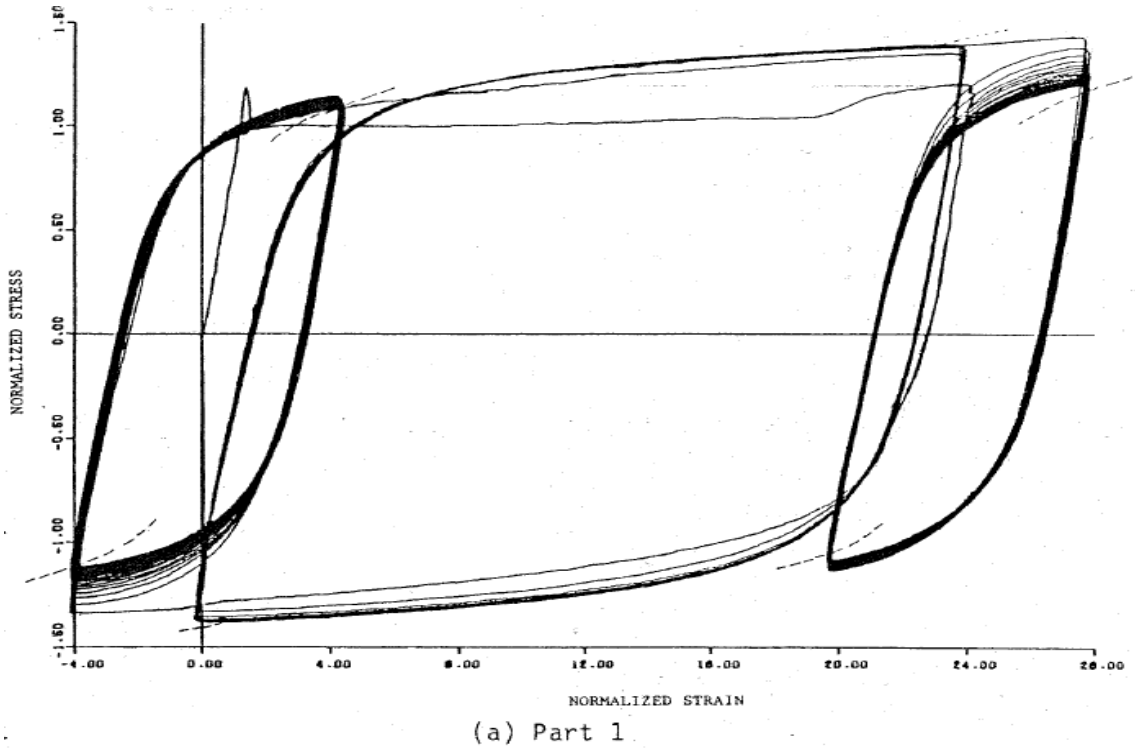

Figure 3.6 Experimental cyclic stress-strain curves for A36 steel (Cofie, 1983).

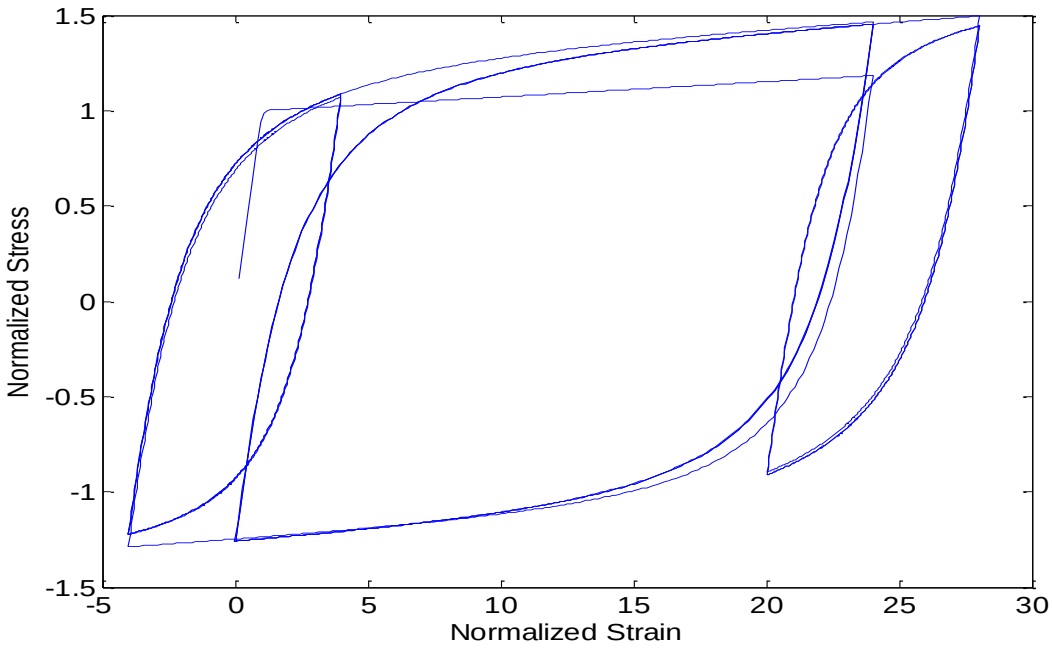

Figure 3.7: Numerical stress-strain curves for A36 steel simulated from OpenSEES.

3.2.2 Modeling of SMA Braces

The superelastic behavior of SMA is simulated using a uniaxial constitutive model proposed by Fugazza (2003). The basic assumption is that stress-strain relationships of SMAs are represented by a series of linear curves whose extension depends on the transformation experienced. The numerical SMA model is implemented in OpenSEES by using the command of the "SMA" material. Figure 3.8 presents parameters needed to simulate SMA behavior which are modulus of elasticity for a*ustenite* and *martensite* phases (E_{SMA}), *austenite* to *martensite* starting stress (loading plateau stress, σ_s^{AS}), *austenite* to *martensite* finishing stress (σ_f^{AS}), *martensite* to *austenite* starting stress (unloading plateau stress, σ_s^{SA}), *martensite* to *austenite* finishing stress (σ_f^{SA}) and superelastic plateau strain length (ε_L). Values of these parameters are provided in Table 3.4. SMA braces are also assumed to have no strength degradation during cyclic loading (Fugazza, 2003). The buckling-restraining mechanism for SMA brace is modeled similarly as in BRBs. The hysteresis behavior is modeled as shown in Figure 3.9.

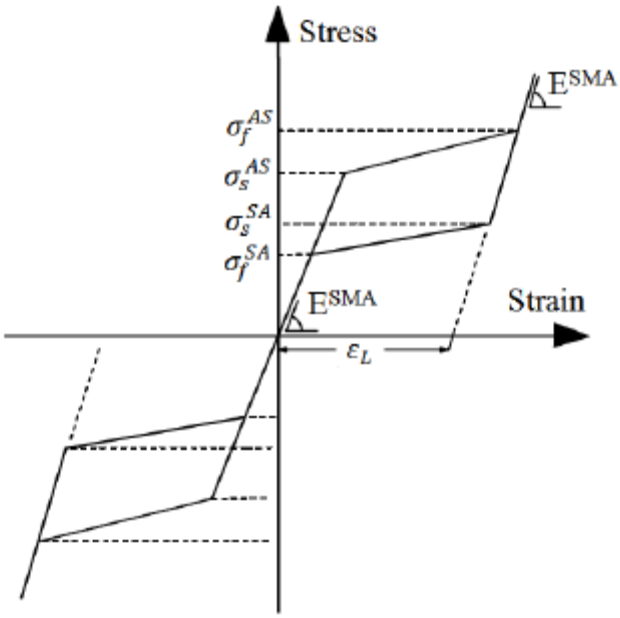

Figure 3.8 Constitutive model of SMA (Fugazza, 2003).

Table 3.4 Adopted mechanical properties of SMA (DesRoches et al., 2004).

Quantity	Values (Model-3/Model-2)
E_{SMA}	6000 ksi
σ_s^{AS}	60 ksi
σ_f^{AS}	90 ksi
σ_s^{SA}	60 ksi / 75 ksi
σ_s^{SA}	30 ksi / 45 ksi
ε_L	4.5%

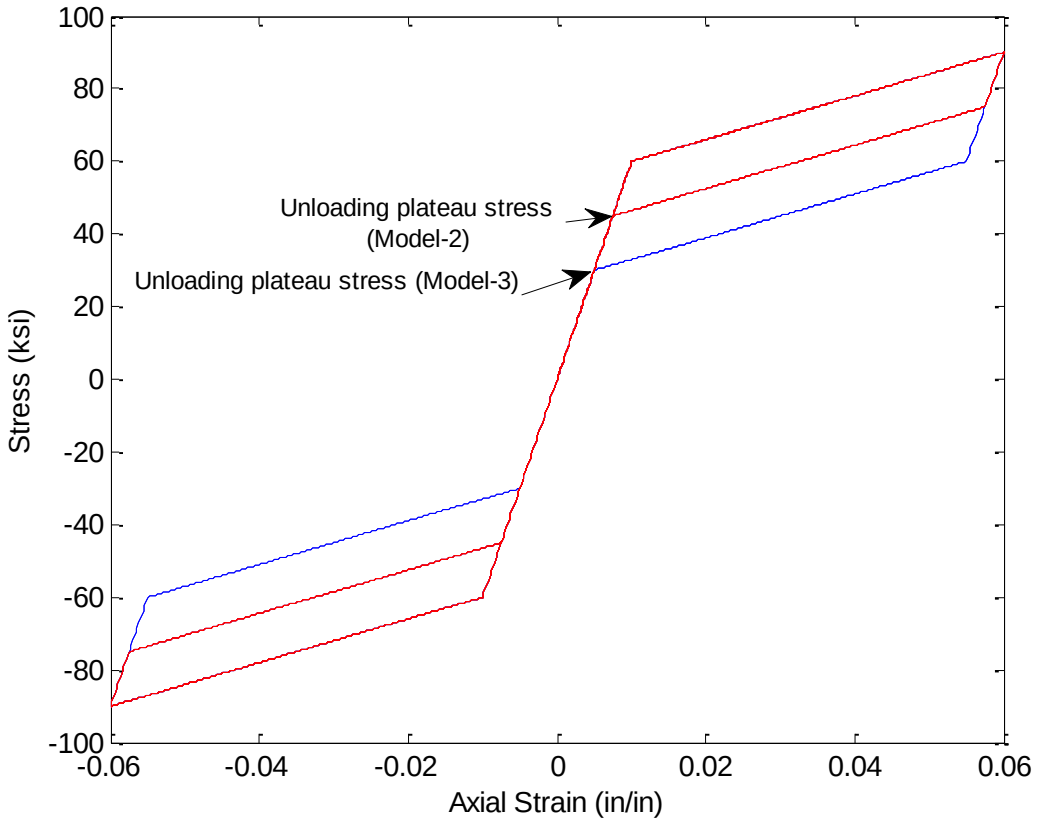

Figure 3.9 Stress-Strain curves for SMA used in Model-2 and Model-3.

3.3 Selected Earthquake Ground Motions

A set of 60 horizontal ground motion records were used to analyze the behavior of three frame models by using NTHA. These ground motions consisted of three suites of 20 ground motions corresponding to threeseismic hazard level of 2%, 10% and 50% probability of exceedance in 50 years. The ground motions were developed for the FEMA-SAC steel project study on steel moment-resisting frames (Somerville et al.,1997). The mean response spectrum from the 10% ground motion set matches the 1997 NEHRP design spectrum, modified from soil type of S_B-S_C to soil type S_D and

having a hazard specified by the 1997 USGS maps (FEMA 302). The spectral accelerations of all three ground motion suites are shown in Figures 3.10, 3.11 and 3.12. Figure 3.13 plots the design response spectrum based on the latest mapped spectral accelerations in USGS.

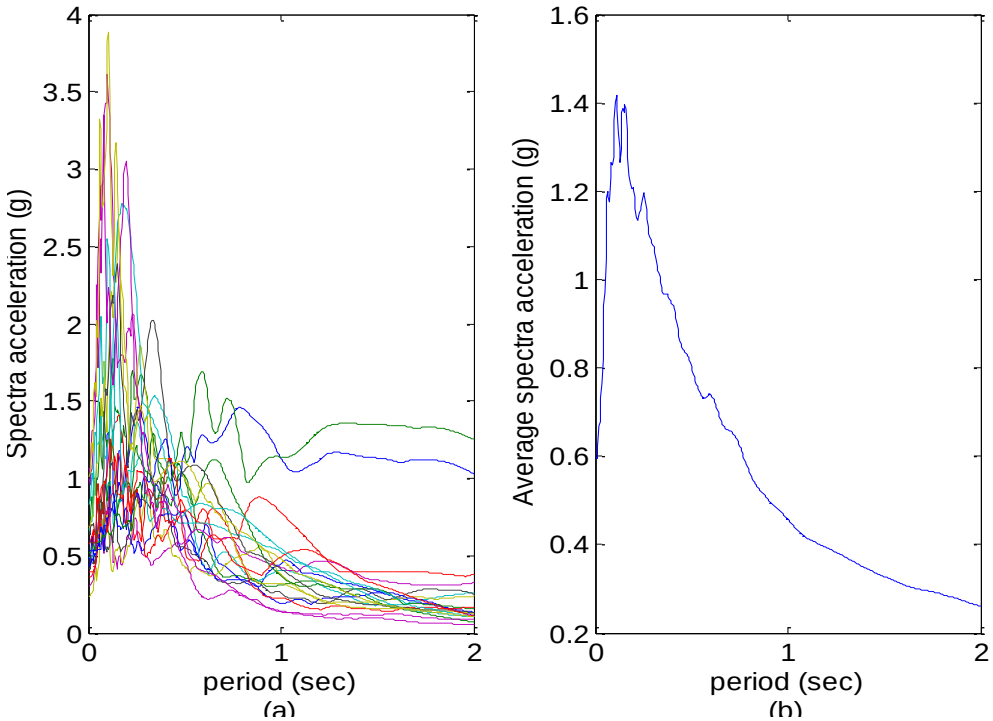

Figure 3.10 (a) Spectral accelerations and (b) the mean spectral acceleration of 20 ground motion records having 10% probability of exceedance in 50 years.

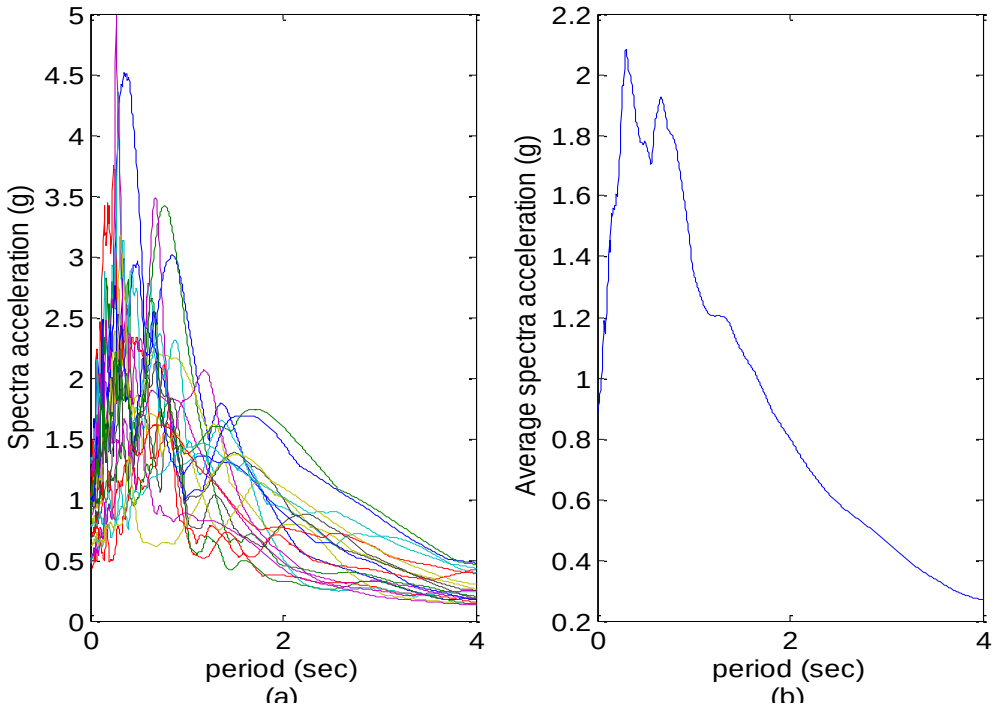

Figure 3.11 (a) Spectral accelerations and (b) the mean spectral acceleration of 20 ground motion records having 2% probability of exceedance in 50 years.

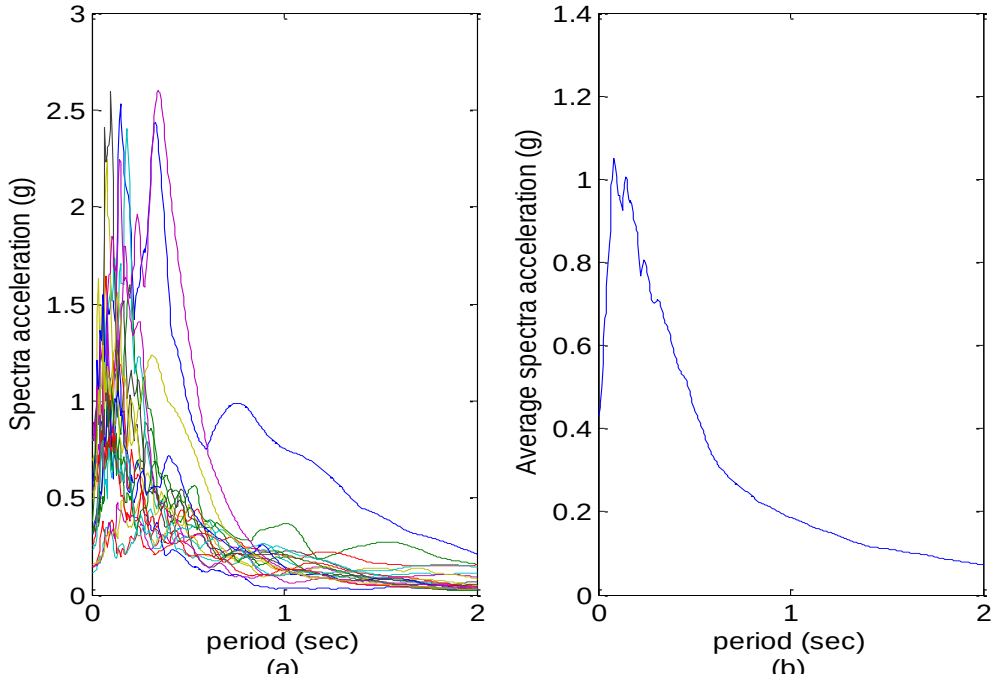

Figure 3.12 (a) Spectral accelerations and (b) the mean spectral acceleration of 20 ground motion records having 50% probability of exceedance in 50 year.

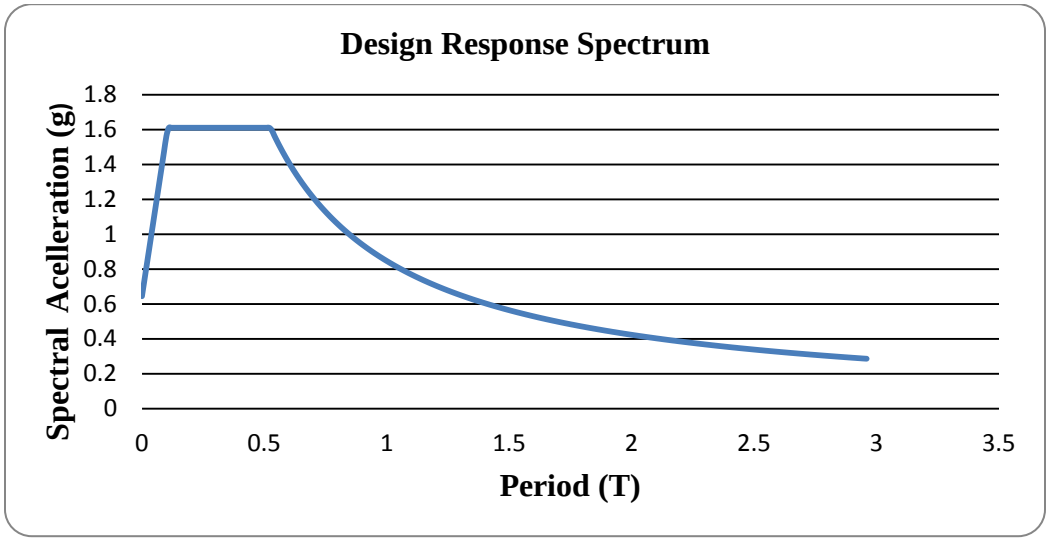

Figure 3.13 Design Response Spectrum.

From the comparison of the average spectral acceleration (generated from LA01~LA02) in Figure 3.10 and the design response spectrum (generated according to the current data in USGS, 2013) in Figure 3.13, it was found that an up scaling factor of 1.16 would be necessary for all ground motions to be compatible to current seismic hazard in downtown Los Angeles. The designed equivalent lateral force for the models is consistent with the design ground motion suite.

CHAPTER 4

GENERAL METHODS FOR PREDICTION OF SEISMIC DEMANDS

4.1 General Analysis Methods

There are four main analysis procedures have been developed to predict the values of various seismic response parameters when structures are subjected to earthquake ground motion which include linear static analysis, nonlinear static pushover analysis, nonlinear time history analysis and incremental dynamic analysis. The last three procedures are reviewed below including their advantages and disadvantages. In this thesis, only nonlinear static pushover analysis and nonlinear time history analysis procedures are employed.

4.1.1 Nonlinear Static Pushover Analysis

Nonlinear static pushover analysis (NSPA) is used to analyze a structure incorporating the nonlinear load-deformation characteristics of individual component under seismic events. In NSPA, the earthquake induced forces are represented approximately by equivalent static lateral forces. Then, these static lateral forces are applied increasingly at floor levels, in addition to permanent vertical loads, until the target displacement is reached or until instability occurs. The purposes of NSPA is to estimate the seismic demands imposed by design ground motion on structural systems and its components and comparing these demands to the available capacities at the interested level of

performances. The evaluation is based on an assessment of important performance parameters such as roof drift, interstory drift, inelastic element deformation as well as connection deformations (Krawinkler and Saraviratna, 1998).

An important issue in NSPA is target displacement. It is an estimate of the global displacement of the structure expected to experience in a design earthquake. The target displacement is usually measured by roof displacement at the center of mass of the structure. In NSPA, the roof displacement of the equivalent SDOF structure is transformed to the roof displacement of the actual MDOF structures through the use of a shape vector and transforming equation. A key assumption in NSPA is that the shape vector is assumed to remain constant regardless of the deformation levels through time history. Therefore, the reasonable results will be obtained only when the deformation responses of structures are mainly dependent on the first mode (FEMA-355C). When dealing with NSPA, the analysts should be aware that the structures might have strength and stiffness degradations including P-Δ effects which affect the force-displacement curve prediction or even lead to the dynamic instability of the structures. In order to account these effects and provide better predictions on the structures' performance, some modifications to the previous NSPA procedures has been made such as the adjustment of maximum displacement ratio, or the development a new coefficient to account for cyclic degradation in strength and stiffness (FEMA-440).

In addition to target displacement, the lateral load pattern also plays a critical role in evaluating seismic demand of structures in NSPA. It represents and bounds the distribution of inertia forces, or equivalent lateral force, in a design earthquake. The variation of inertia forces distribution due to the intensity of the earthquake as well as its

duration leads to the concerns about the accuracy of the responses of structures in the analysis when using only one invariant lateral loading pattern. Krawinkler and Seneviratna (1998) suggested that the results in one invariant pattern are likely to be reasonable when the structure responses are not severely affected by higher mode effects (or the first mode governs structures) and only one yielding mechanism is detected. Therefore, it is suggested to use multiple load patterns (uniform, triangular, SRSS patterns or a pattern from present code) to bound for the variation in the inertia force distribution. It allows analysts to understand more accurately about the structure's responses, and to capture different yielding patterns and any soft story mechanism. However, Krawinkler and Seneviratne (1998) also stated that using any of these invariant load patterns still can't account for the redistribution of inertia forces which might occur during strength or stiffness degrading. In order to have better results, it is suggested to have an adaptive load pattern which can change respectively with the time variant distribution of inertia force. One example of calculation of the distribution of inertia forces is shown below:

$$C_i = \frac{(w_x \times {h_x}^k)}{\sum_{i=1}^{n}(w_i \times {h_x}^k)} \quad (4.1)$$

in which i. and x represent the floor level, C_i is the distribution factor at i^{th} level; w_i is floor weight at the level i^{th} and h is the height from the base to the floor level i^{th} (ASCE Standard 7-10).

4.1.2 Nonlinear Time History Analysis

If nonlinear time history analysis (NTHA) is selected for seismic analysis of a building, the mathematical model directly incorporating the nonlinear load-deformation characteristics of individual components of the building will be subjected to a suite of ground motion time histories to obtain forces and displacements. Although the procedure for performing an NTHA is very similar to that of NSPA, response calculations in NTHA are carried differently. In NTHA, the design displacement is determined directly through dynamic analysis using ground motion time histories, not by using target displacement as in nonlinear static pushover analysis (ASCE Standard 41-06). However, structure's responses obtained from NTHA can be highly sensitive to characteristics of individual ground motion which requires the analysis to be carried out with more than one ground motion record. It suggested using minimum 3 to 7 ground motion records. If less than 7 ground motion records are used, the maximum demand in the sample might be used for the design. If 7 or more records are used, the maximum demand will be calculated as the average of maximum demands. In the present study, a set of total 60 ground motion records is used. Although NTHA requires much more numerical effort than NSPA, NTHA is capable of providing the results with lower uncertainties than that of NSPA because it takes into accounts higher mode effects and strength degradation including P-Δ effects.

4.1.3 Incremental Dynamic Analysis

Incremental dynamic analysis (IDA) is a sequence of nonlinear time history analyses. In IDA, the structural model is subjected to one or more ground motion record(s) in which

each record is scaled to different levels of intensity to predict more thoroughly structural performance under seismic events. Shome et al. (1998) demonstrated that scaling ground motion records to a target spectral acceleration is one of the most efficient ways to predict structural seismic demands under that particular intensity level. It is due to the fact that, in IDA, the structural performances are investigated from elasticity to yielding and finally collapse. Usually results from an IDA are represented by plots of Engineering Design Parameter (EDP) vs. Intensity Measure (IM). While the EDP can be measured by maximum interstory drift ratio, maximum drift ratio or base shear, the IM is usually measured by "first-mode" spectral acceleration, $S_a(T_1)$ and PGA. In IDA, the analysis will terminate at the point that the analysis doesn't not converge or the slope of the line drop by 20% of the initial slope, whichever comes first (Vamvatsikos and Cornell, 2002).

4.2 Engineering Demand Parameters and Earthquake Intensity Measures

An Engineering Demand Parameter (EDP) of a structure is a quantity that can be recorded from an analysis which is used to evaluate performances of the structure under static lateral forces or dynamic loadings. There are many possible choices for EDPs such as: roof drift ratio (RDR), interstory drift ratio (ISDR), floor accelerations, joint rotations, etc. Analysts can choose different EDPs depending on what type of analysis they are using and performance level they are interested in.

A ground motion Intensity Measure (IM) is a quantity that describes the "strength" of an earthquake ground motion. The main purpose of IM is to predict the response of a structure under an earthquake ground motion. Traditional IMs are Peak

Ground Acceleration (PGA) and Spectral Acceleration at the fundamental period of the structure (S_a). Luco and Cornell (2001) have suggested using S_a as an IM rather than using PGA because it provides smaller conditional dispersion by using the same set of ground motions. However, S_a also contains two shortcomings since it doesn't account for higher mode effects and the period elongation in the inelastic response range of structure. Furthermore, Padgett et al. (2008) have shown that the selection of PGA provides better results on the basis of increased efficiency and practicality, especially for recorded ground motions while $S_a(T_1)$ has slight advantages over PGA when synthetic motions are used.

In this study, the relationship between RDR and Base Shear (or Pushover Curve) will be plotted to assess the performance of the frames in NSPA. The results from NTHA are used to generate the relationship between IMs and median structural demands, EDPs for performance assessment purposes. The relationship between IMs and EDPs can be described by the following equation (Shome and Cornell, 1999):

$$EDP = m \times IM^n \times \varepsilon \tag{4.2}$$

where ε is a random variable with median = 1. For convenience, the variable, ε, is assumed to be constant at 1. The coefficient *m* and *n* can be determined by performing a linear regression analysis of *ln*(EDP) on *ln*(IM).

The efficiency of the relationship is determined using Equation 4.3. It measures the dispersion of demand from NTHA results about the estimated median demand.

$$\beta_{EDP|IM} = \sqrt{\sum \frac{(\ln(EDP_i) - \ln(m.IM^n))^2}{N-2}} \tag{4.3}$$

where EDP_i is the i^{th} realization of the demands from the NTHA and *N* is number of NTHAs performed. In this study, the Equation 4.3 is employed to determine whether

PGA or $S_a(T_1)$ is a more efficient IM for each frame model. In this study, Equation 4.3 is employed to determine whether PGA or $S_a(T_1)$ is a more efficient IM for each frame model.

4.3 Structural Performance Levels

Performance-based assessment of structures requires performance levels for both structural and nonstructural components to meet specified requirements with certain confidence. The performance levels are defined based on acceptance criteria which relate to allowable earthquake-induced forces and deformations for components of the structure. These levels are usually identified quantitatively in terms of EDPs such as drift ratio, permanent drift, brace displacement, joint rotation, etc. FEMA-273 and ASCE Standard 41-06 recommended four different levels of structural performance which are described below:

- Operational (O): This level indicates very light overall damage in structure. Structures have no permanent drift, retains original strength and stiffness. All systems required for normal operation are still functional. This refers that all structural components are still elastic range without any yielding.
- Immediate Occupancy (IO): This level allows very limited structural damage has occurred after the earthquake. The overall strength and stiffness of structures systems remain nearly the same to what they have before the earthquake. No permanent drift occurs. This level corresponds to approximately 0.7% interstory

or roof drift for steel braced frames according FEMA-273 or ASCE Standard 7-10.

- Life Safety (LS): It warns significant damage has occurred to the structure but some margin against either partial or total structural collapse remains. Some structural elements and components are severely damaged but haven't resulted in large falling debris. Many braces yield and connections may fail. FEMA-273 and ASCE Standard 41-06 recommended 1.5% drift or 0.5% permanent drift for steel braced frames for this level.
- Collapse Prevention (CP): The building is on the verge of experiencing partially collapse or totally collapse. Severe damages to the structure have occurred including degradation of strength and stiffness and large permanent lateral deformation such as extensive yielding in beams and columns, failure in braces or connections. For steel braced frames, extensive yielding and 2% drift or 2% permanent drift are set for the CP level (FEMA-273 and ASCE Standard 41-06).

Since BRBFs perform better than conventional steel braced frames if they are subjected to the same seismic loads, the performance levels for BRBFs are developed in Table 4.1. They are based on the FEMA-273 recommendations and recent results on BRBFs testing. Fahnestock (2007) showed that BRBFs with improved connection details can experience up to 4.8% story drifts before failures, which was much higher the drift limit for CP in FEMA-273, under maximum considered earthquakes (MCE). Table 4.2 also provides performance levels for SMA braces based on SMA mechanical properties, which were summarized in Table 3.4. All levels below are estimates rather than precise prediction of structure's performance. In general, the SMA braces used for hybrid BRB-

SMA frame systems are expected to remain intact during a seismic event so as to restore the building. Within a 6% strain limitation the superelastic SMA wires still provide recentering capacity with extremely small residual deformation for the self-centering SMA braces developed by Yang et al., 2010. However, when the demand strain exceeds a strain between 6-9%, the stress starts to increase sharply until about five times the forward transformation yield stress and then the wires suddenly break. This high strength of SMA is not taken into account in the design for the adjacent beams and columns. Therefore, if a SMA brace is stretched beyond 6% during an earthquake, the SMA brace will not break but the adjacent beams and columns will be damaged earlier than the SMA brace, leading to undesired collapse.

Table 4.1 Structural performance levels for BRBFs.

Performance Levels	Drift	Permanent Drift	Damage States
O	0.2%	0.05%	1st yielding of braces
IO	0.5%	0.15%	Minor yielding of braces
LS	2.5%	0.3%	Extensive yielding of braces
CP	4.5%	0.7%	Braces or connections fails

Table 4.2 Structural performance levels for SMA braces.

Performance Levels	Elongation	Damage States
O	1%	Yield strain, ε_y , of SMA
IO	2.5%	Major yielding of SMA braces
LS	4.5%	Superelastic strain length, ε_L , of SMA
CP	6%	Strain limit to prevent from second strain hardening

CHAPTER 5

SEISMIC PERFORMANCE ASSESSMENTS FOR MODEL FRAMES

5.1 General Analysis Procedures

The seismic behavior and performance of three model frames (model-1, model-2 and model-3) described in Chapter 3 are assessed based on the following procedures:

- Eigenvalue analyses are carried out to determined dynamic characteristics of the systems such as fundamental period, mode shapes and lateral loading patterns.
- NSPAs are to identify general characteristics of the systems such as overall ductility, yielding patterns, soft-story mechanisms.
- NTHAs are used to determine the system capacities and responses to a set of ground motions. Both global demands and local demands are inspected.

5.2 Eigenvalue Analysis for Model-1

From eigenvalue analysis, the periods of this model for the first three modes are 0.406s, 0.177s and 0.149s. The first three mode shapes are shown in Figure 5.1. The magnified-displacement shapes of the frame under three mode shapes are shown in Figure 5.2, 5.3 and 5.4.

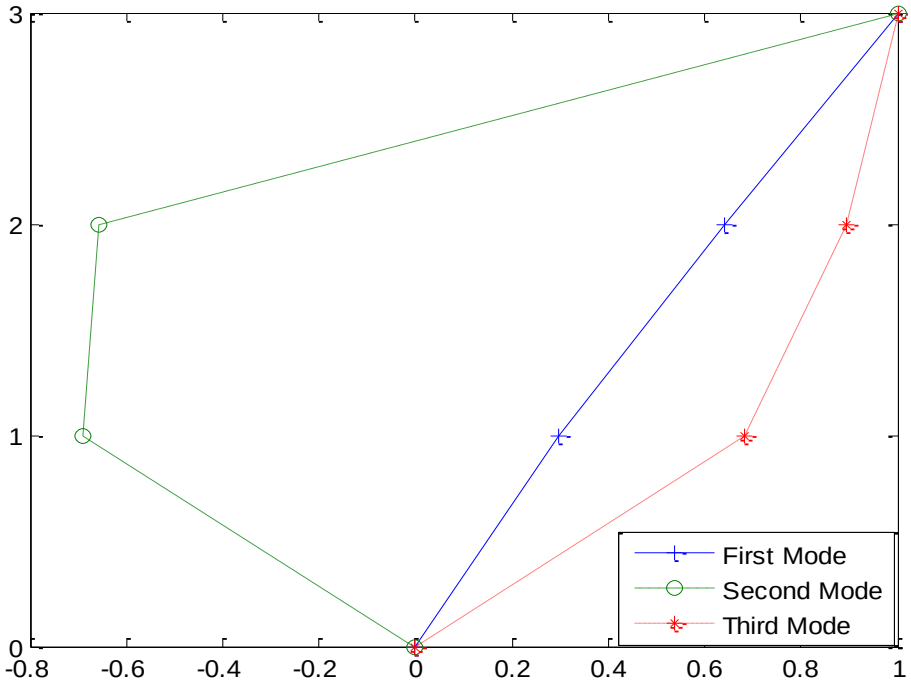

Figure 5.1 First three mode shapes for Model-1.

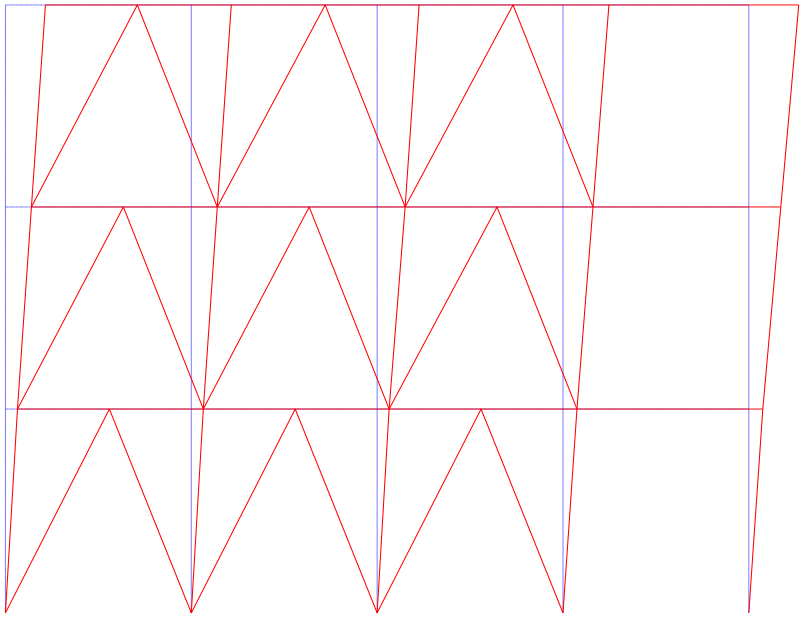

Figure 5.2 Magnified-displacement of Model-1 under the first mode.

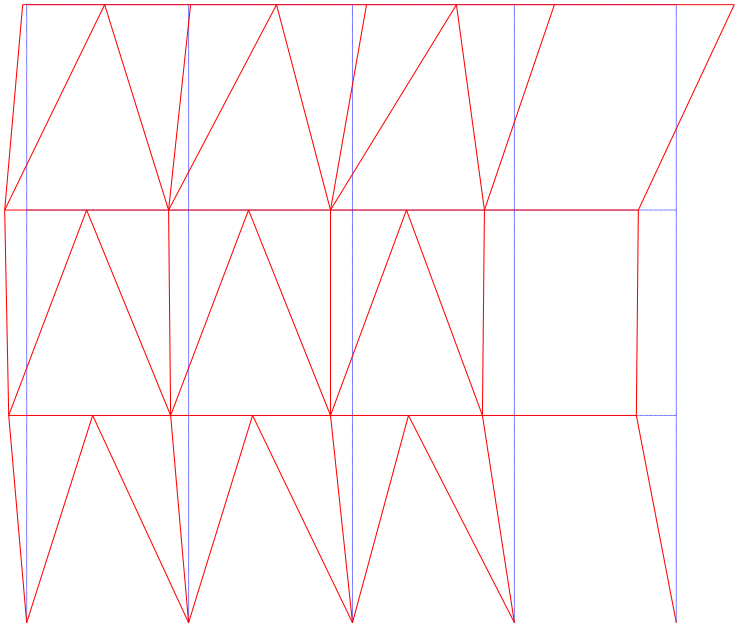

Figure 5.3: Magnified-displacement of Model-1 under the second mode.

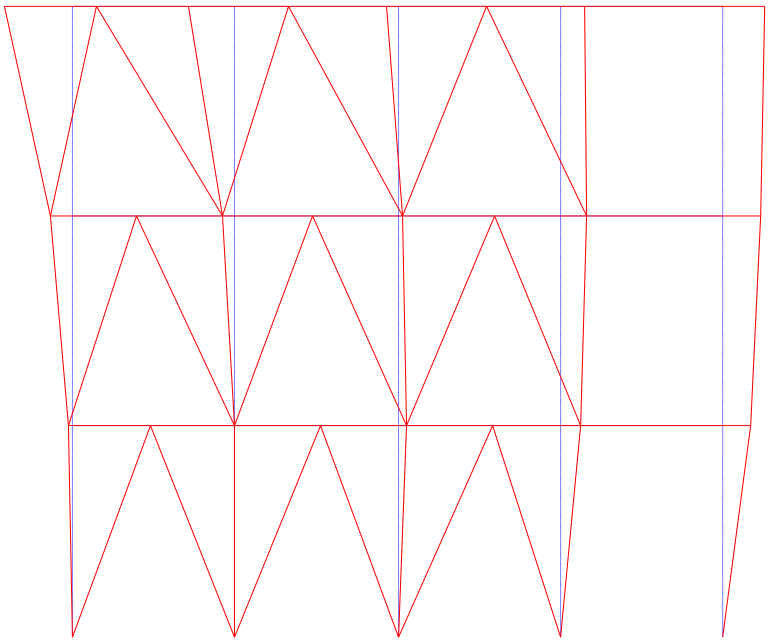

Figure 5.4: Magnified-displacement of Model-1 under the third mode.

5.2 Nonlinear Static Pushover Analysis for Model-1

Since the 1st mode was shown to be strongly dominant compared to other modes for Model-1 in eigenvalue analysis, the static behavior is assessed through NSPA employing only the 1st mode lateral loading pattern. The lateral loading pattern for first mode is summarized in Table 5.1. The model is pushed to the roof target displacement of 3.47% roof drift ratio (RDR) without losing any lateral strength; then, it is pulled back until the roof achieves zero displacement. The pushover curve plots roof drift ratio vs. base shear ass shown in Figure 5.5.

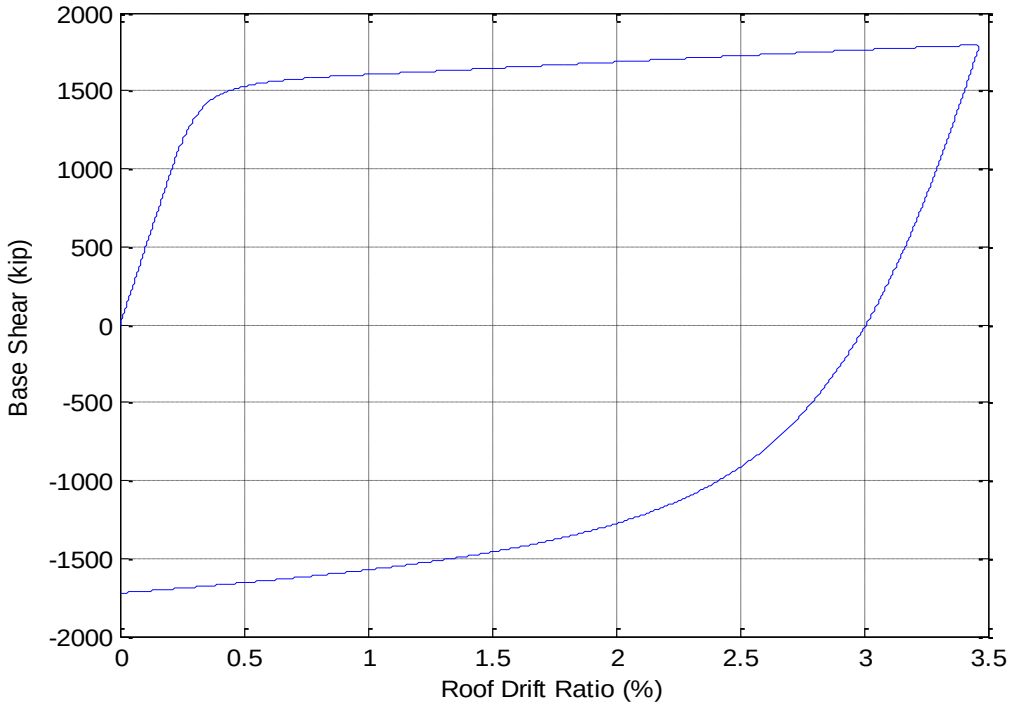

Figure 5.5 Pushover curve for Model-1 under the first mode lateral loading pattern.

Table 5.1 First mode lateral loading pattern for Model-1 under NSPA.

Story Level	First mode
3	0.990
2	0.611
1	0.301

The pushover curve indicates the sequence of yielding in Model-1. Compression yielding (CY) occurs in the right BRBs, followed by tension yielding (TY) in the left BRBs. Beams and columns remain elastic. CY occurs in the order from the 3rd to 2nd to 1st story. The yielding in compression braces starts at 0.24% (RDR) in the 3rd story and ends at 0.4% RDR in the 1st story. The TY starts right before CY finishes at 0.39% RDR and ends 0.71% RDR. TY occurs in the 2nd story, then in 3rd story and in 1st story at last. The Model-1 frame continues being pushed into hardening range and reaches the target RDR of 3.47%.

The base shear in Figure 5.5 at yield point is roughly 1500 kips which is greater than the total design base shear, 750 kips. The difference in strength is due to consideration of the expected yield strength of BRBs in the simulation. After the yield point, the base shear slowly increases to 1800 kips at target RDR. The permanent drift, a drift when the lateral loads are released until zero, is 3% RDR. The base shear is about -1700 kips when the frame is pulled back completely to zero RDR. The large residual RDR is due to yielding in the BRBs.

To determine the possibility of any soft-story mechanism, pushover curves for interstory drift ratios are plotted in Figure 5.6. The maximum ISDR which occurs in the roof and the 2nd story are 4.2% and 3.9% respectively. At that time, the 1st story has only

2.2% ISDR. Therefore, it can be stated that roof and the 2nd story are the most critical stories for NSPA. In a similar pattern, the roof level has the highest permanent deformation, followed by 2nd story, then 1st story.

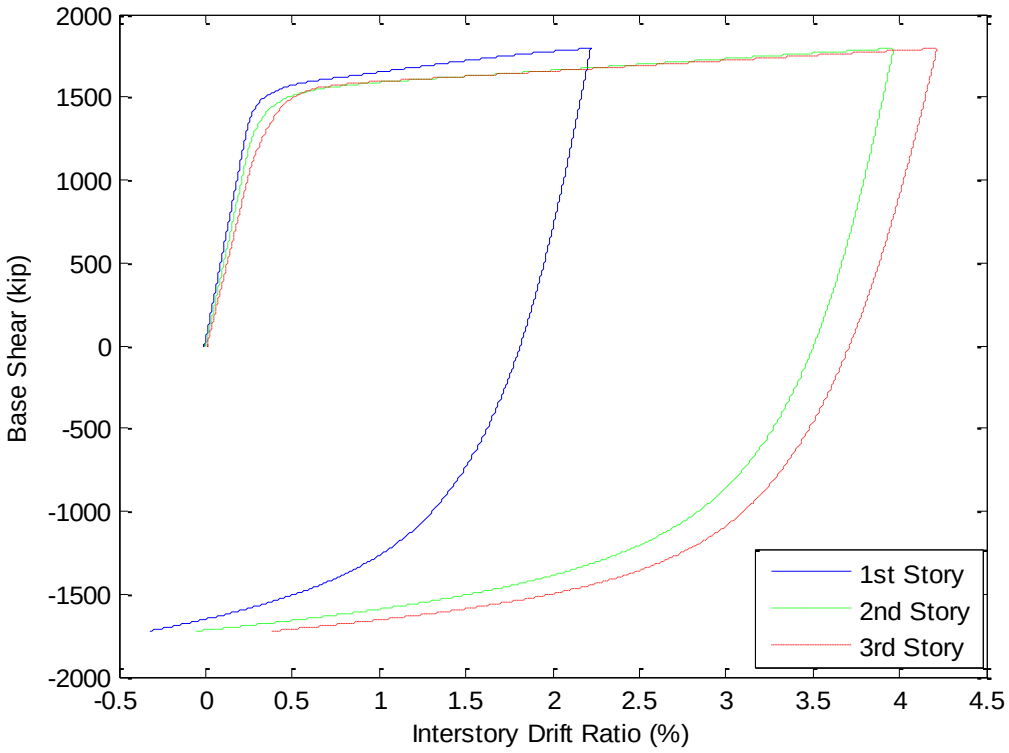

Figure 5.6 Interstory drifts for Model-1.

5.3 Nonlinear Time History Analysis for Model-1

The seismic demands on Model-1 are also examined using NTHAs with three suites of total 60 ground motions corresponding to a seismic hazard level of 2%, 10% and 50% probability of exceedance in 50 years. In order to interpret global responses of Model-1, maximum ISDRs vs. PGA and $S_a(T_1)$ curves are plotted in Figures 5.7 and 5.8,

respectively. Regression equations in the figure shows that the dispersion measure, $\beta_{D|IM}$, in the PGA plot is higher than that in $S_a(T_1)$ plot. Therefore, $S_a(T_1)$ is selected as IM for this model. The average of maximum ISDRs for all 60 ground motions is 0.8725%. The 2%/50yr suite produces an average of maximum ISDR equal to 1.4260%. The 10%/50yr suite and the 50%/50yr suite have the average maximum ISDRs of 0.7664% and 0.4252% respectively. This indicates that the maximum ISDRs are approximately linearly correlated with intensity measures.

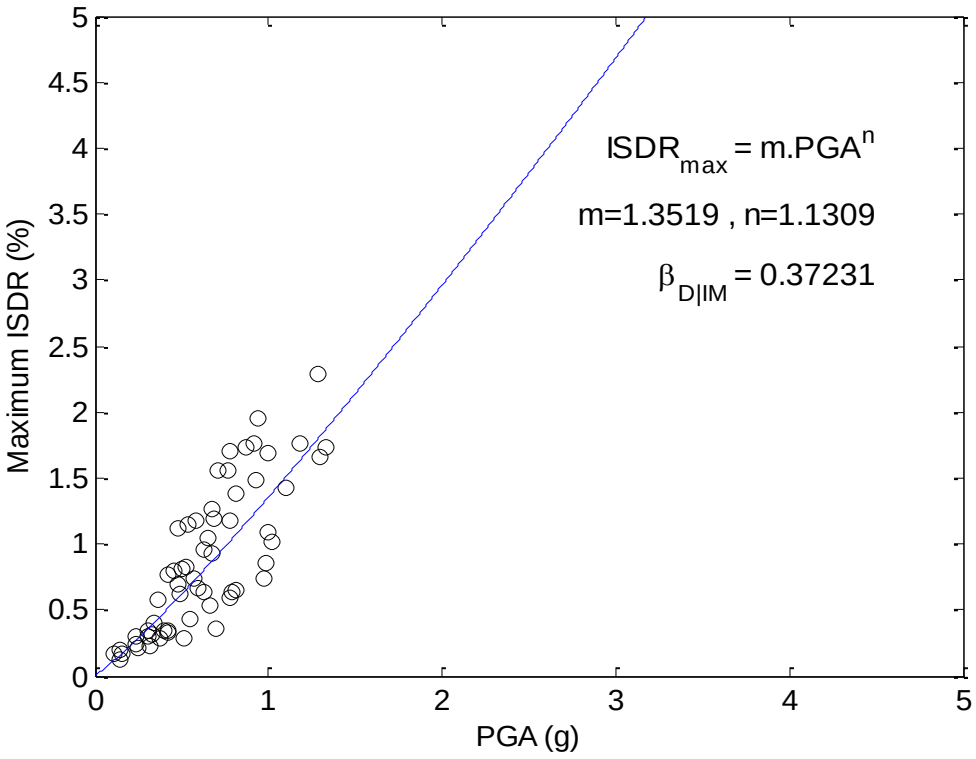

Figure 5.7 Relationship between maximum ISDR and PGA for Model-1.

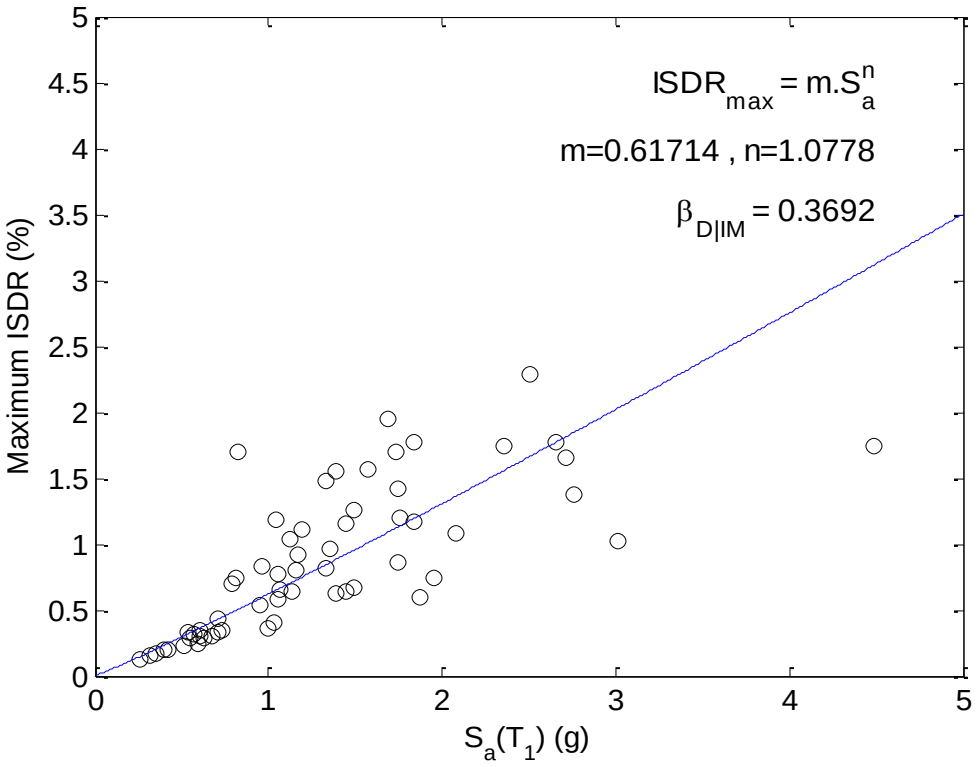

Figure 5.8 Relationship between maximum ISDR and $S_a(T_1)$ for Model-1.

The results of NTHAs for local demands are plotted as ISDR vs. $S_a(T_1)$ in Figures 5.9, 5.10 and 5.11 for the 1st to 3rd story, respectively. The 1st story ISDR and the 2nd story ISDR shows very similar responses with coefficients *m* and *n* are nearly equal for both stories. The 3rd story has smaller average change in ISDR for each unit change in $S_a(T_1)$ compared to that in the 1st and 2nd stories due to smaller values in the *m* and *n* coefficients. The maximum ISDRs for the 1st, 2nd and 3rd story are 2.288%, 2.257% and 1.871% respectively. These maximum ISDRs occur under the same LA21 ground motion which has 2% probability of exceedance in 50 years. The occurrences of maximum ISDR by story and the average of ISDRs are given in Table 5.2, which indicate that the maximum ISDRs tend to occur in the 1st story, especially when the intensity increases. It is due to column demands concentrate at the 1st story level. This finding is inconsistent

with the results of NSPA where the upper stories were identified as the most critical stories.

Table 5.2 Statistical data for ISDR by story for Model-1.

Story Level	Max ISDR/GM	Mean ISDR	Max ISDR occurrences (2% / 10% / 50% ground motions)
1	2.288%/LA21	0.853%	34 (18 / 14 / 2)
2	2.257%/LA21	0.833%	23 (2 / 6 / 15)
3	1.871%/LA21	0.598%	3 (0 / 0 / 3)

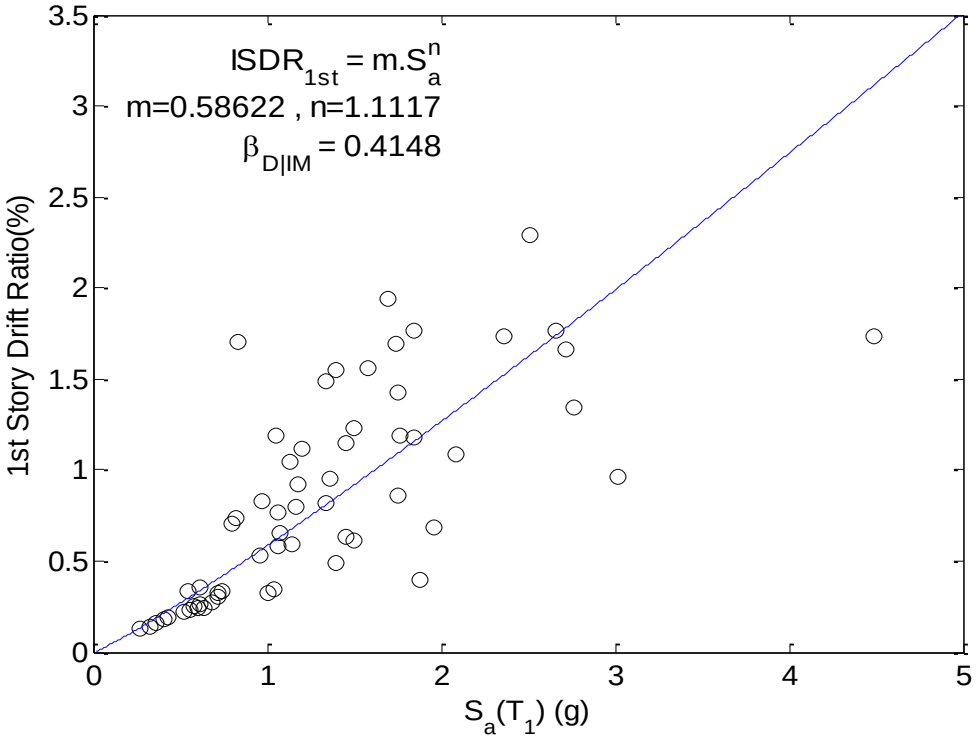

Figure 5.9 Relationship between the 1st interstory drift and $S_a(T_1)$ for Model-1.

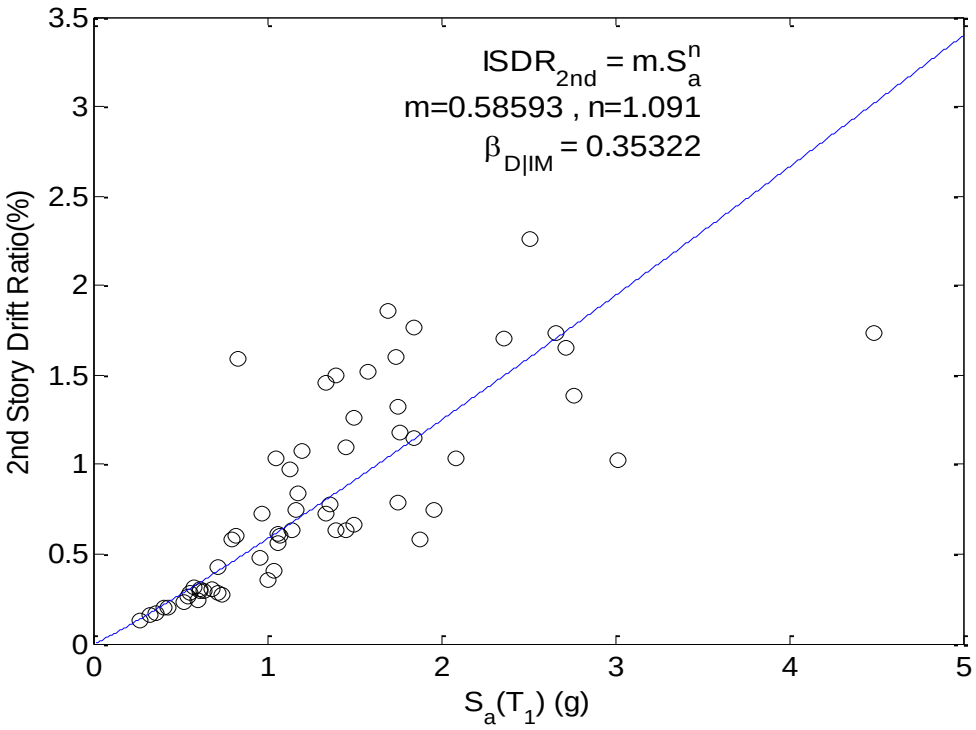

Figure 5.10 Relationship between the 2nd interstory drift and $S_a(T_1)$ for Model-1.

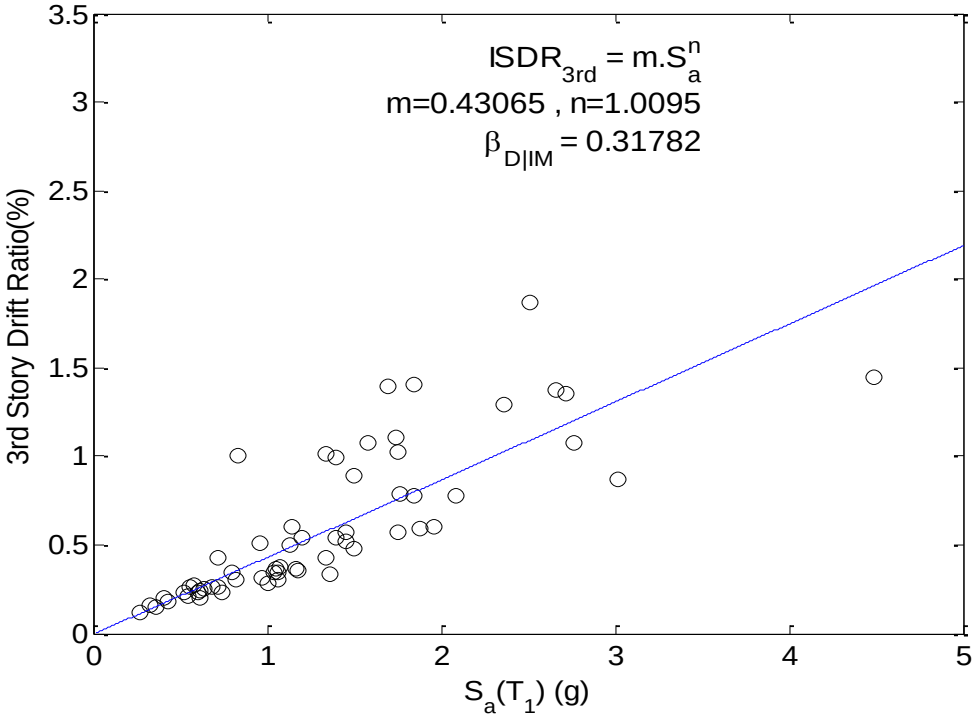

Figure 5.11 Relationship between the 3rd interstory drift and $S_a(T_1)$ for Model-1.

In order to check the effectiveness of SMA braces in the rehabilitated frame (Model-2) and the retrofitted frame (Model-3), permanent drift ratio (PDR) was also examined in both global and local levels. Figures 5.12 and 5.13 compare maximum PDR with respect to $S_a(T_1)$ and PGA. Similar to maximum ISDRs, under the same unit change, the average change in maximum PDR is larger for PGA than that for $S_a(T_1)$; However, the discrepancy between two curves is narrowed. This is because the difference in values of coefficient *m* is now small. The larger coefficient, $\beta_{D|IM}$, in the PGA plot indicates PGA produces more dispersion in median PDRs than $S_a(T_1)$. The average maximum PDR for all 60 ground motions is 0.202%. The average maximum PDRs classified by seismic hazard levels of 2%/50yr, 10%/50yr and 50%/50yr ground motion suites are 0.372%, 0.156% and 0.077%, respectively. It indicates that maximum PDR increases when the ground motion intensity increases.

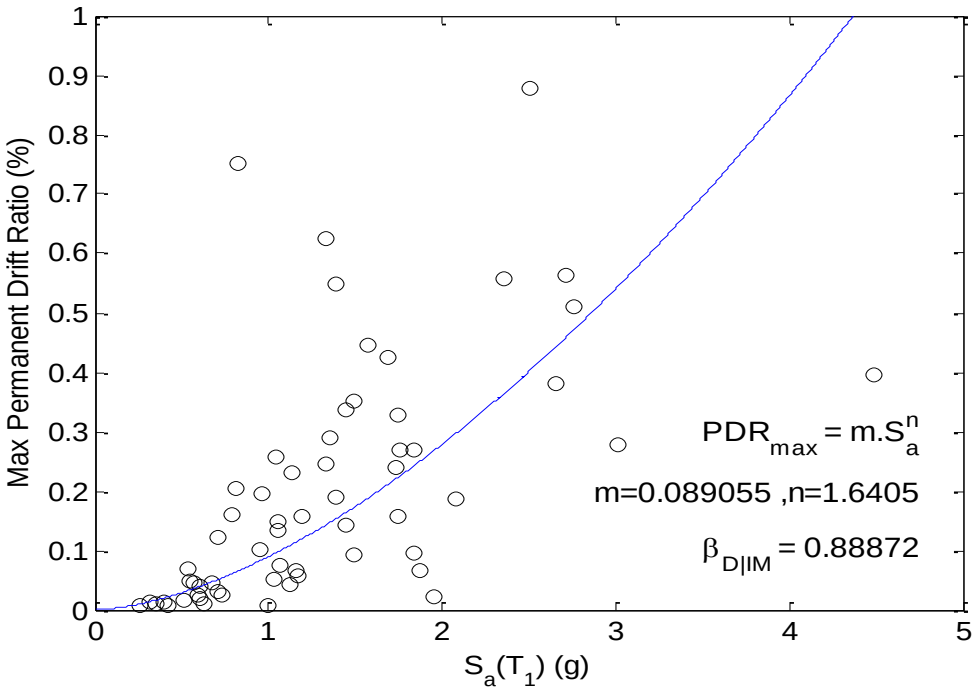

Figure 5.12 Relationship between maximum PDR and $S_a(T_1)$ for Model-1.

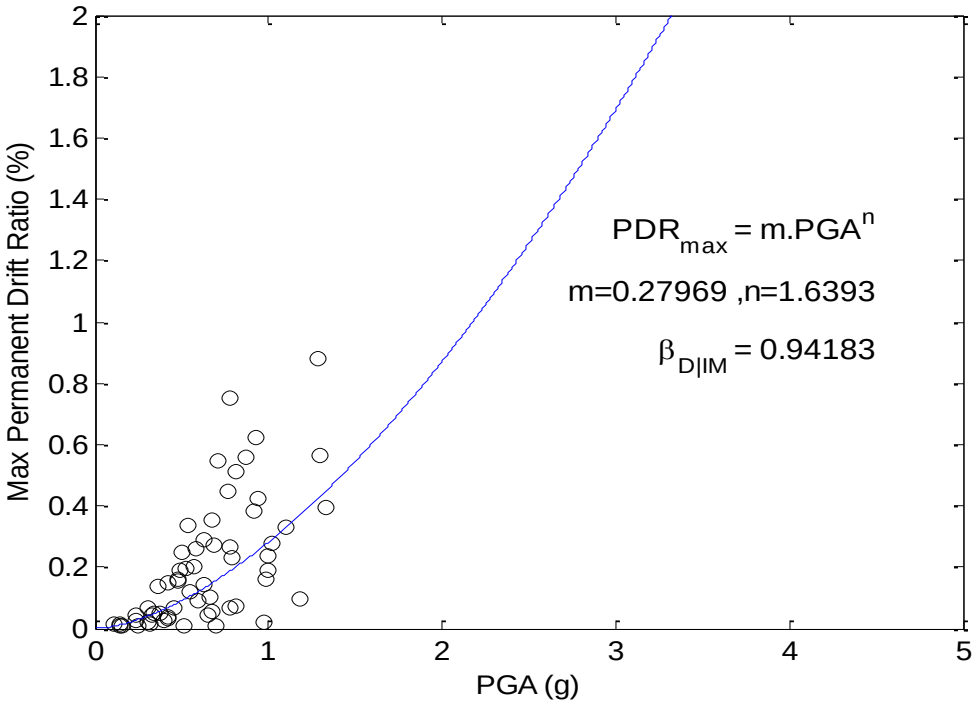

Figure 5.13: Relationship between maximum PDR and PGA for Model-1

The PDRs with respect to $S_a(T_1)$ for the 1st, 2nd and 3rd story are shown in Figure 5.14, 5.15 and 5.16 respectively. The trend of PDR responses in three stories is opposite to that of ISDR responses; that is, the 3rd story has highest maximum PDR, followed by the 2nd story, and followed by the 1st story. The maximum PDRs for the 1st, 2nd and 3rd story are 0.7471%, 0.8336% and 0.877% respectively. All these maximum cases occurred in the LA21 ground motion. Table 5.3 shows that the 2nd story has the largest number of occurrences of maximum DPR as well as the highest average DPR among three stories. This indicates that the maximum PDR tends to occur in the 2nd story; especially when the intensity increases.

Table 5.3 Statistical data for PDR by story for Model-1.

Story Level	Max PDR/GM	Mean PDR	Max PDR occurrences (2% / 10% / 50% ground motions)
1	0.747% / LA21	0.162%	19 (4 / 8 / 7)
2	0.834% / LA21	0.186%	23 (9 / 8 / 6)
3	0.878% / LA21	0.149%	18 (7 / 4 / 7)

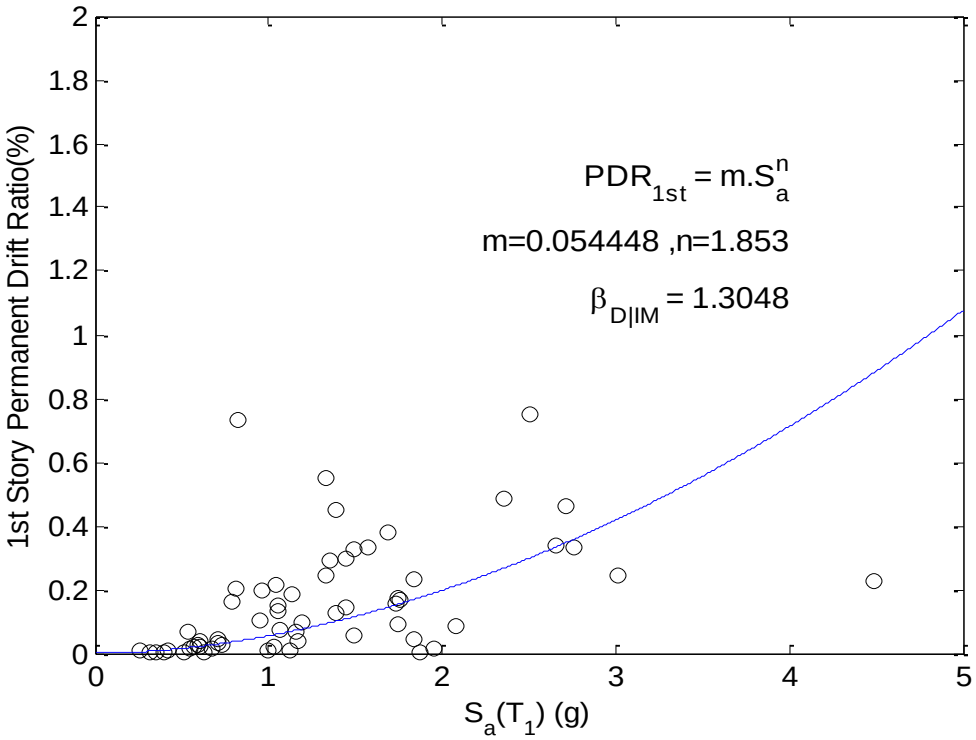

Figure 5.14 Relationship between the 1st interstory PDR and $S_a(T_1)$ for Model-1.

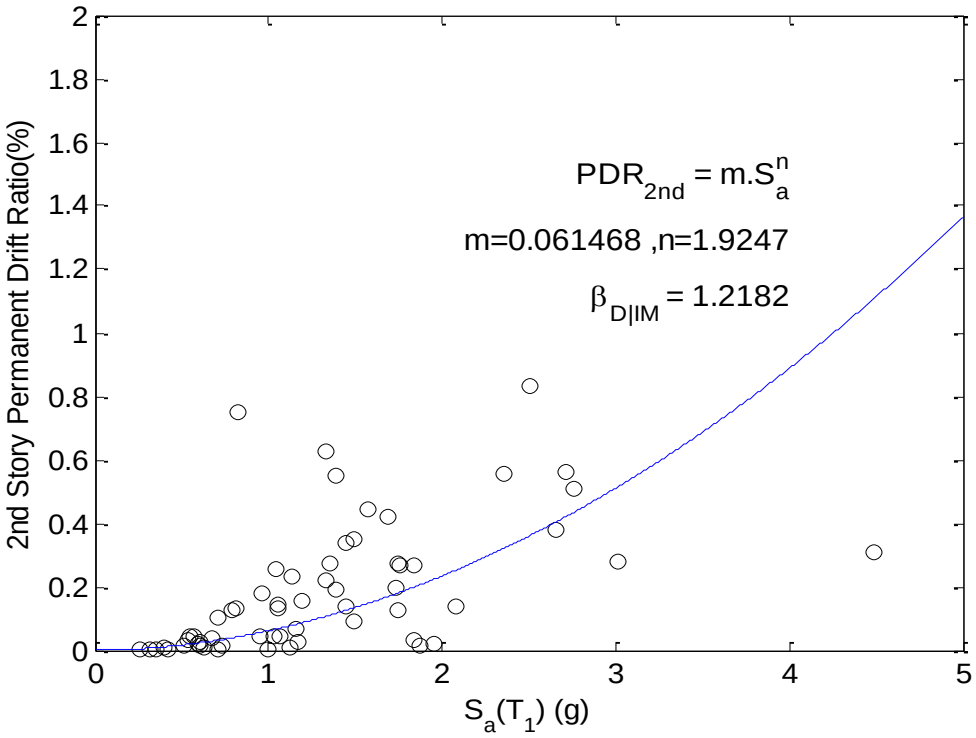

Figure 5.15 Relationship between the 2nd interstory PDR and $S_a(T_1)$ for Model-1.

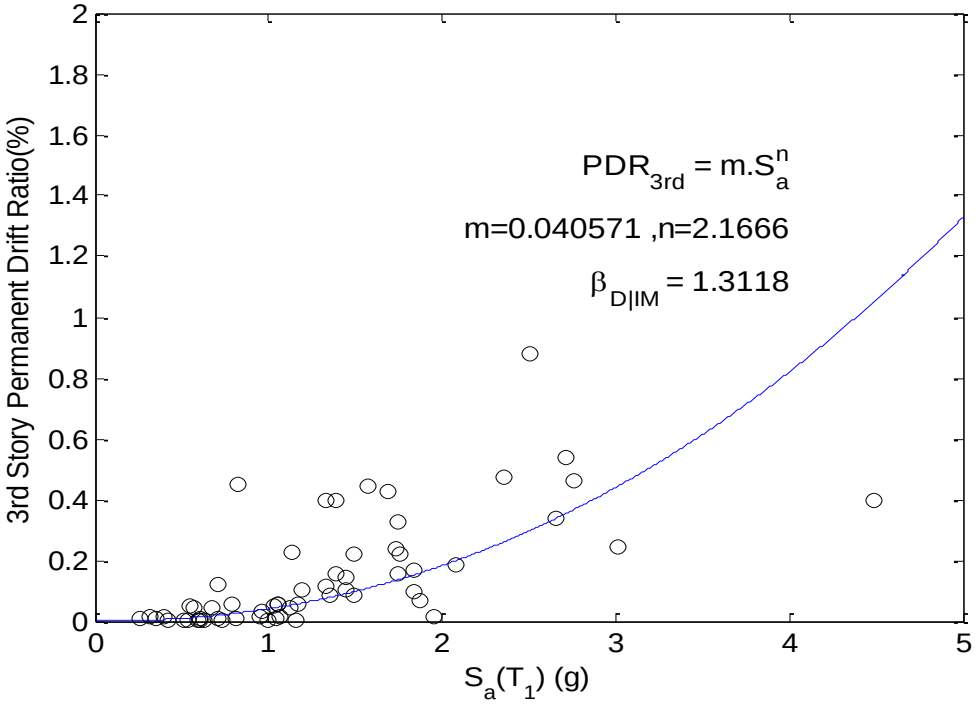

Figure 5.16 Relationship between the 3rd story PDR and $S_a(T_1)$ for Model-1.

5.5 Eigenvalue Analysis for Model-2

The 1st, 2nd and 3rd mode periods of this structure are 0.328s, 0.143s and 0.127s respectively. The fact that Model-2 has smaller periods compared with the periods of Model-1 indicates Model-2 is stiffer. This is reasonable because this rehabilitated frame has been added SMA braces in the fourth bay. The first three mode shapes are shown in Figure 5.17. The magnified-displacement shapes of the frame for the first three mode shapes are shown in Figure 5.18, 5.19 and 5.20.

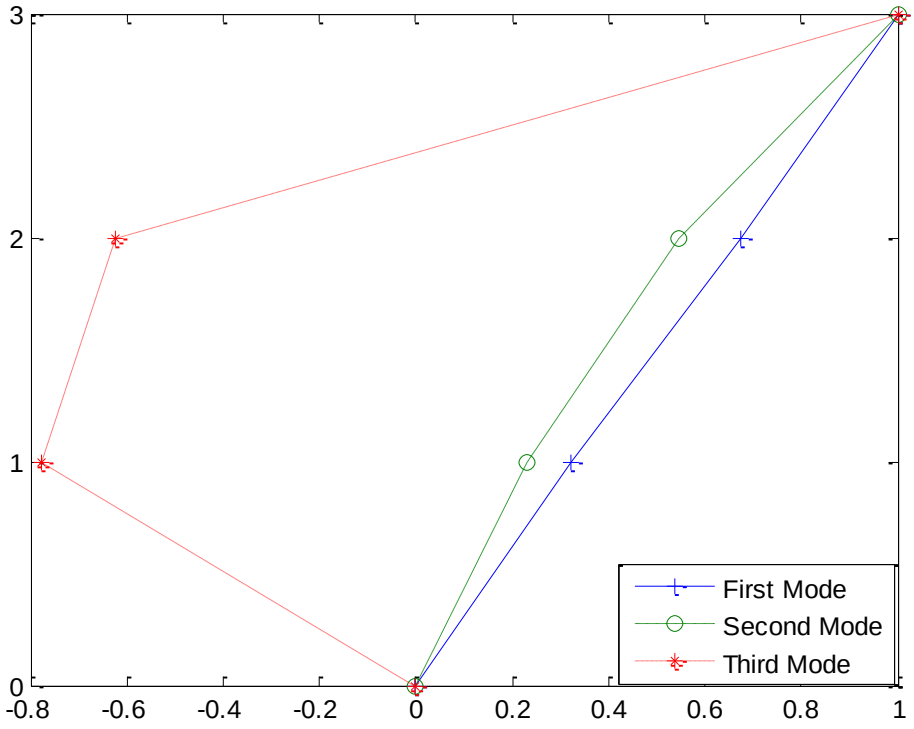

Figure 5.17 First three mode shapes for Model-2.

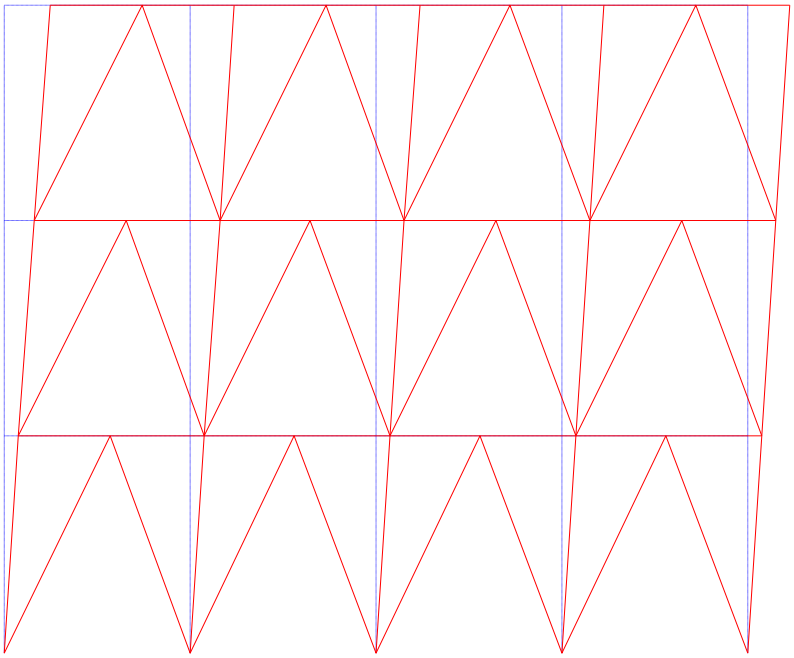

Figure 5.18 Magnified-displacement of Model-2 under the first mode.

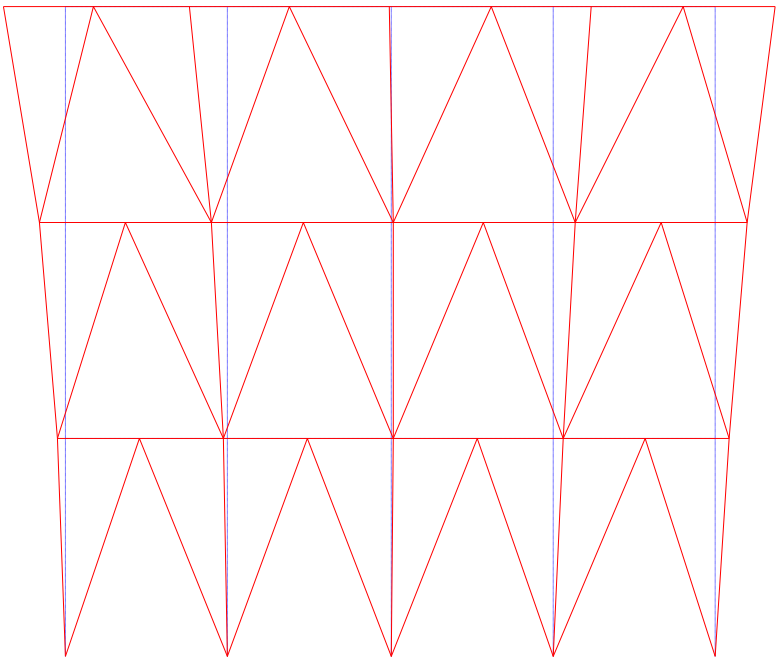

Figure 5.19 Magnified-displacement of Model-2 under the second mode.

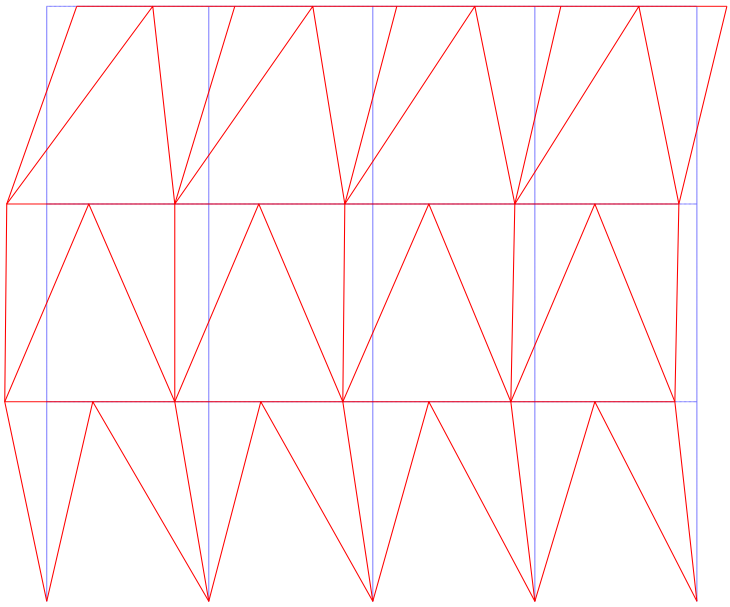

Figure 5.20 Magnified-displacement of Model-2 under the third mode.

5.6 Nonlinear Static Pushover Analysis for Model-2

The static behavior of Model-2 was assessed using NSPA under the first mode of structure. The lateral loading pattern for the first mode is summarized in Table 5.4, which is very similar with that in Model-1. With the same procedure, the model is pushed slowly to the same target RDR of 3.47%; then, it is pulled back until roof displacement equals zero. Comparison of pushover curves for Model-1 and Model-2 is shown in Figure 5.21.

Table 5.4 First mode lateral loading pattern for Model-2 under NSPA.

Story Level	First mode
3	0.990
2	0.6061
1	0.2892

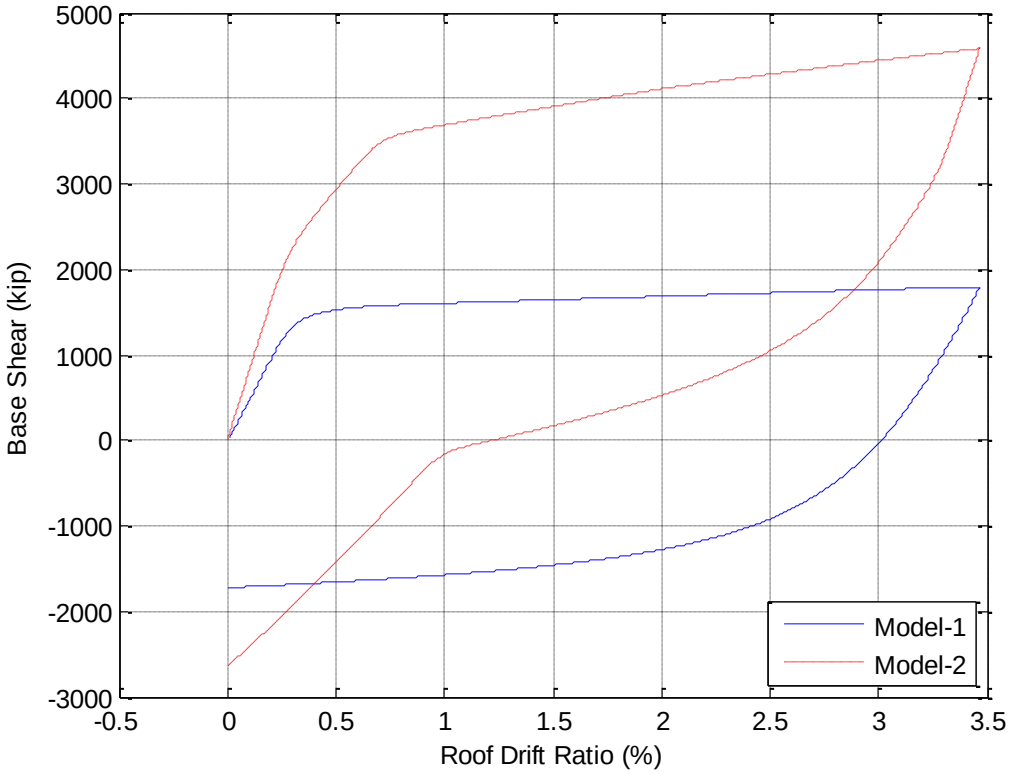

Figure 5.21 Comparison of pushover curves between Model-1 and Model-2

The first CY in the right BRBs starts at 0.15% RDR and the last CY in the right BRBs occurs at 0.23% RDR. TY in the left BRBs begins right after the last CY at 0.24% RDR and ends at 0.42% RDR. CY and TY occurrences start from the 2nd to 3rd story then to 1st story. The first CY in the left SMA braces occurs at 0.57% RDR and the last one occurs at 0.68% RDR. The first TY in the left SMA braces occurs at 0.61% RDR while the last TY of SMA is at 0.8% RDR. Overall, the time for all braces to yield is from 0.15% RDR to 0.8% RDR. Exterior column base in the SMA bay yields at 0.5% RDR.

Until 2.62% RDR, all column bases have yielded and in the order from the right exterior column to the left exterior column. Beams still remain elastic but right at the border.

Figure 5.21 shows the overstrength factor (Ω_o) for Model-2 is about 2.6 (4580/1750 = 2.6) at the target RDR. It is important to note that unlike the Model-1 with 3.1% permanent RDR, Model-2 has a much smaller deformation of 1.2% RDR in Figure 5.21. Although the permanent deformation in Model-2 is substantially reduced, the permanent deformation would have been reduced more if the column size could be increased to reduce the degree of yielding in the column bases.

To determine the possibility of any soft-story mechanism, pushover curves for interstory drift ratios are plotted against base shear as shown in Figure 5.22. The 2nd story has the highest 4.0% ISDR. At the same time, ISDRs for the 3rd story and 1st story are 3.6% and 2.8% respectively. It indicates that the 2nd story is the weakest one under NSPA. No soft-story mechanism occurs in this frame. With respect to residual deformation, the roof and 2nd story have 1.4% residual ISDR while the 1st story has a 0.8% residual ISDR.

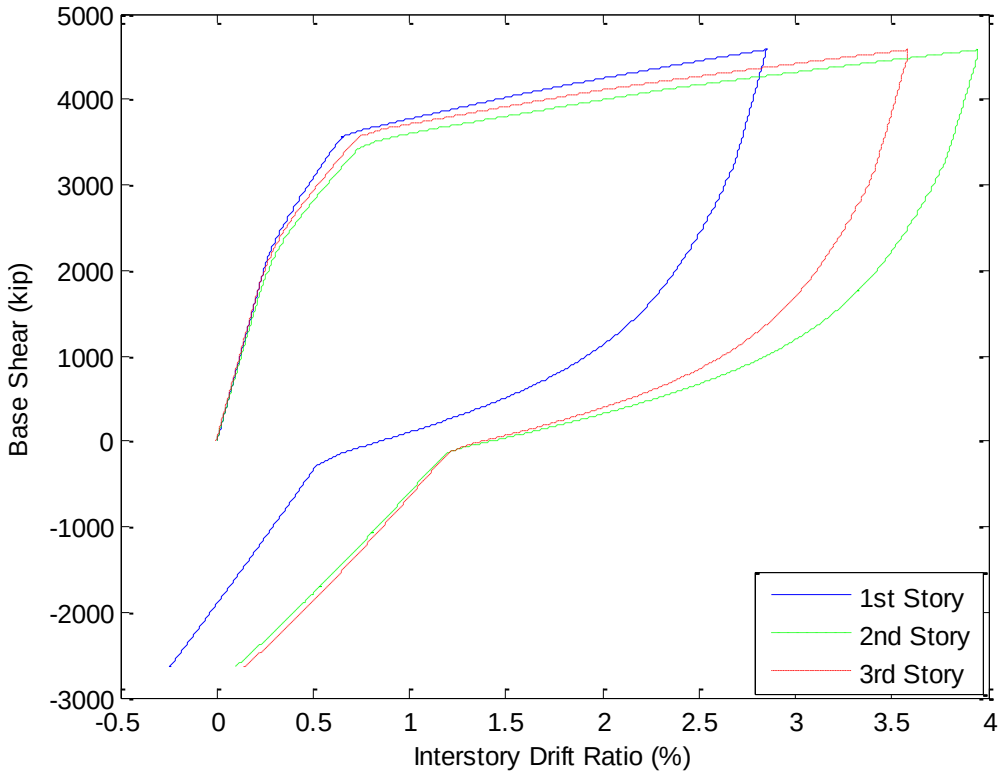

Figure 5.22 Interstory drifts for Model-2.

5.7 Nonlinear Time History Analysis for Model-2

From the results from NTHA, Model-2 produces an average of 0.567% maximum ISDRs while it was 0.873% in Model-1. Comparison of Model-1 and Model-2 is summarized in Table 5.5. Similar to Model-1, Model-2 has shown a linear relationship between the maximum ISDRs and intensity of ground motions. Table 5.5 indicates Model-2 has smaller values in term of maximum ISDRs in all categories. It is attributed to the presence of SMA, which made Model-2 stiffer compared to Model-1. Also, the average maximum ISDR is reduced 52% for the 2%/50yr ground motion suite while it is reduced only 34% and 16% for the 10%/50yr and 50%/50yr ground motion suites. Figure 5.24

indicates that reduction in ISDRs becomes larger as the intensity of GM increases. It means that the effect of rehabilitation on seismic demand is substantial.

Table 5.5 Statistical data for maximum ISDR for Model-1 and Mode-2.

Frame	Mean	Mean of 2%/50yr suite	Mean of 10%/50yr suite	Mean of 50%/50yr GM suite
Model-1	0.873%	1.426%	0.766%	0.425%
Model-2	0.567%	0.833%	0.502%	0.356%

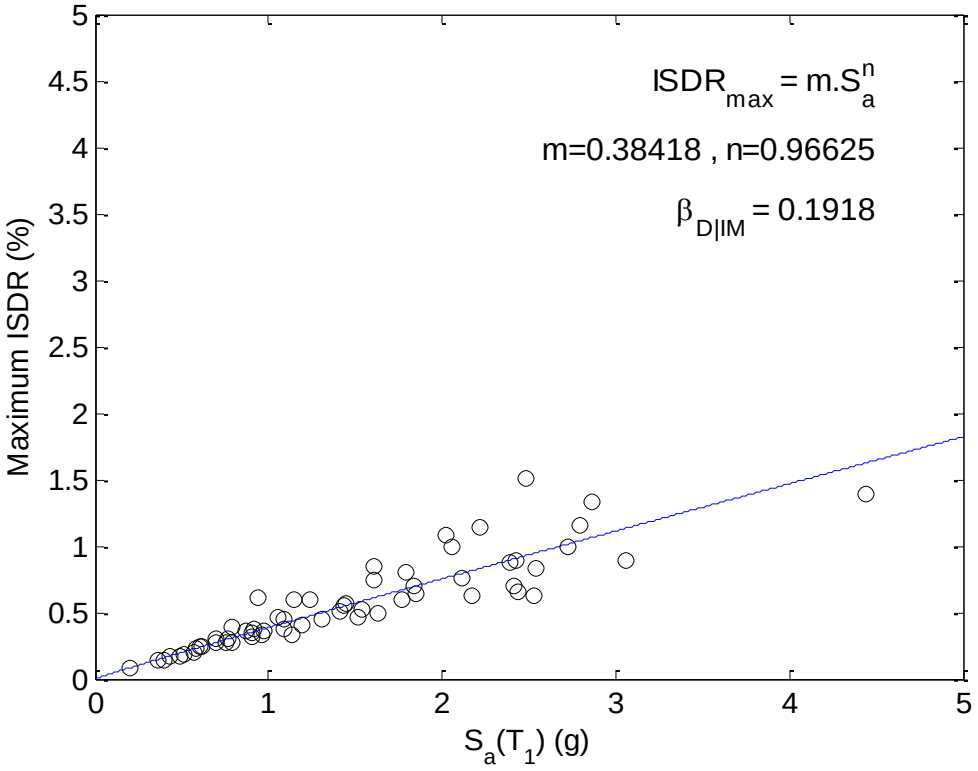

Figure 5.23 Relationship between maximum ISDR and $S_a(T_1)$ for Model-2.

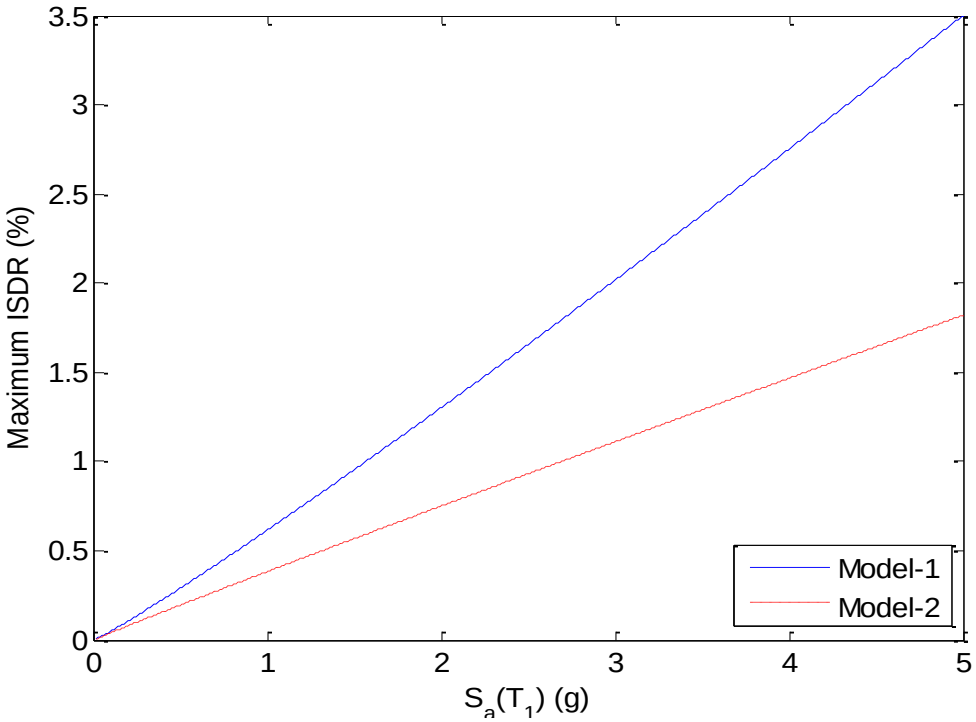

Figure 5.24 Comparison of global seismic demand relationships for Model-1 and Model-2.

Seismic demands at the local levels are also examined, as shown Figure 5.25, 5.26 and 5.27. The results show that the 1st and 2nd stories have similar demands while the 3rd story has slightly smaller demand on ISDR. Statistical data of interstory drift ratios is summarized in Table 5.6. The data follows the same trend as the as-built model; the 1st story has the highest values in all categories, then followed by the 2nd story and then the 3rd story. Out of 20 2%/50yr ground motion, the maximum ISDR occurred in the 1st story 17 times. It indicates when the intensity increases, the 1st story tends to be the most critical one.

Table 5.6 Statistical data of ISDR by story for Model-2.

Story Level	Max ISDR/GM	Mean ISDR	Max ISDR occurrences (2% / 10% / 50% ground motions)
1	1.510%/LA21	0.544%	31 (17 / 6 / 8)
2	1.383%/LA28	0.525%	18 (3 / 9 / 6)
3	1.267%/LA28	0.442%	11(0 / 5 / 6)

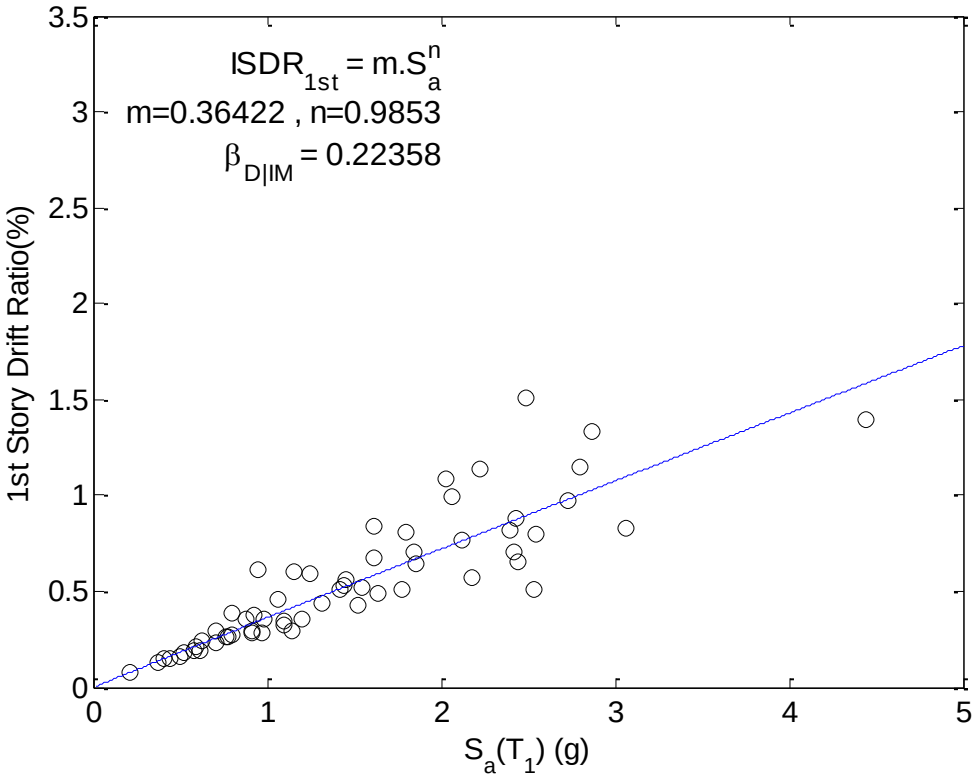

Figure 5.25 Relationship between the 1st interstory drift and $S_a(T_1)$ for Model-2.

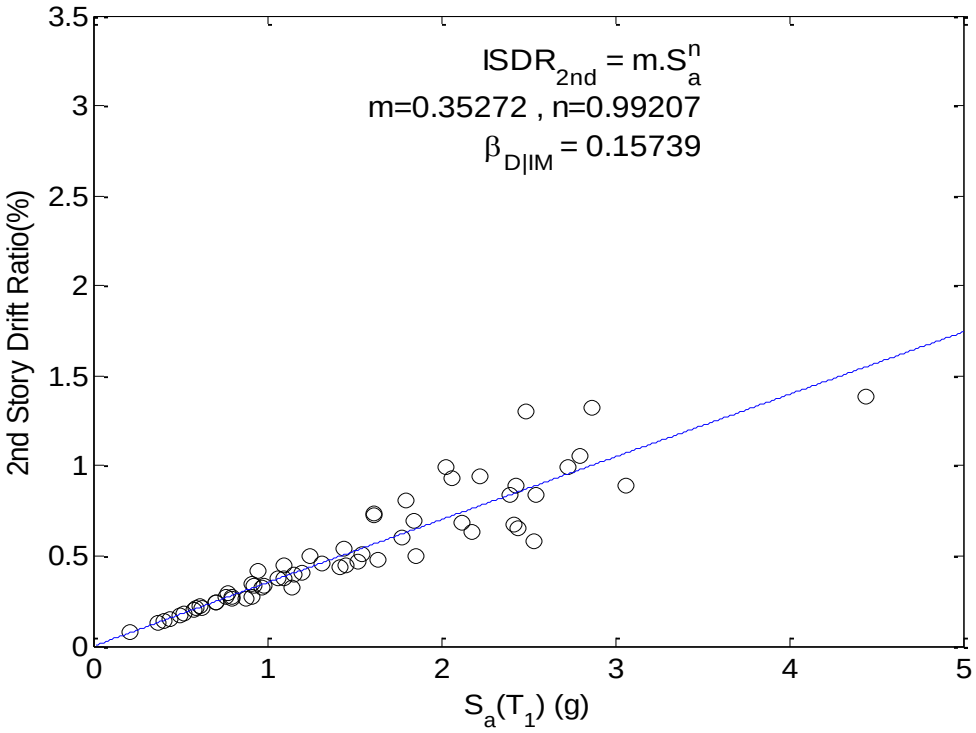

Figure 5.26 Relationship between the 2nd interstory drift and $S_a(T_1)$ for Model-2.

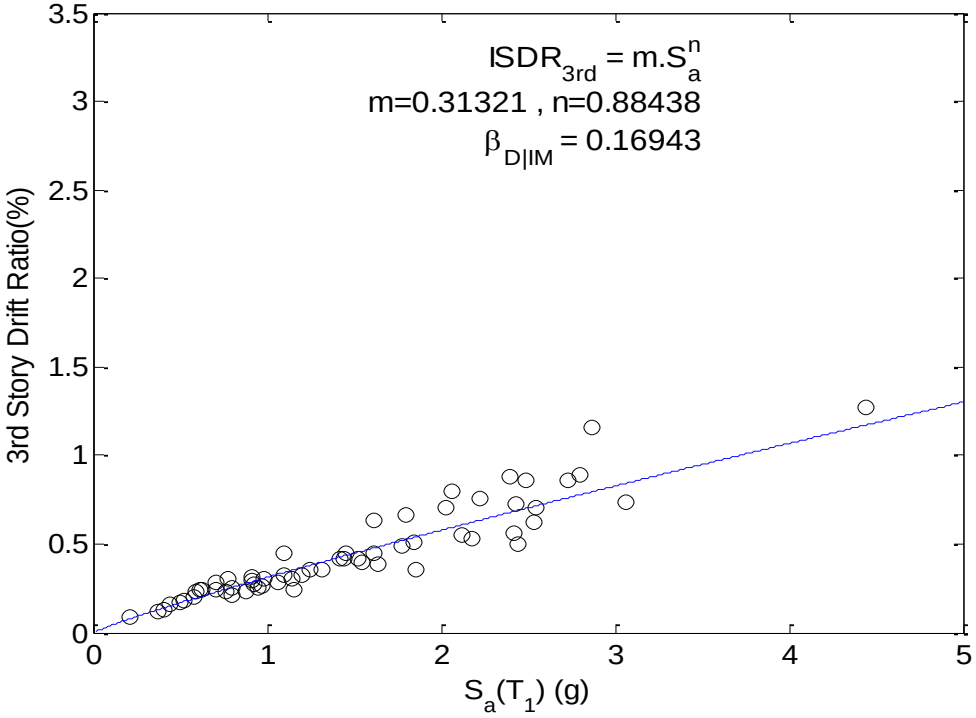

Figure 5.27 Relationship between the 3rd interstory drift and $S_a(T_1)$ for Model-2.

Permanent deformation was also examined in both global and local levels. The relationship between maximum permanent drift ratio and ground motion intensity for Model-2 is shown in Figure 5.28. Figure 5.29 compares that relationship for both Model-2 and Model-1. It can be seen that Model-2 has much lower permanent deformation than Model-1 and the effectiveness in permanent deformation increases as the ground motion intensity increases. The maximum PDR for 2%/50yr suite, 10%/50yr suite and 50%/50yr suite are 0.1149%, 0.1144% and 0.075% respectively. Table 5.7 states that Model-2 has a mean of maximum PDR of 0.044% compared to 0.202% in Model-1. The reduction is more than 78% ((0.202-0.044)/0.202 = 78.3%) meaning that adding additional SMA braced bay is significantly effective on reducing permanent deformation.

The comparison of permanent deformation by story between two models is summarized in Table 5.8. It shows that the maximum permanent deformation tends to occur in the 2nd story in Model-1, while tending to occur in the 1st story for Model-2. The 2nd story of Model-2 has maximum PDR of 1.114% under the LA12 record while the max PDR for that story in Model-1 occurs under the LA21 record. It means a more intensive earthquake isn't necessary to create larger residual deformation in a particular story.

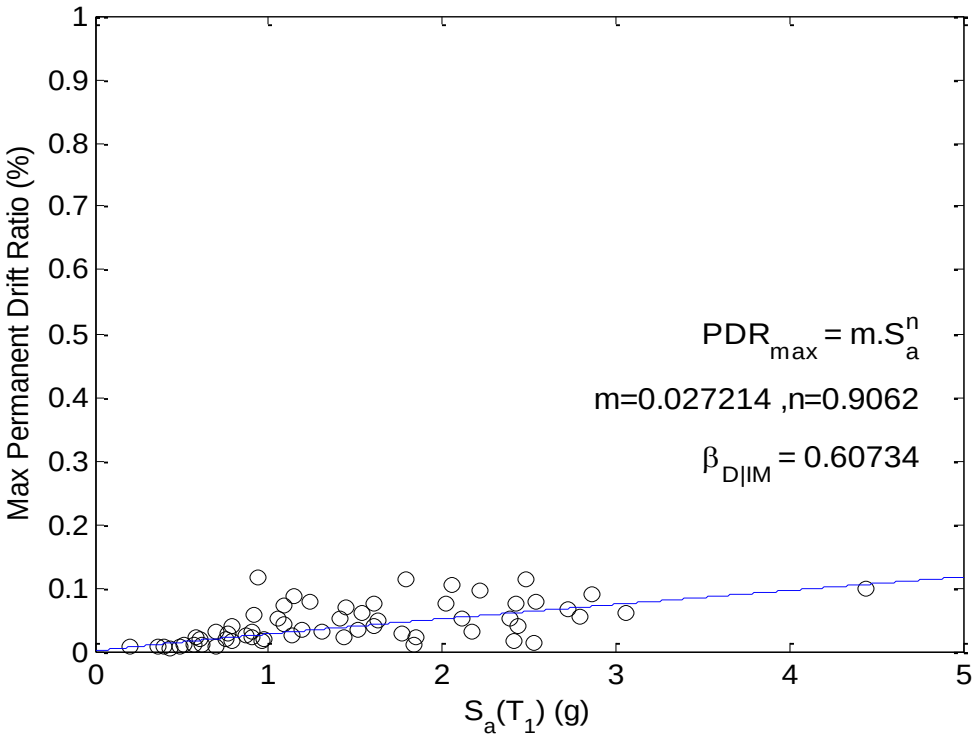

Figure 5.28 Relationship between maximum PDR and $S_a(T_1)$ for Model-2.

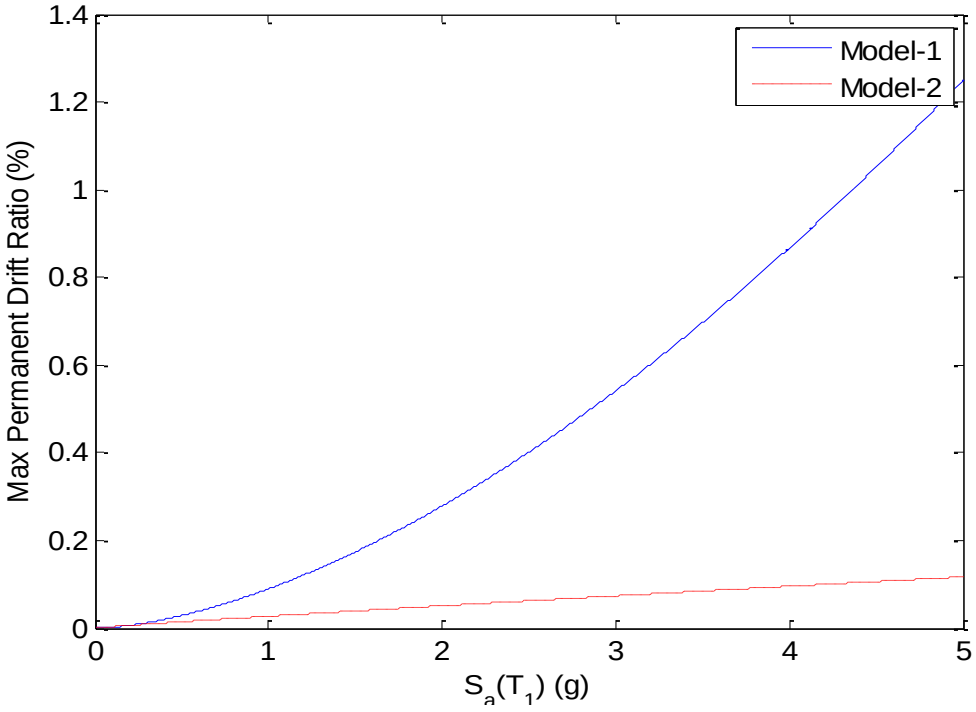

Figure 5.29 Comparison of maximum PDR for Model-1 and Model-2.

Table 5.7 Statistical data for maximum PDR for Model-1 and Model-2.

Frame	Mean	Mean of 2%/50yr suite	Mean of 10%/50yr suite	Mean of 50%/50yr GM suite
Model-1	0.202%	0.372%	0.156%	0.077%
Model-2	0.044%	0.064%	0.041%	0.027%

Table 5.8 Statistical data of permanent drift by story for Model-2 and Model-1.

Story	Model	Max PDR/GM	Mean PDR	Max PDR occurrences
1	2	0.115%/LA38	0.034%	26
	1	0.747%/LA21	0.162%	19
2	2	0.114%/LA12	0.031%	15
	1	0.834%/LA21	0.186%	23
3	2	0.099%/LA36	0.028%	19
	1	0.878%/LA21	0.149%	18

Seismic demand on SMA braces is shown in Figure 5.30. It shows that all the data points are less than 6% strain limit, indicating that the design of SMA braces are designed satisfactory. The maximum strain demand of the SMA brace is 2.48%. The SMA braces have mean of maximum strain demands of 1.21%, 0.67% and 0.48% for the 2%/50yr, 10%/50yr and 50%/50yr respectively. It indicates that demands in SMA braces increase as the intensity of ground motion increases.

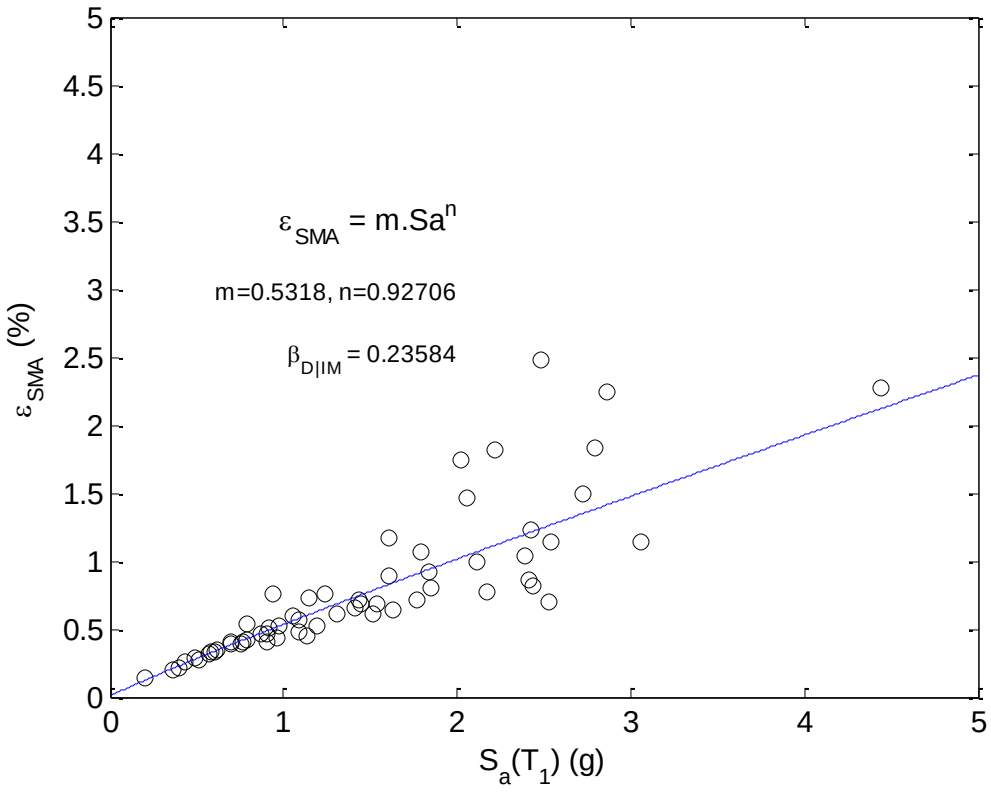

Figure 5.30 Relationship between SMA strain and $S_a(T_1)$ for Model-2.

5.8 Eigenvalue Analysis for Model-3

This retrofitted frame, Model-3 has 1st, 2nd and 3rd mode periods equal to 0.458s, 0.182s and 0.149s, respectively. It has the highest period among three models which, is a little softer than the as-built model. All braces have been redesigned based on seismic-induced lateral load from the as-built model. The first three mode shapes are shown in Figure 5.31. The magnified-displacement shapes of the frame for the first three mode shapes are shown in Figure 5.32, 5.33 and 5.34.

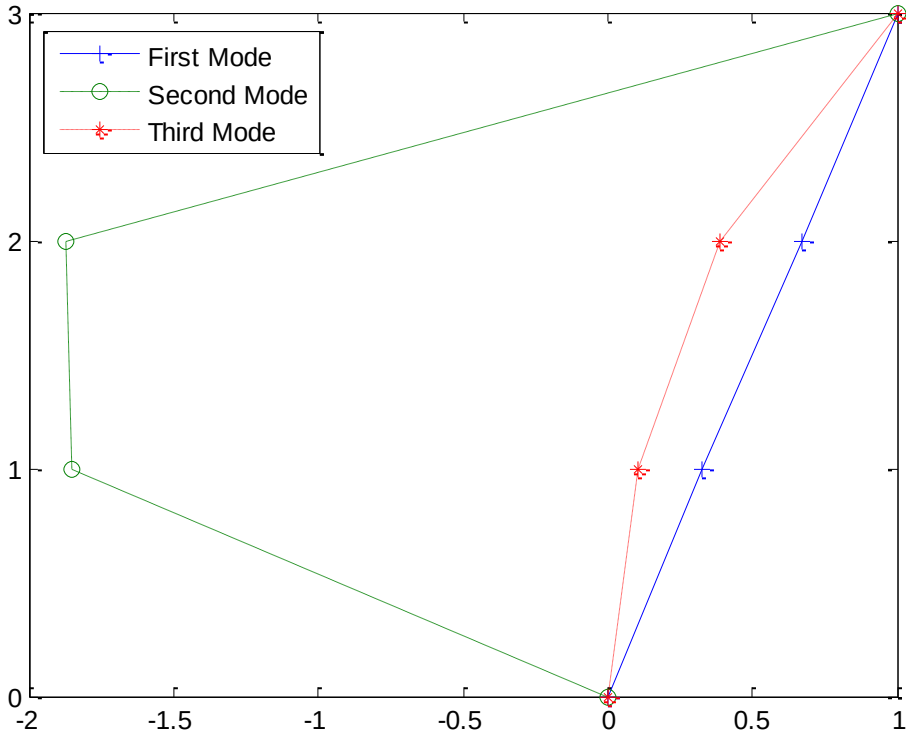

Figure 5.31 First three mode shapes for Model-3.

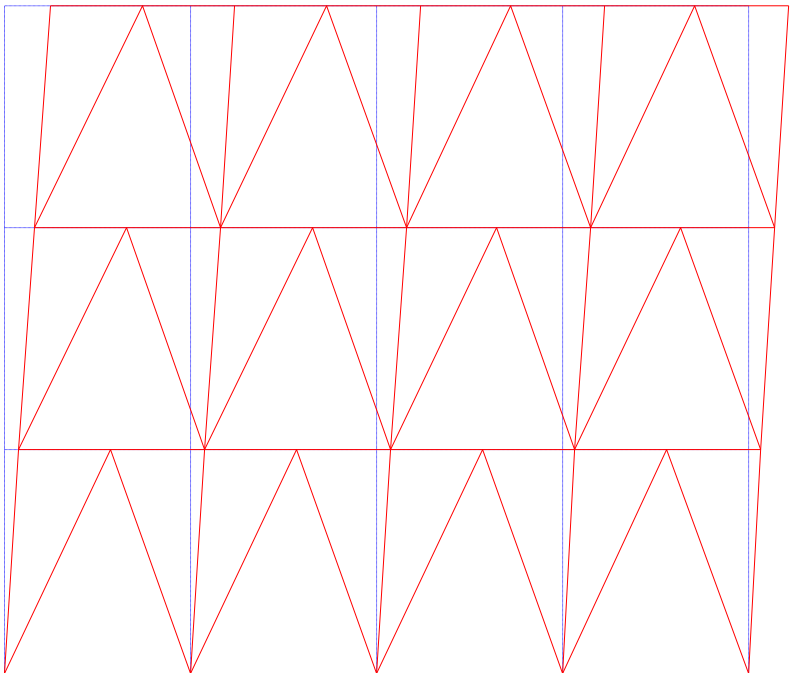

Figure 5.32 Magnified-displacement of Model-3 under the first mode.

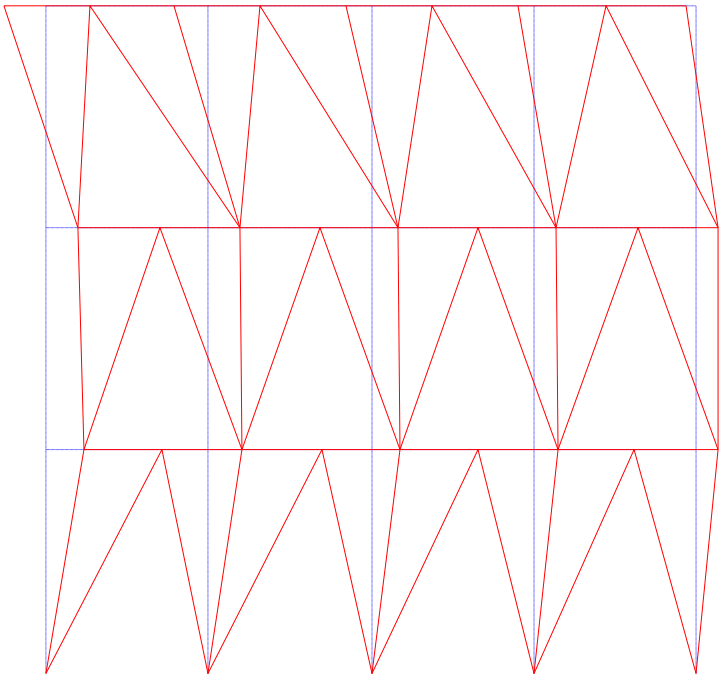

Figure 5.33 Magnified-displacement of Model-3 under the second mode.

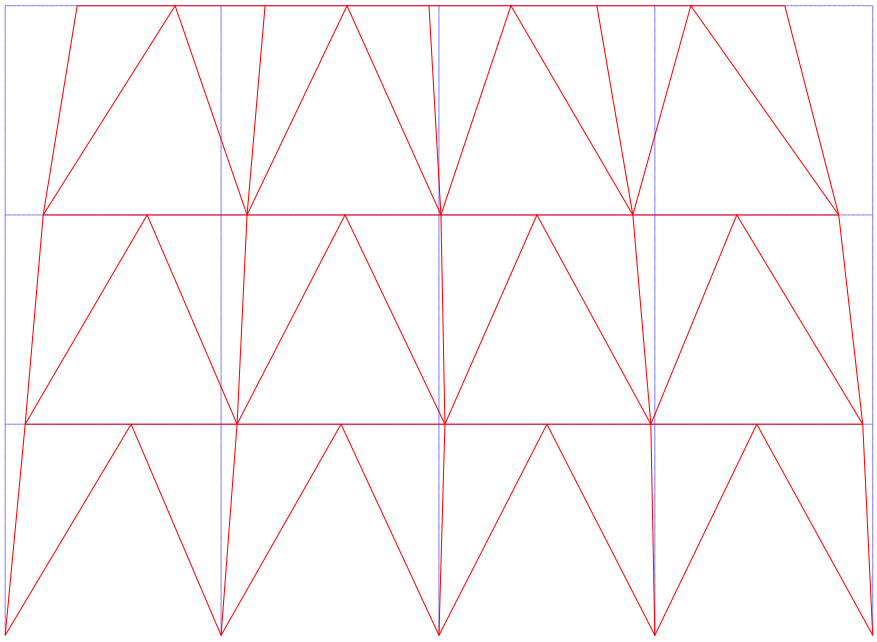

Figure 5.34: Magnified-displacement of Model-3 under the third mode.

5.9 Nonlinear Static Pushover Analysis for Model-3

Static behavior of Model-3 was assessed using NSPA under the first mode of structure. The lateral loading pattern is summarized in Table 5.9. Comparing with the other models, it indicates that all three models have very similar the 1st mode lateral loading pattern. With the same procedure, the model is pushed to the same target RDR of 3.47%; then, it is pulled back until roof displacement equals zero. Comparison of pushover curves for all three models is shown in Figure 5.35.

Table 5.9 First mode lateral loading pattern for Model-3 under NSPA.

Story Level	First mode
3	0.990
2	0.606
1	0.290

Yielding in this retrofitted model occurs in the sequence from CY to TY and to column yielding. The first CY in the right BRBs starts at 0.13% RDR and the last CY in BRBs occurs at 0.17% RDR. TY in the left BRBs begins after the last CY at 0.31% RDR and ends at 0.66% RDR. All CYs and TYs start at the 2nd story. The CY stage in the left SMA braces occurs between 0.4% RDR and 0.43% RDR. The TY stage in SMA braces occurs between 0.48% RDR and 0.59% RDR. Overall, the yielding duration for all braces is from 0.13% RDR to 0.66% RDR. It indicates Model-3 braces start and finish yielding sequence earlier than the other models. While Model-2 has extensive yielding in column, columns in Model-3 just slightly yielded. The first yield in column starts at 1% RDR and the last yield is at 2.4% RDR. Beams still remain elastic.

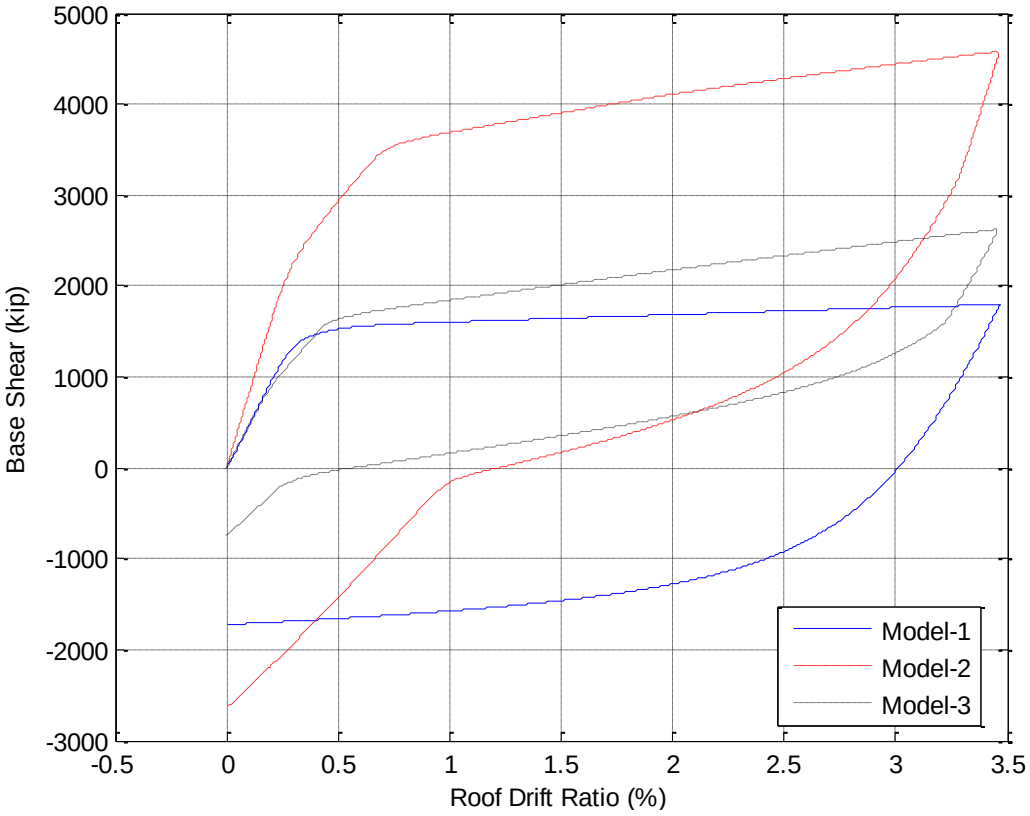

Figure 5.35 Comparison of pushover curves for three models.

Figure 5.35 compares pushover capacities of all three models. It indicates that Model-3 has similar lateral resisting strength as Model-1, which is as expected. However, the base shear of Model-3 at the target RDR is slightly larger than Model-1 because SMA braces have a little larger strain hardening ratio compared to BRBs. Among three models, Model-3 is shown to have the smallest permanent deformation about 0.5% RDR. It indicates effect of retrofitting in Model-3 is efficiency, even better than the rehabilitation option in Model-2, while remain a similar lateral resistance to the as-built conventional BRBF model.

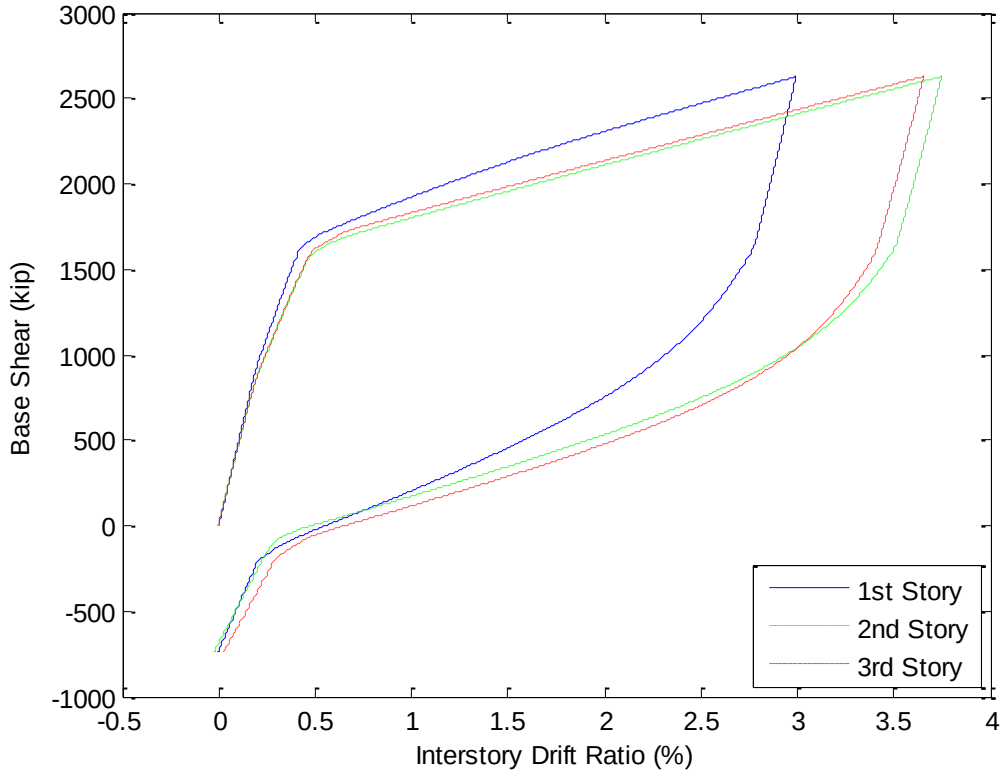

Figure 5.36 Interstory drifts for Model-3.

Comparison of interstory drifts is shown in Figure 5.36. It seems seismic demands are distributed more uniformly than the as-built model and rehabilitated model. The maximum ISDRs are 3.65% RDR, 3.75% RDR and 3.0% RDR for the 3rd, 2nd and 1st story respectively. No soft-story mechanism occurs in this frame. Also all stories are shown to have the similar residual displacements.

5.7 Nonlinear Time History Analysis for Model-3

Seismic demand relationship for Model-3 is shown in Figure 5.37. Figure 5.38 indicates Model-3 exhibit the largest seismic demand among the three models. However, the seismic demands for the retrofitted model are merely slightly larger than the as-built BRB

model. It can be explained by the fact that the difference in seismic demands is proportional to the difference between fundamental periods. Model-3 has a mean of maximum ISDRs for all 60 ground motion records at 0.95%. The maximum value is 2.224% ISDR occurred under LA21 ground motion which is slightly smaller than that of Model-1. The average maximum ISDRs are 1.45%, 0.861% and 0.535% for the 2%/50yr, 10%/50yr and 50%/50yr ground motion suites, respectively. Comparison of seismic demands between three models is summarized in Table 5.10. It indicates that Model-3 has the largest values in all categories, but is comparable to Model-1. The discrepancy between Model-3 and Model-1 are very small due to the fact that SMA braces have smaller elastic modulus than BRBs. It can be concluded that the retrofitting option in Model-3, designed by using the proposed force distribution between the BRB and SMA braces, is comparable to the Model-1.

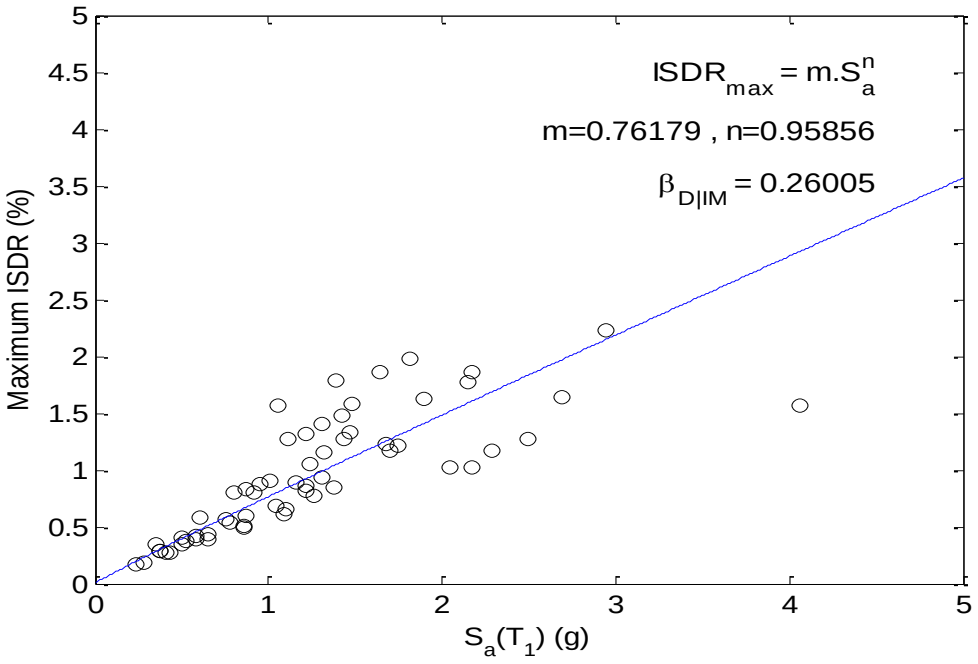

Figure 5.37 Relationship between maximum ISDR and $S_a(T_1)$ for Model-3.

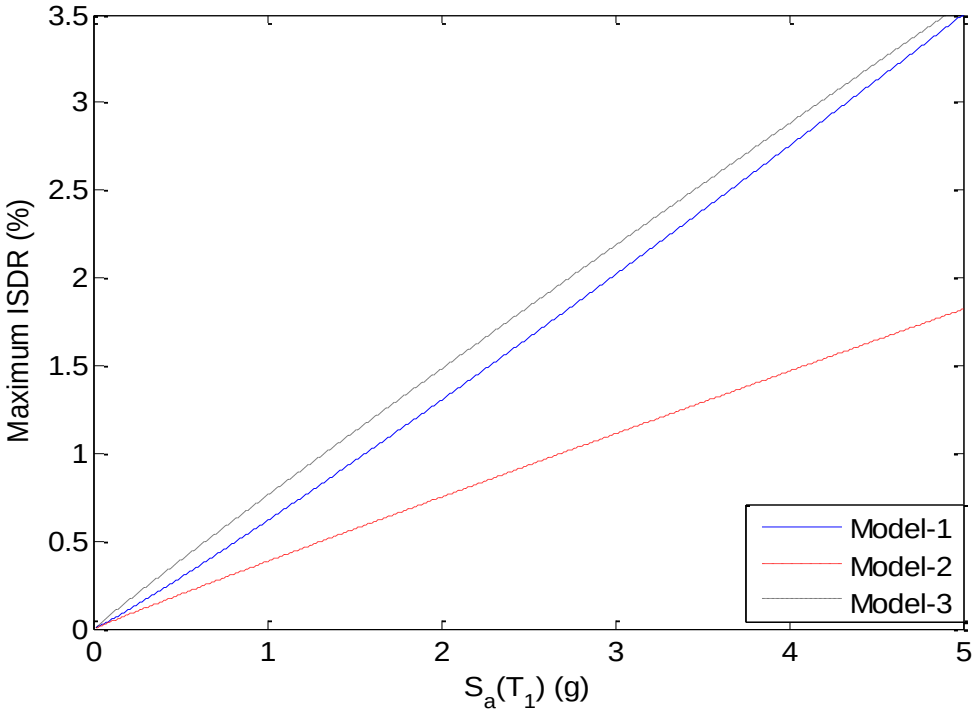

Figure 5.38 Comparison of global seismic demand relationships for all three models.

Table 5.10 Statistical data for maximum ISDR for all three models.

Frame	Mean	Mean of 2%/50yr suite	Mean of 10%/50yr suite	Mean of 50%/50yr GM suite
Model-1	0.873%	1.426%	0.766%	0.425%
Model-2	0.567%	0.833%	0.502%	0.356%
Model-3	0.950%	1.45%	0.861%	0.535%

Seismic demands at three local levels are also examined in Figure 5.39, 5.40 and 5.41. They show that all three stories have very similar demands. Statistical data of interstory drift is summarized in Table 5.11. Similar to Model-1, all maximum ISDRs occurs under ground motion LA21 and tend to locate at the 1st and 2nd story levels, but

the distribution of mean ISDRs along the height of the building is more uniform than the other two models.

Table 5.11 Statistical data of ISDR by story for Model-3.

Story Level	Max ISDR/GM	Mean ISDR	Max ISDR occurrences (2% / 10% / 50% ground motions)
1	2.224%/LA21	0.904%	25 (15 / 9 / 1)
2	2.191%/LA21	0.921%	25 (5 / 8 / 12)
3	1.940%/LA21	0.804%	10 (0 / 3 / 7)

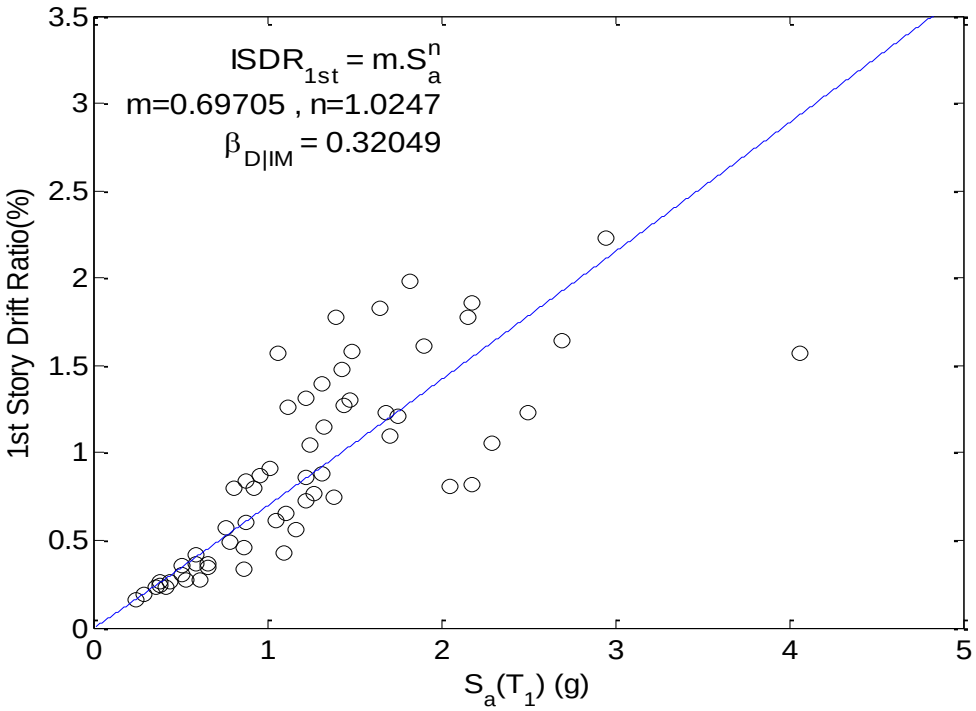

Figure 5.39 Relationship between the 1st interstory drift and $S_a(T_1)$ for Model-3.

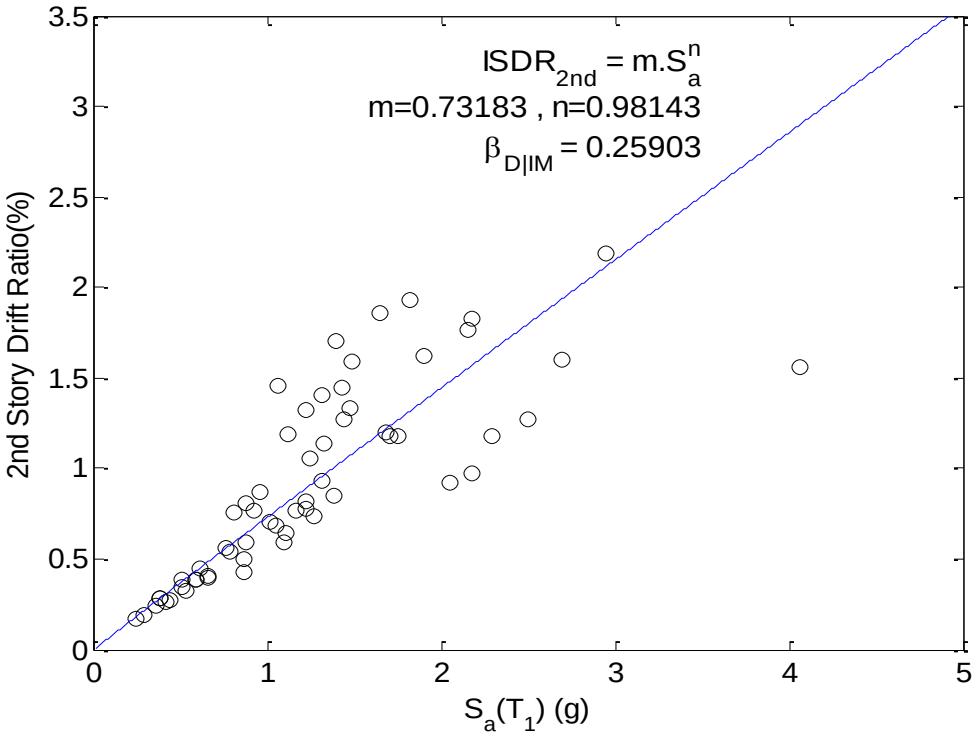

Figure 5.40 Relationship between the 2nd story drift and $S_a(T_1)$ for Model-3.

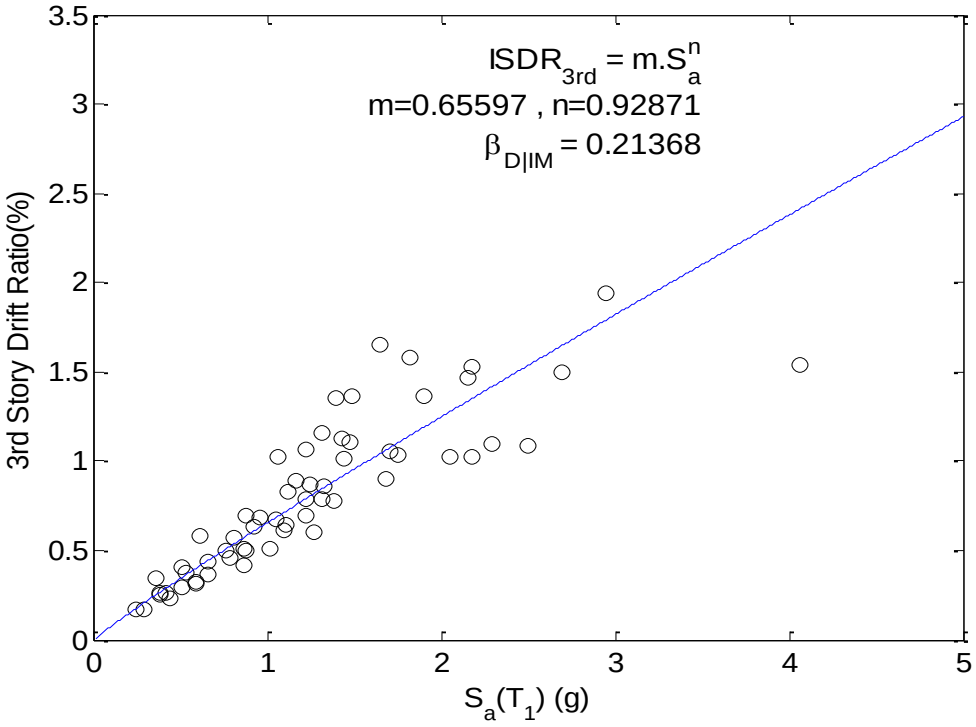

Figure 5.41 Relationship between the 3rd interstory drift and $S_a(T_1)$ for Model-3.

Permanent deformation was also examined in both global and local levels. The relationship between maximum PDR and $S_a(T_1)$ for Model-3 is shown in Figure 5.42. Comparison of permanent deformation for three models is shown in Figure 5.43. It indicates Model-3 has the lowest permanent deformation. As the same trend for Model-2, the reduction in permanent deformation in Model-3 tends to increase with intensity of earthquakes. However, the difference between Model-2 and Model-3 are negligible for small earthquakes. The mean of maximum PDR for 2%/50yr suite, 10%/50yr suite and 50%/50yr suite are 0.041%, 0.033% and 0.024%, respectively, as summarized in Table 5.12. The reduction in average maximum PDR in Model-3 compared to Model-1 is more than 83% ((0.202-0.033)/0.202 = 83%) while reduction is 78.2% in Model-2. It is attributed to smaller yielding of column in Model-3.

The comparison of permanent deformation by story between three models is summarized in Table 5.13. It shows that maximum permanent deformation tends to occur in the 1st story in Model-2, in the 2nd story for Model-1 and in the 3rd story for Model-3. Each story in Model-3 has the mean and maximum PDR smaller compared with that story in Model-2 and Model-1. Overall, the retrofitted frame, Model-3, is very efficient in reducing permanent deformation under intense earthquakes.

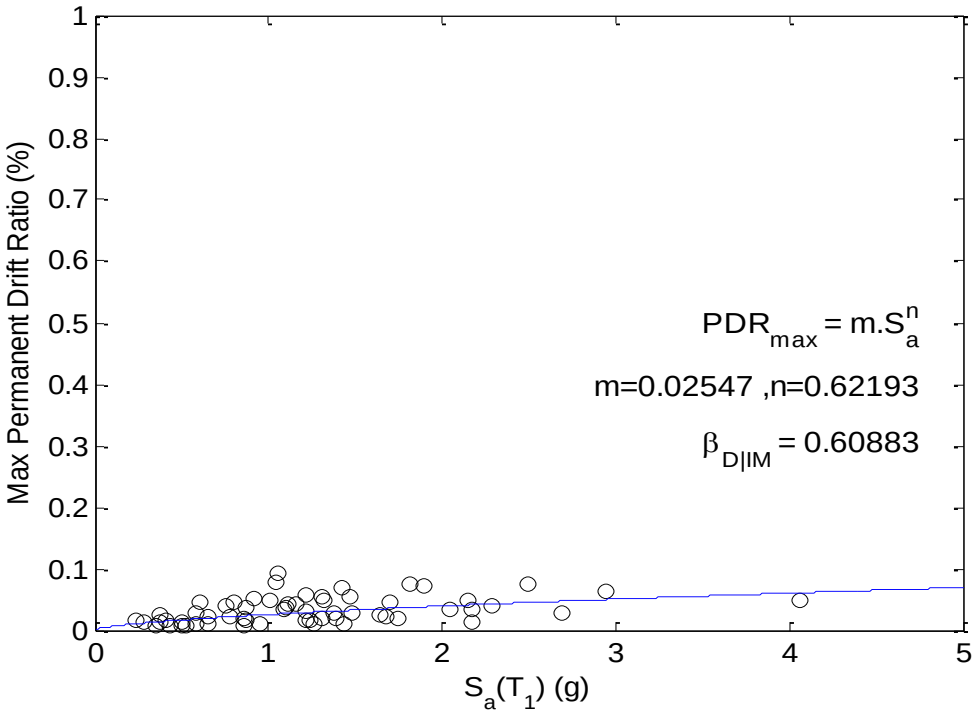

Figure 5.42 Relationship between maximum PDR and $S_a(T_1)$ for Model-3.

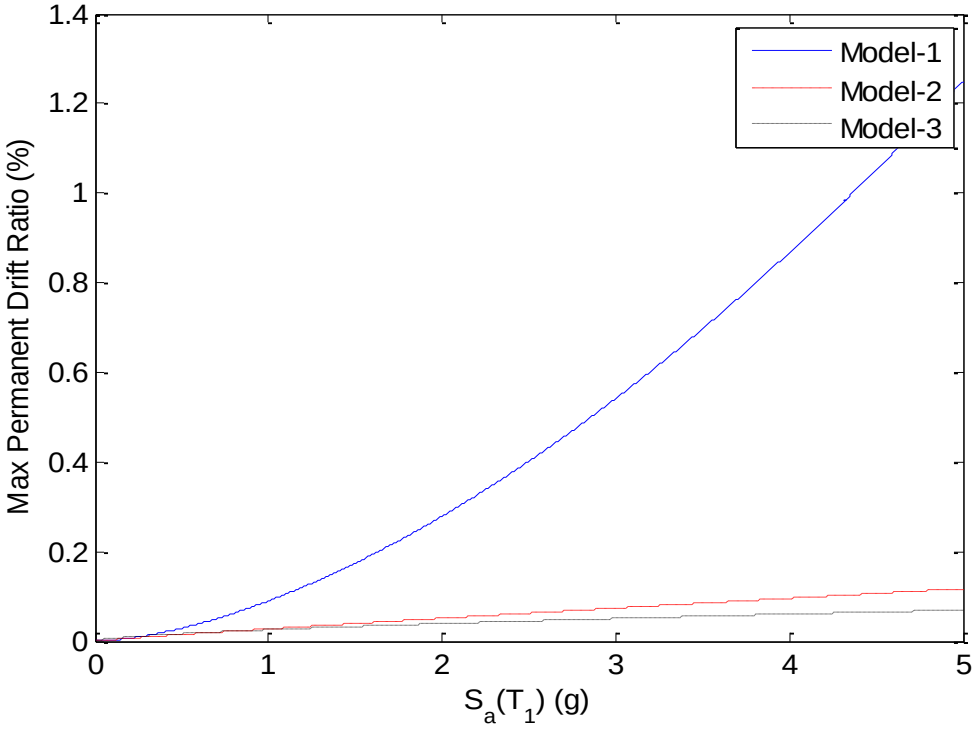

Figure 5.43 Comparison of permanent drift for three models.

Table 5.12 Statistical data for maximum PDR for three models.

Frame	Mean	Mean of 2%/50yr suite	Mean of 10%/50yr suite	Mean of 50%/50yr GM suite
Model-3	0.033%	0.041%	0.033%	0.024%
Model-2	0.044%	0.064%	0.041%	0.027%
Model-1	0.202%	0.372%	0.156%	0.077%

Table 5.13 Statistical data of permanent drift by story for three models.

Story	Model	Max PDR/GM	Mean PDR	Max PDR occurrences
1	3	0.092%/LA38	0.021%	23
	2	0.115%/LA38	0.034%	26
	1	0.747%/LA21	0.162%	19
2	3	0.089%/LA38	0.022%	12
	2	0.114%/LA12	0.031%	15
	1	0.834%/LA21	0.186%	23
3	3	0.084%/LA38	0.025%	25
	2	0.099%/LA36	0.028%	19
	1	0.878%/LA21	0.149%	18

Seismic demand relationship on SMA braces is shown in Figure 5.44. It shows all the data points satisfy 6% strain limit. The maximum strain demand of SMA braces is 5.76% and the mean of that is 2.3% for all 60 ground motions. The average maximum strain demands for the 2%/50yr, 10%/50yr and 50%/50yr suites are 3.75%, 2.04% and 1.12% respectively. Figure 5.45 shows the demand for SMA braces in Model-3 is much larger than Model-2. It is due to the area of SMA braces in Model-3 is designed much smaller than in Model-2. Therefore, Model-3 tends to be more cost-effective than Model-2.

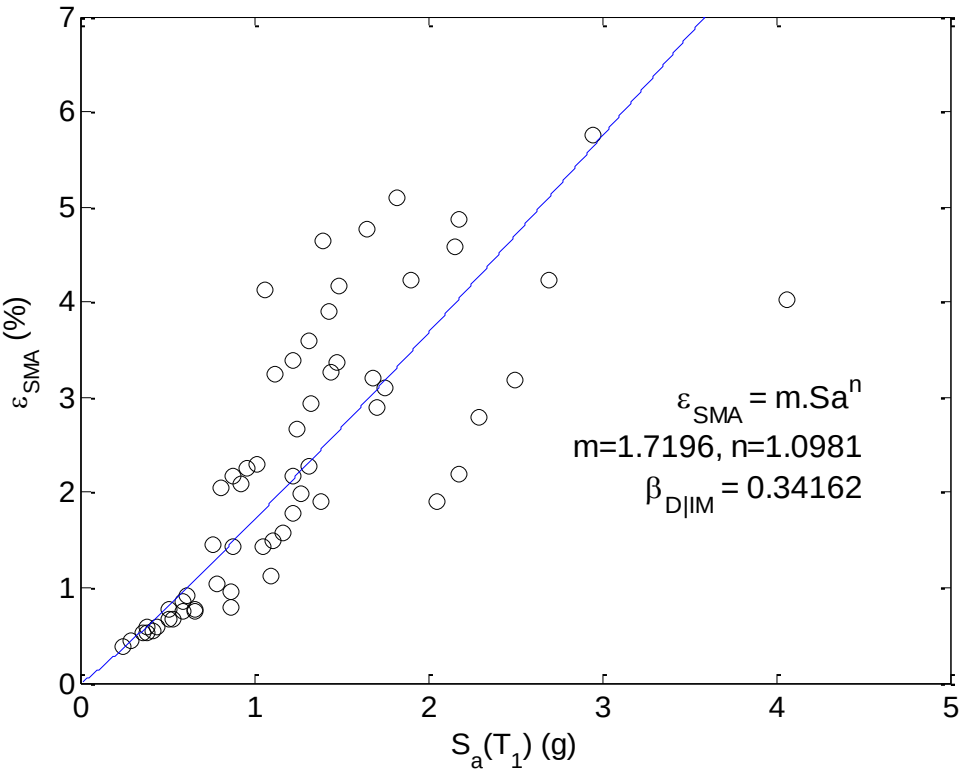

Figure 5.44 Relationship between SMA strain and $S_a(T_1)$ for Model-3.

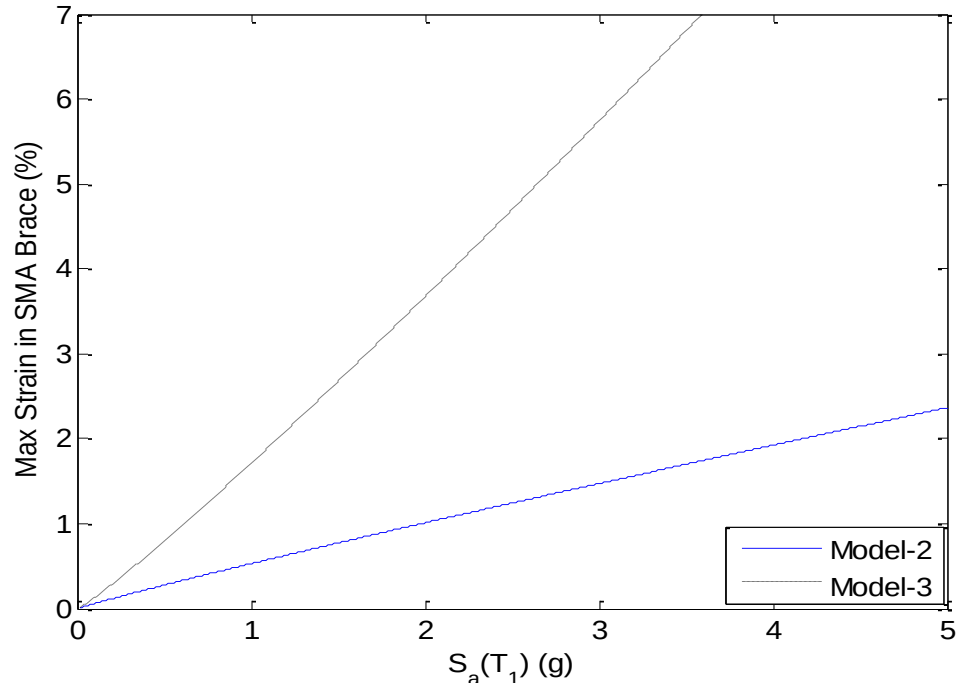

Figure 5.45 Comparison of seismic demands on SMA braces for Model-2 and Model-3.

CHAPTER 6

FRAGILITY ASSESSMENTS OF AS-BUILT AND HYBRID FRAMES

6.1 Probabilistic Seismic Demand Analysis

Probabilistic seismic demand analysis is carried out to estimate the mean annual probability of exceeding a certain demand level (in term of EDP), for a given earthquake intensity level (IM). It can be expressed in the following equation (Kinali and Elllingwood, 2007).

$$P[EDP \geq \kappa | IM] = 1 - \Phi\left(\frac{\ln(\kappa) - \ln(m.IM^n)}{\beta_{EDP|IM}}\right) \quad (6.1)$$

in which κ is a demand level of interest and $\beta_{EDP|IM}$ is dispersion of demand given an *IM* (*EDP*, *IM*, *m*, and *n* are already defined in Equation 4.2).

In this thesis, uncertainty in structural capacity of the frames is neglected. Song and Ellingwood (1999) have found that variability in frame structural characteristics had only a small contribution to the overall response variability of the frame, compared to that of the variation in ground motion intensities. Thus, the yield strength, expected yield strength, modulus of elasticity of the beams and columns as well as SMA material properties are assumed to be deterministic and were set equal to their mean values in this study. Also, uncertainty in defining performance levels is neglected because research to define damage states of the frames is beyond the scope of this thesis.

6.2 Assessment of Interstory Drifts

The seismic fragility curves for the as-built BRB, rehabilitated and retrofitted hybrid BRB-SMA models, corresponding to Model-1, Model-2 and Model-3, respectively, were calculated with respect to the four damage states found in FEMA-273 or in ASCE Standard 41-06: operational (O), immediate occupancy (IO), life safety (LS), and collapse prevention (CP) (the detailed descriptions of these damage stages are defined in Section 4.3), as shown in Figures 6.1-6.3. The system limit states are applicable to all the frame models and are given in Table 4.1. The maximum interstory drift ratio was selected as the engineering demand parameter (EDP). The seismic fragility curves were calculated through the median and dispersion values obtained from the probability seismic demand analysis summarized in Chapter 5. In order to interpret the seismic fragility curves for the as-built, rehabilitated and retrofitted models, the mean spectral acceleration for each ground motion suite at the structural fundamental period was used to calculate the probability of exceedance of each damage state under a seismic hazard level. The results are summarized in Table 6.1.

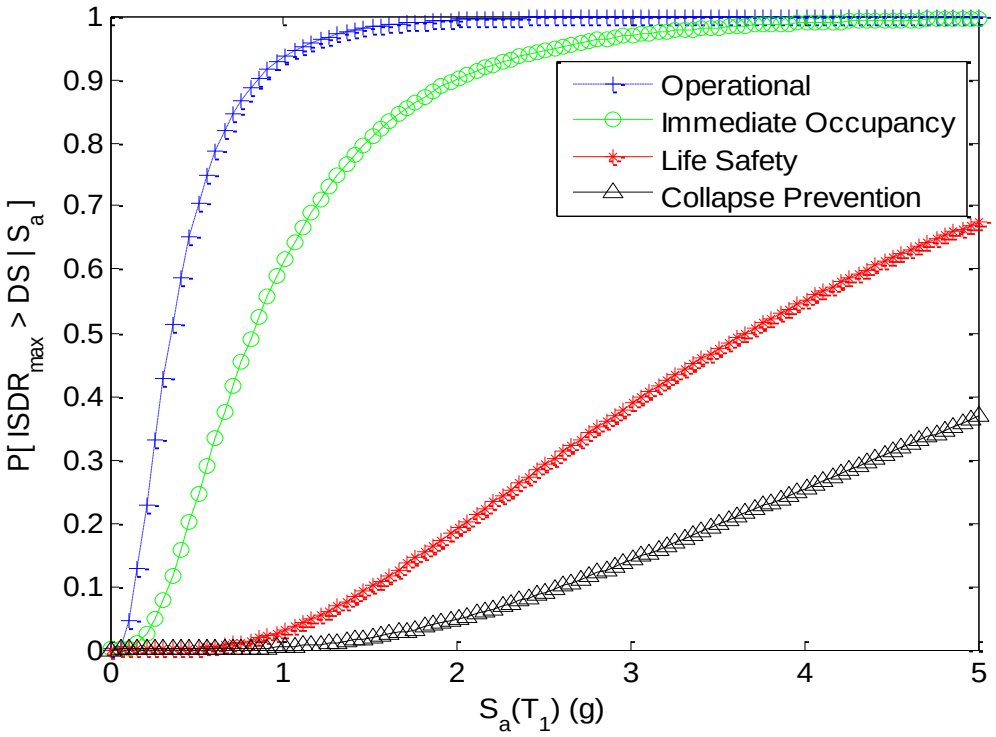

Figure 6.1 Seismic fragility curves for Model-1.

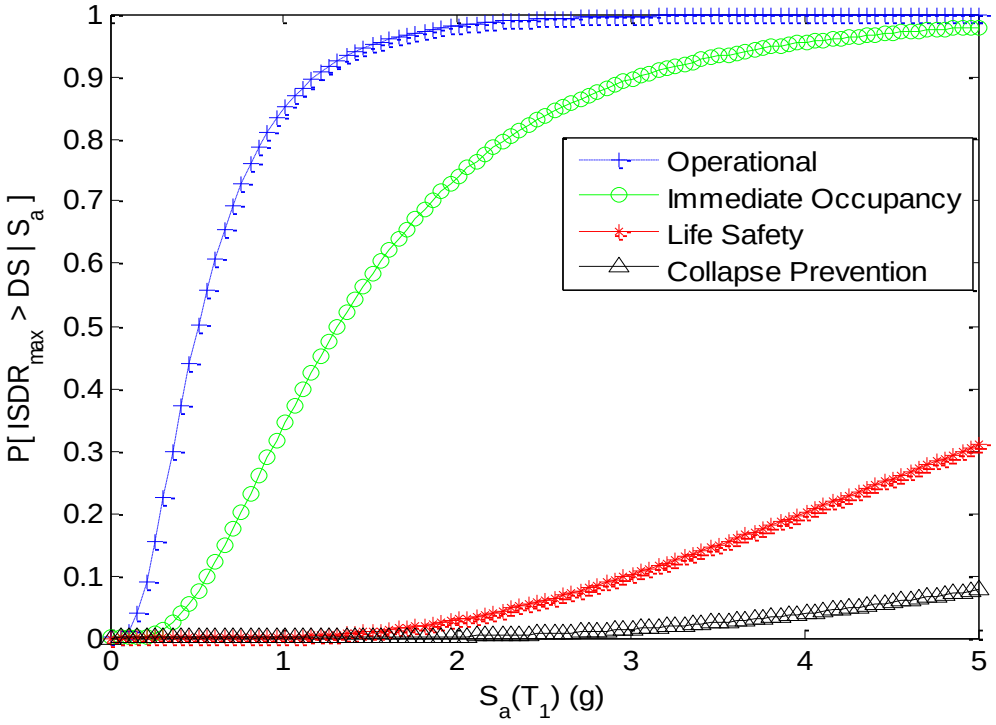

Figure 6.2 Seismic fragility curves for Model-2.

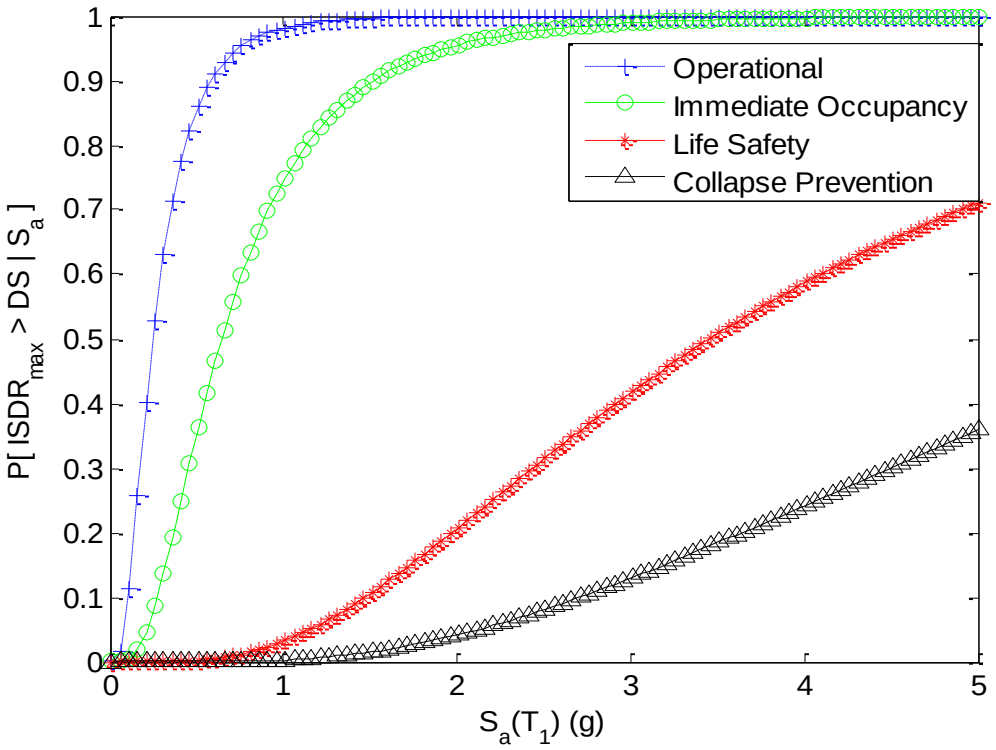

Figure 6.3 Seismic fragility curves for Model-3.

Table 6.1 Probability of exceeding a damage state under seismic hazard levels.

Hazard Level	Model	$S_a(T_1)$ (g)	O (0.2%)	IO (0.5%)	LS (2.5%)	CP (4.5%)
2%/50yr	1	1.838	99.73	91.20	12.30	1.88
	2	2.011	98.16	74.13	2.98	0.25
	3	1.778	99.44	90.40	19.65	5.02
10%/50yr	1	0.941	95.13	58.95	1.11	0.07
	2	1.025	85.64	35.31	0.18	0.01
	3	0.842	94.21	63.45	3.47	0.46
50%/50yr	1	0.567	78.95	26.55	0.08	0.00
	2	0.697	68.38	16.77	0.02	0.00
	3	0.523	83.71	40.26	0.81	0.07

The following inferences can be drawn from the above results:

- Model-2 has the smallest probability of exceedance for all damage states. It is because the rehabilitation method, which described in Chapter 3, makes it the strongest model.

- The Probability of exceeding the CP damage state for Model-2 is negligible for all cases when the spectral acceleration is less than 2.0g.
- Even though Model-3 has slightly higher damage state probabilities across the board than Model-2, the difference is very small.
- The superior performance of Model-2 to the other models becomes more apparent when the intensity increases.

6.3 Assessment of Permanent Drifts

In order to investigate the effectiveness of retrofitted and rehabilitated models, the seismic residual performance of three models is assessed using permanent drifts as an EDP. The four damage states for permanent drifts corresponding to O, IO, LS and CP were already defined in Table 4.1. Fragility curves for three models are shown in Figures 6.4, 6.5 and 6.6. Again, the mean spectral acceleration for each ground motion suite at the structural fundamental period are used to calculate the probability of exceedance for each limit state, and the results are provided in Table 6.2.

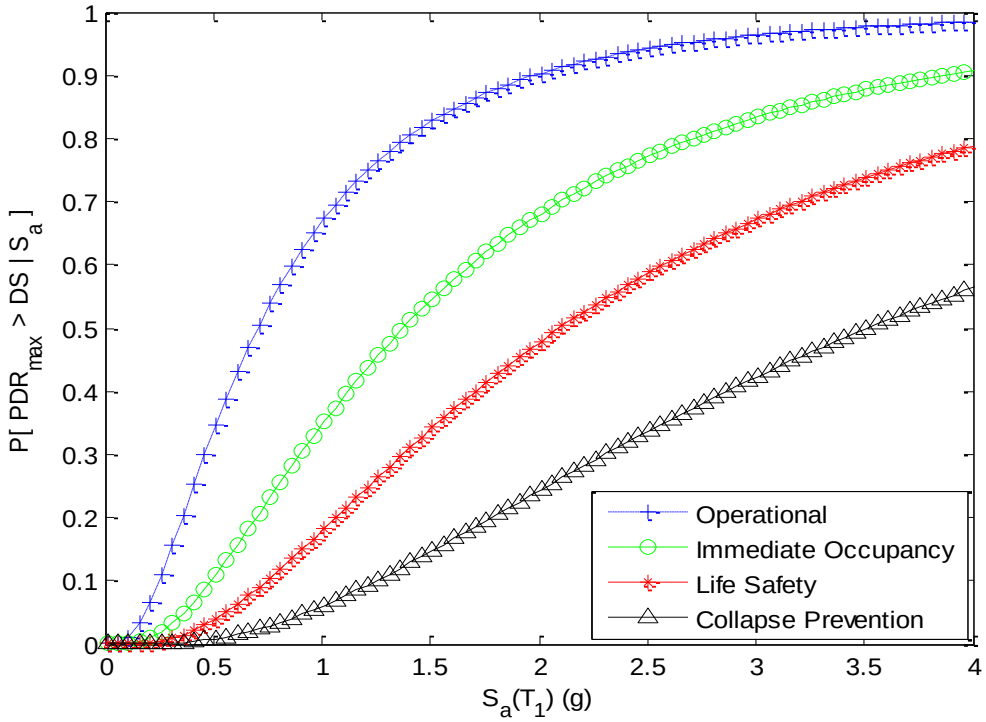

Figure 6.4 Seismic fragility curves for permanent drift of Model-1.

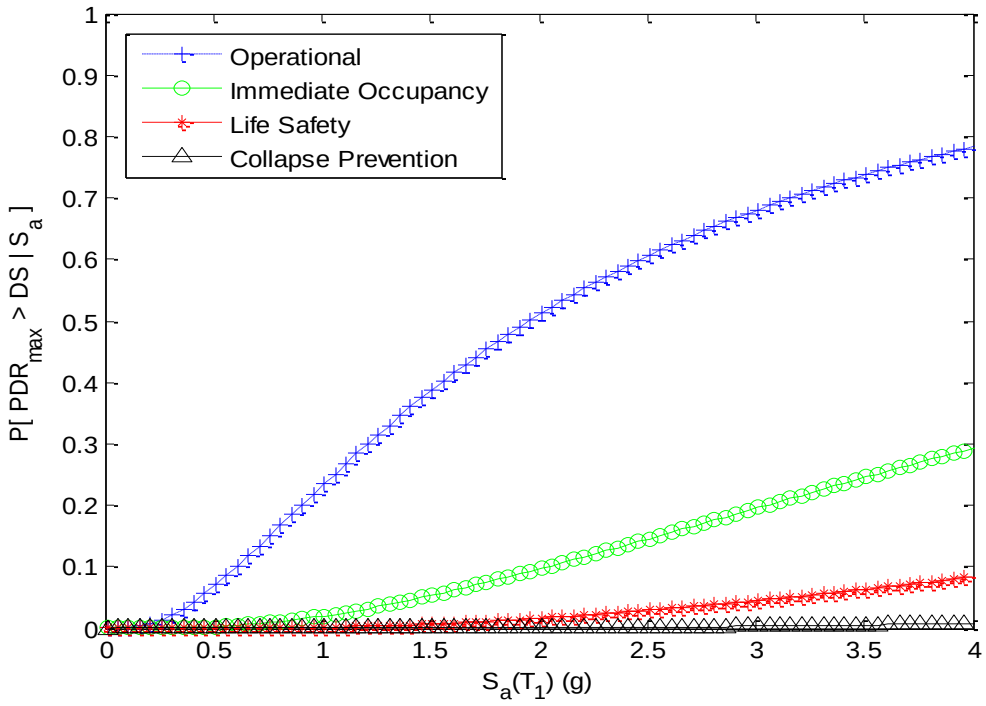

Figure 6.5 Seismic fragility curves for permanent drift of Model-2.

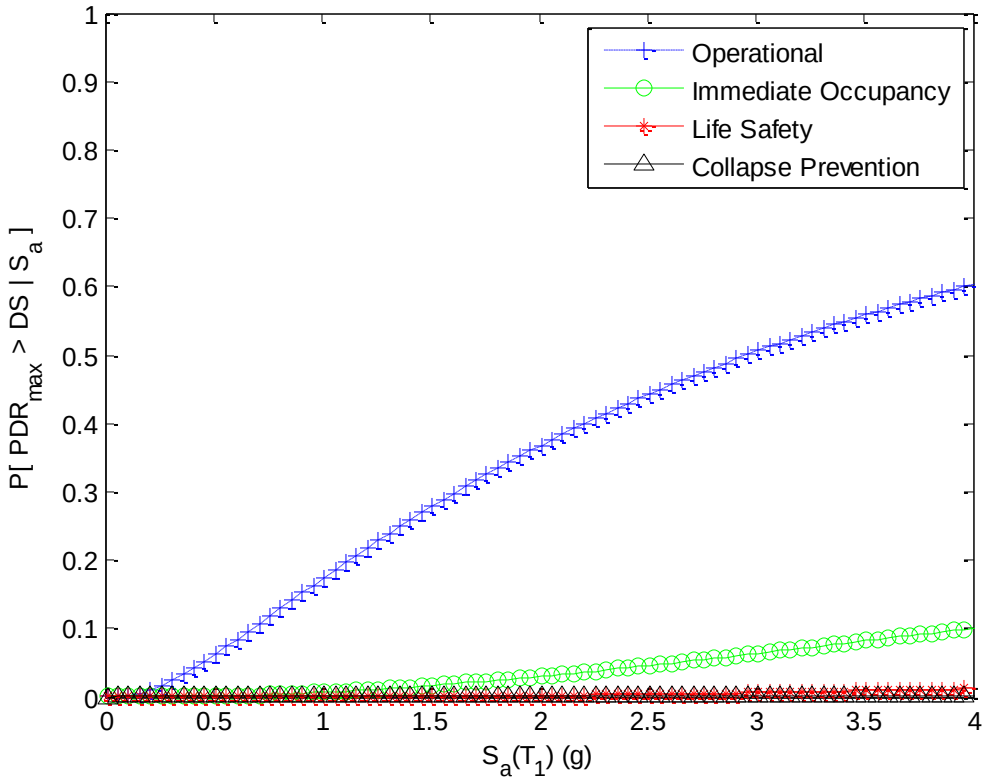

Figure 6.6 Seismic fragility curves for permanent drift of Model-3.

Table 6.2 Probability of exceeding a damage state under seismic hazard levels in term of permanent drift.

Hazard Level	Model	$S_a(T_1)$ (g)	O (0.05%)	IO (0.15%)	LS (0.3%)	CP (0.7%)
2%/50yr	1	1.838	88.30	64.07	43.52	21.10
	2	2.011	51.19	9.74	1.65	0.08
	3	1.778	32.86	2.36	0.16	0.00
10%/50yr	1	0.941	64.08	31.95	16.04	5.13
	2	1.025	23.97	2.10	0.21	0.01
	3	0.842	13.67	0.42	0.02	0.00
50%/50yr	1	0.567	39.47	13.64	5.26	1.19
	2	0.697	12.94	0.70	0.05	0.00
	3	0.523	6.74	0.12	0.00	0.00

The following inferences can be drawn from the results presented in Table 6.2:

- Model-2 and Model-3 have superior performance in term of permanent drifts to Model-1. The probability of exceeding the CP limit is close zero for Model-2 and Model-3 while it is 21.1% for Model-1.
- Model-1 has extremely high permanent drifts under severe earthquakes.
- As the levels of damage state increases, probability of exceedance drops faster for Model-2 and Model-3 than for Model-1.
- Model-3 has better performance in all cases compared to Model-2, but the difference is very small for severe damage states.
- As the hazard level increases, the probability of exceeding a certain permanent drift increases; the increases is especially pronounced for the as-built frame.

6.4 Assessments of Seismic Demand of SMA Braces

The seismic fragilities of SMA braces are calculated for four performance levels defined in Table 4.2. The maximum strain in the brace experienced during a ground motion record is used as the corresponding EDP. The seismic fragilities of Model-2 and Model-3 are shown in Figures 6.7 and 6.8. The mean annual probabilities of exceedance for both models using mean spectral acceleration at fundamental period are summarized in Table 6.3.

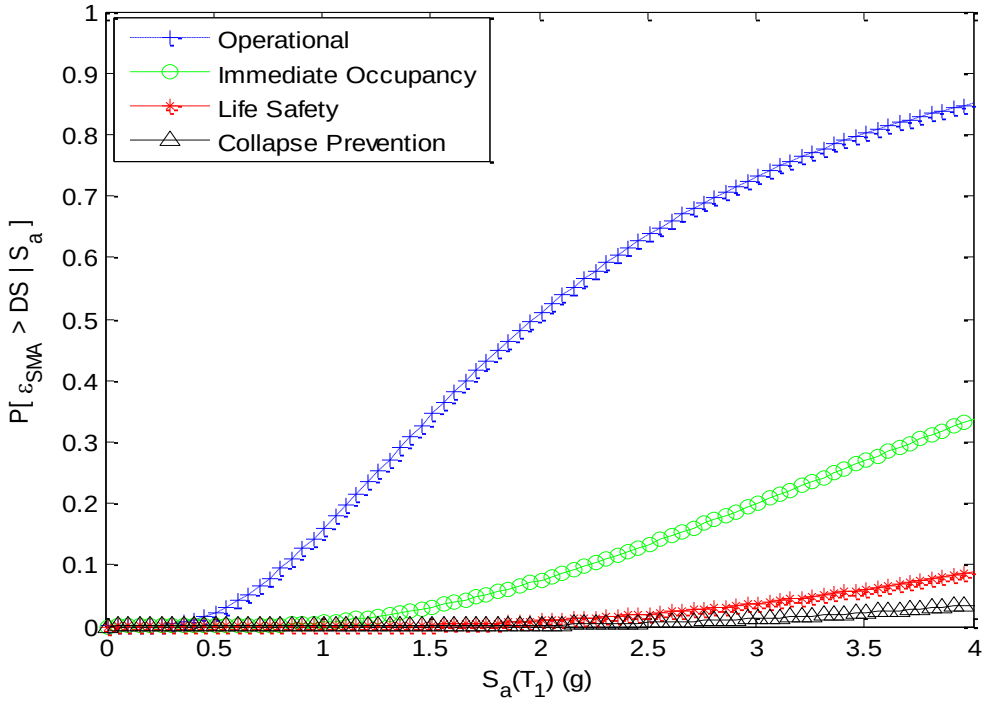

Figure 6.7 Seismic fragilities for SMA braces in Model-2.

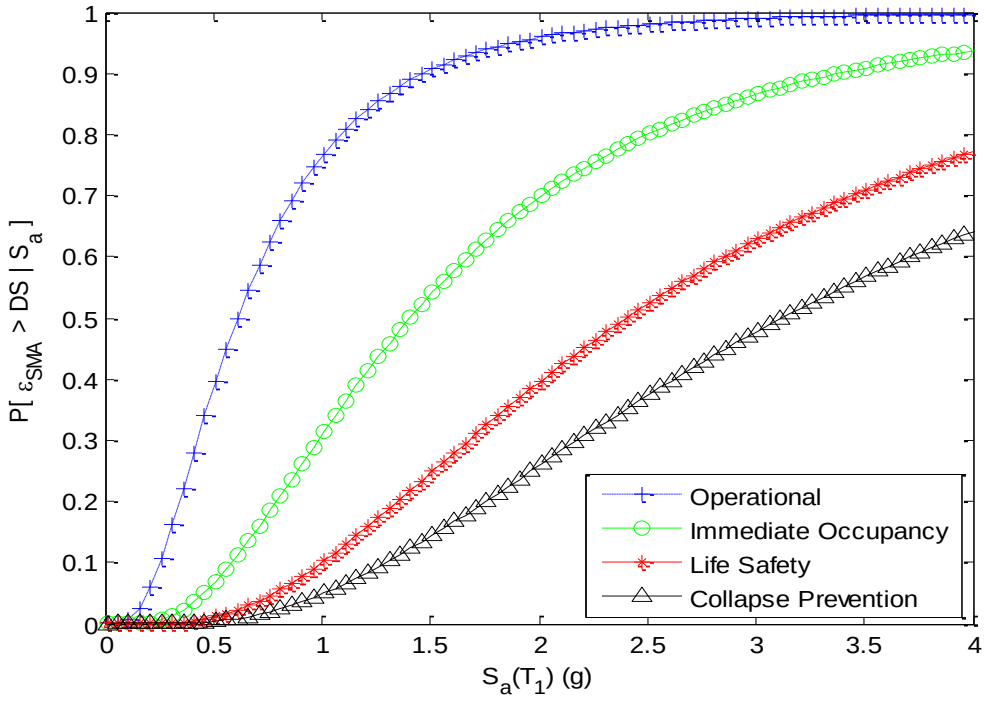

Figure 6.8 Seismic fragility curves for SMA braces in Model-3.

Table 6.3 Probability of exceeding a damage state under seismic hazard levels for SMA braces.

Hazard Level	Model	$S_a(T_1)$ (g)	O (1.0%)	IO (2.5%)	LS (4.5%)	CP (6.0%)
2%/50yr	2	2.011	52.74	0.01	0.00	0.00
	3	1.778	99.97	77.47	16.70	3.53
10%/50yr	2	1.025	0.5	0.00	0.00	0.00
	3	0.842	84.94	4.97	0.04	0.00
50%/50yr	2	0.697	0.00	0.00	0.00	0.00
	3	0.523	32.93	0.09	0.00	0.00

The following inferences can be made from the results Table 6.3:

- SMA braces in Model-2 have almost zero probability of exceedance for all cases except the operational damage state under 2%/50yr earthquake events.
- Under 2%/50yr events, the probability of exceeding the CP limit, which is also the strain limit to prevent the degradation in recentering properties of SMA, in Model-3 is 3.53%. It indicates that the effectiveness of SMA braces on recentering capacity is still guaranteed with very high confidence level.
- The SMA braces in Model-2 and Model-3 have similar probabilities of exceedance for IO, LS and CP damage states under 10%/50yr and 50%/50yr events.

CHAPTER 7

CONCLUSIONS AND RECOMMENDATIONS FOR FURTHER STUDY

7.1 Conclusions

This thesis presented a comparative study of the seismic performance of a conventional three story BRBF designed for downtown Los Angeles, with the rehabilitated and retrofitted models of this frame containing innovative SMA braces. Nonlinear static pushover analyses and nonlinear time history analyses were carried out to compare the maximum interstory drifts, permanent drifts of the frames and SMA braces' demand. Finally, fragility analyses were used to estimate the probabilities of exceeding certain limits of structural response, given increasing intensities of ground motions. The effects of SMA braces on permanent deformation were discussed as well as the effect of the variation of ground motion intensities. The general conclusions drawn from the results of this study can be summarized as follows:

- The results from NTHA agree with the NSPA results where the 2nd story was identified as the most critical story for 10%/50yr and 50%/50yr events. However, as the intensity increases, the interstory drifts tend to accumulate in the 1st story.
- Rehabilitated and retrofitted models have more uniform distribution of inelastic response along the height of the structure compared to the as-built BRBF.
- While the demands in the as-built and retrofitted frames are very similar in term of maximum interstory drift, the maximum ISDR in the rehabilitated frame with

additional strength provided from SMA braces is 35% less than the maximum ISDR in the as-built frame.

- As the ground motion intensity increases, the improvement in performance in term of maximum interstory drift of rehabilitated frame becomes more apparent compared to that of the other models.
- SMA braces provide both rehabilitated and retrofitted frames with excellent recentering capacities with an average reduction of 79% and 83% maximum residual drift, respectively. The retrofitted frame has the larger reduction in permanent drift because it has only slightly yielding in base columns while the rehabilitated frame had major yielding in columns.
- Comparing between rehabilitating and retrofitting frames, the retrofitting frame yields larger demands in SMA braces, but the demand doesn't exceed the SMA strain limitation, meaning that the SMA braces can be reused.
- In 2%/50yr events, the rehabilitated and retrofitted models has a mean of 9.74% and 2.36% probability of exceeding the IO permanent drift limit (which is defined as 0.15% drift ratio) respectively (64.07% for the as-built frame). The very small permanent deformation observed suggests that these frames can resume their original configurations after severe earthquakes.

7.2 Further research suggestions

Further research suggestions are summarized as follows:

- More refined modeling techniques are suggested in order to account for the contribution of gravity frames and non-structural elements to lateral force resistance. A 3D analysis of the building is recommended to account for the building irregularities and torsional effects.
- Since the OpenSEES platform did not provide any buckling-restrained brace element in its library, the buckling-restrained braces modeled in this thesis used nonlinear beam-column element with the designed steel core area and the realistic moment of inertia to account for the effect of the concrete-filled tube. Although the cyclic strain hardening was simulated in the brace model, the effect of little higher strength in compression than in tension wasn't simulated yet. Therefore, better modeling of the braces is suggested. Also, the prismatic members in OpenSEES didn't take into account lateral buckling and lateral-torsional buckling behaviors.
- The performance levels for the frames and SMA braces assessed in this study are estimates rather than precise prediction. Therefore, more experiments might be needed to define more accurately damage states or performance levels for the frame. It will help to provide seismic fragility results with a higher confidence level.
- Previous researches has shown that using synthetic ground motions or recorded ground motions might produce large differences in the demand results (Kinali and Ellingwood, 2007) which might increase the uncertainty in fragility results, even their intensities were scaled to match. It is suggested to use both types of ground motion in the analyses to better account for those variations.

APPENDIX A

DESIGN CALCULATION FOR SMA LENGTH

Design Procedure for SMA Length:

$$V_{Design} = \Phi V_n \geq V_u$$

$$\Phi V_n = \Phi V_{SMA.f} + \Phi V_S \geq V_u \quad (1)$$

The requirement for the hybrid devices to have a flag shape hysteresis including re-centering capacity:

$$\Phi V_{SMA.r} \geq \Phi V_S \quad (2)$$

Also,

$$V_{SMA.r} = \alpha \cdot V_{SMA.f} \quad (3)$$

in which α is the ratio between the forward transformation yield stress to the reverse transformation yield stress

From eq. (1), (2) and (3), it yields

$$\Phi V_{SMA.f} \geq \frac{1}{1+\alpha} \cdot V_u$$

$$\Phi V_{SMA.r} \geq \frac{\alpha}{1+\alpha} \cdot V_u$$

$$\Phi V_S = \frac{\alpha}{1+\alpha} \cdot V_u$$

Requirement for deformation capacity:

$$\delta_{SMA} = 6\% \cdot L_{SMA}$$

The elongation of SMA is restricted to 6% maximum

$$\delta_{SMA} \geq \delta_{demand} \cdot SF$$

where SF is Safety Factor

Hence,

$$L_{SMA} \geq \frac{\delta_{demand} \cdot SF}{6\%} \tag{4}$$

Requirement for recentering capacity to meet permissibly maximum residual deformation δp

$$\delta_{SMA.r} = \frac{\alpha \cdot \sigma_{yf} \cdot L_{SMA}}{E_{SMA}}$$

$$\delta_{SMA.r} \leq \delta_p$$

Hence,

$$L_{SMA} \leq \frac{E_{SMA}}{\alpha \cdot \sigma_{yf}} \cdot \delta_p \tag{5}$$

From (4) and (5), we can find the upper bound and lower bound of SMA length as below:

$$\frac{\delta_{demand} \cdot SF}{6\%} \leq L_{SMA} \leq \frac{E_{SMA}}{\alpha \cdot \sigma_{yf}} \cdot \delta_p$$

REFERENCES

AISC. (2010) “Seismic Provisions for Structural Steel Buildings”, American Institute of Steel Construction, Inc., ANSI/AISC 341-10.

ASCE. (2010) "Standard-Minimum Design Loads for Buildings and Other Structures, 7-10", American Society of Civil Engineers.

ASCE. (2007) "Seismic Rehabilitation of Existing Buildings", American Society of Civil Engineers., ASCE/SEI 41-06.

Asgarian, B., Moradi, S. (2011) “Seismic Response of Steel Braced Frames with Shape Memory Alloy Braces”, Journal of Construction Steel Research; 67, 65-74.

Auricchio, F., Fugazza, D., DesRoches, R. (2006) “Earthquake Performance of Steel Frames with Nitinol Braces.”, Journal of Earthquake Engineering, Vol 10, 1-22.

Rowshandel, B., Reichle, M., Wills, C., Cao, T., Petersen, M., Branum, D., Davis, J. (2005) "Estimation of Future Earthquake Losses in California", California Geological Survey.

Clark, P., Aiken, L., Kasai, K., Ko, E., Kimura, I. (1999) “Design Procedures for building Incorporating Hysteretic Damping Devices”, Proceeding of the 69th Convention of the SEAOC.

Clark, P.W., Aiken, I.D., Kasai, K., Kimura, I. (2000) “Large-Scale Testing of Steel Unbonded Braces for Energy Dissipation”, Structures Congress 2000: Advanced Technology in Structural Engineering.

Cofie, N.G. (1983) “Cyclic Stress-Strain and Moment Curvature Relationships For Steel Beams and Columns”, PhD Dissertation, Department of Civil Engineering, Standford University, Standford, CA.

DesRoches, R., McCormick, J., Delemont, M. (2004) "Cyclic Properties of Superelastic Shape Memory Alloy Wires and Bars", Journal of Structural Engineering; 130(1), 38-46.

Dolce, M., Cardone, D. (2001) “Mechanical Behavior of Shape-Memory Alloys for Seismic Applications. 2: Austenite NiTi Wires Subjected to Tension.”, International Journal of Mechanical Sciences; 43(11), 2657-2677.

FEMA. 273 (1997) “NEHRP Guidelines for the Seismic Rehabilitation of Buildings”, Federal Emergency Management Agency, Washington, DC.

FEMA. 302 (1997) "NEHRP Recommended Provisions for Seismic Regulations for New Buildings", Federal Emergency Management Agency, Washington, DC.

FEMA. 355-C (2000) "State of the Art Report on Systems Performance of Steel Moment Frames Subject to Earthquake Ground Shaking", Federal Emergency Management Agency, Washington, D.C.

FEMA. 440 (2005) "Improvement of Nonlinear Static Seismic Analysis Procedures", Federal Emergency Management Agency, Washington, D.C.

Fahnestock, L.A., Sause, R., Ricles, J.M. (2007) "Experimental Evaluation of a Large-Scale Buckling-Restrained Braced Frame", Journal of Structural Engineering, 133:1205-1214.

Fugazza, D. (2003) "Shape-Memory Alloy Devices in Earthquake Engineering: Mechanical Properties, Constitutive Modelling and Numerical Simulations" Master Dissertation, European School for Advanced Studies in Reduction of Seismic Risk, Pavia, Italy.

Kinali, K., Ellingwood, B.R. (2007) "Application of the Capacity Spectrum Method to Steel Frames in the Central and Eastern United States", Proceedings of the Thematic Conference on Computational Methods in Structural Dynamics and Earthquake Engineering, ECCOMAS.

Kinali, K., Ellingwood, B.R. (2007) "Seismic Fragility Assessment of Steel Frames for Consequence-Based Engineering: A Case Study for Memphis, TN", Engineering Structures.

Krawinkler, H., Seneviratna, G.D.P.K. (1998) "Pros and Cons of a Pushover Analysis of Seismic Performance Evaluation." Engineering Structures, Vol.20, 452-464.

Lopez, W.A., (2001) "Design of Unbonded Braced Frame" Proceedings 70th Annual Convention of SEAOC, Sacramento, CA.

Lopez, W.A., Sabelli, R. (2004) "Seismic Design of Buckling-Restrained Braced Frames" Structural Steel Educational Council.

Luco, N., Cornell, C.A. (2001) "Structure-Specific Scalar Intensity Measures for Near-Source and Ordinary Earthquake Ground Motions", Submitted for Publication: Earthquake Spectra.

McCormick, J., DesRoches, R., Fugazza, D., Auricchio, F. (2007) "Seismic Assessment of Concentrically Braced Steel Frames with Shape Memory Alloy Braces", Journal of Structural Engineering; 133:862-870.

McCormick, J., Tyber, J., DesRoches, R., Gall, K., Maier, H.J. (2007) "Structural Engineering with NiTi. II: Mechanical Behavior and Scaling", Journal of Engineering Mechanics; 133: 1019-1029.

Moradi, S., Alam, M.S., Asgarian, B. (2013) "Incremental Dynamic Analysis of Steel Frames Equipped with NiTi Shape Memory Alloy Braces" The Structural Design of Tall and Special Buildings.

Ocel, J., DesRoches, R., Leon, R.T., Hess, W.G., Krumme, R., Hayes, J.R., Sweeney, S. (2004) "Steel Beam-Column Connections Using Shape Memory Alloys", Journal Structural Engineering; 130(5): 732-740.

Otsuka, K., Wayman, C.M. (1998) "SHAPE MEMORY MATERIALS", United Kingdom, Cambridge University Press.

Padgett, J., Nielson, B., DesRoches, R. (2008) "Which Ground Motion Intensity Measure is most Appropriate for Conditioning Demand Models for Bridge Portfolios", Structures Congress (2008).

Ryhanen, J. (1999) "Biocompatibility Evaluation of Nickel-Titanium Shape Memory Metal Alloy", Acedemic Dissertation, Medicine School, University of Oulu, Oulun Yliopisto, OULU.

Sabelli, R., Mahin, S., Chang, C. (2003) "Seismic Demands on Steel Braced Frame Buildings with Buckling-Restrained Braces", Engineering Structures, 25(5), 655-666.

Sarno, L.D., Elnashai, A.S. (2008) "Bracing Systems for Seismic Retrofitting of Steel Frames", Journal of Constructional Steel Research: 65 (2009), 452-465.

Shome, N., Cornell, C.A. (1999) "Probabilistic Seismic Demand Analysis of Non-linear Structures", Report No. RMS-35, RMS Program, Stanford University.

Shuhaibar, C., Lopez, W.A., Sabelli, R. (2002) "Buckling-Restrained Braced Frames", Proceedings of Seminaron Reponse Modification Technologies for Performance-Based Seismic Design, 321-328.

Somerville, P., Smith, N., Punyamurthula, S., Sun, J. (1997) "Development of Ground Motion Time Histories for Phase 2 of FEMA/SAC Steel Project", SAC-BD/97-04

Song, J., Ellingwood, B.R. (1999) "Probabilistic Modeling of Steel Moment Frames with Welded Connections", Engineering Journal, AISC; 36(3), 129-137.

Uang, C.M., Kiggins, S. (2006) "Reducing Residual Drift of Buckling-Restrained Braced Frames as a dual system.", Engineering Structures, 28(11), 1525-1532.

Vamvatsikos, D., Cornell, C.A. (2002) "Incremental Dynamic Analysis", Earthquake Engineerings and Structural Dynamics; 31:491-514.

Yang, C.S., DesRoches, R., Leon, R.T. (2010) "Design and Analysis of Braced Frames with Shape Memory Alloy and Energy-absorbing Hybrid Devices", Engineering Structures; 32:498-507.